2013

Submarine Groundwater Discharge to the York River Estuary: Quantifying Groundwater Flux and Potential for Biogeochemical Cycling

Jenna Lynn Luek
College of William and Mary - Virginia Institute of Marine Science

Submarine groundwater discharge to the York River estuary: Quantifying groundwater flux and potential for biogeochemical cycling

---

A Thesis

Presented to

The Faculty of the School of Marine Science

The College of William and Mary in Virginia

In Partial Fulfillment

Of the requirements for the Degree of

Master of Science

By

Jenna Lynn Luek

2013

APPROVAL SHEET

This thesis is submitted in partial fulfillment of
The requirements for the degree of
Master of Science

Jenna Lynn Luek

Approved, by the Committee, August 2013

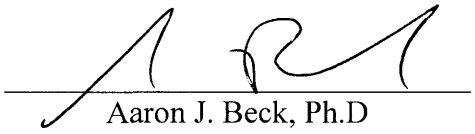

Aaron J. Beck, Ph.D
Advisor

Michael A. Unger, Ph.D

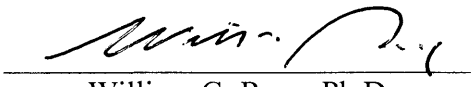

William G. Reay, Ph.D

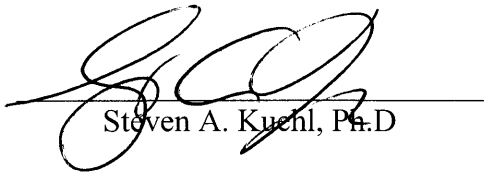

Steven A. Kuehl, Ph.D

Table of Contents

Acknowledgements

I am extremely grateful to the many among the Virginia Institute of Marine Science community for supporting my education, my research and me over the past three years. Without the amazing graduate student community and my fantastic housemates I may not have made it through this program. In particular, I'd like to thank Jenna Spackeen, Hadley McIntosh, and the rest of the chemical oceanography department for their laboratory and moral support. I'd like to thank Alison O'Connor for continuing and growing what I started at the GP site eighteen months ago. Matt Freedman, Carol Hopper-Brill, the CBGS staff, the rest of the GK-12 Year 4 cohort have been amazing friends and mentors who have helped me grow as an educator and a communicator. The CBNERRVA staff and Kelsey Fall and Carissa Wilkerson provided invaluable field support as I collected York River samples. Dr. Linda Schaffner provided critical guidance and support in my graduate education and our community garden project. Dr. Jian Shen has provided essential York River hydrodynamic modeling data that has significantly improved the accuracy of my calculations. My committee members, Drs. Steve Kuehl, Mike Unger, and William Reay, have provided wonderful guidance and insight. I'd like to thank Dr. Aaron Beck, for taking me on as a student midway through my time here at VIMS and for being a fantastic mentor to me. I am extremely grateful to Brandon Conroy for being my best friend and support for the last two years. Finally, I want to thank the late Dr. Rebecca Dickhut for bringing me to the Virginia Institute of Marine Science as an undergraduate and trusting me with her hard earned Antarctic samples. Without her enthusiasm and support I would have never considered a career in marine science. She has been an amazing role model to me and I am honored to have worked with such a fantastic scientist and friend. I feel extremely fortunate to have the continued support of the Dickhut academic family.

Table of Figures

Chapter 1

Chapter 2

List of Tables

Introduction

Fresh groundwater mixes with saline estuarine and coastal ocean waters in an area known as the subterranean estuary (STE) (Moore, 1999). A salinity gradient occurs across the STE similar to surface estuaries and processes such as adsorption and flocculation, ion exchange, and chemical precipitation occur. The STE therefore acts as a source for some compounds and a sink for others (Charette et al., 2008; Moore, 1999). Water flowing through the STE is a combination of water originating in the coastal ocean as well as fresh groundwater derived from upland sources. Water that is cycled through the STE and eventually discharged to the surface is termed SGD. More specifically, SGD is defined as "any and all flow of water on continental margins from the seabed to the coastal ocean, regardless of fluid composition or driving force" (Burnett et al., 2003). Submarine groundwater discharge may be a major contributor to the budget of a wide variety of compounds important to the biogeochemical cycling of the global oceans (Moore, 2010). Understanding this interaction within coastal sediments is imperative to furthering our understanding of the cycling of water and chemicals such as nutrients and contaminants through the subterranean estuary and receiving coastal waters.

SGD is driven by many forces including hydraulic gradients, tidal fluctuations, and wave energy, as well as factors such as salinity and temperature that influence density (Moore, 1999; Moore, 2010; Santos et al., 2012). Additional small scale mechanisms of SGD such as bioirrigation, gas bubble movement, and ripple migration release pore waters (Santos et al., 2012). Local geology can also influence the mobility of groundwater and exacerbate or limit groundwater exchange. The mobility of groundwater through an aquifer depends upon hydraulic conductivity, which is a function of variables

such as the porosity, tortuosity, and grain size distribution of the sediments as well as the viscosity of the flowing liquid. Silts and clays have a lower intrinsic permeability and therefore have lower hydraulic conductivities; unconsolidated sands have a higher hydraulic conductivity and allow for greater advective fresh groundwater flow (Schwarzenbach et al., 2003). Groundwater is stored in saturated sediments known as aquifers that may be confined or unconfined by an upper boundary aquitard. Dredging may alter the flow of SGD as it can breach this aquitard and increase advective flow and interaction with overlying coastal waters (Yehdegho et al., 1997; Moore, 1999). Groundwater from deep aquifers is pumped for municipal, industrial, agricultural and domestic head use. Fresh groundwater potentials and connectivity all flow through the STE (Harsh and Laczniak, 1990; Moore, 1999).

Regional land use patterns and environmental history can strongly affect the observed levels and fluxes of various chemicals such as nutrients, trace metals, and contaminants across the STE (Lapointe et al., 1990; Valeila et al., 1992; Charette and Buesseler, 2004; Ballestero et al., 2004). Shallow aquifers have been shown to be susceptible to anthropogenic contamination, especially in the upper thirty meters (Simmons, 1992; Valeila et al., 1992; Heywood and Pope, 2009). For example, the growth of population around Waquoit Bay [Massachusetts, USA] spurred an increase of nitrogen contamination in shallow coastal wells (Valeila et al., 1992). SGD enriched in nutrients to the coastal ocean was found to be greater than their input via surface pathways (Simmons, 1992) and has been linked to recurrent harmful algal blooms (Hu et al., 2006; Lee and Kim, 2007). SGD has been shown as a route for agricultural additives in shallow coastal aquifers to enter estuarine waters (Gallagher et al., 1996; Ballestero et

al., 2004; Reay, 2004). After years of anthropogenic use, working waterways such as the Chesapeake Bay have been subjected to a slew of natural and manmade chemical compounds. For example, Elizabeth River sediments contain high concentrations of polycyclic aromatic hydrocarbons (PAHs) originating from industrial operations and shipping along the river (Mitra et al., 1999; Conrad et al., 2007).

Measuring Groundwater Discharge

Modern quantitative measurements of watershed groundwater discharge include techniques such as hydrograph separation, water mass balance, measurements of hydraulic gradients. By analyzing long-term stream flow (hydrograph), a base flow can be measured whose assumed source is groundwater. A water mass balance determines groundwater input by measuring all other sources and sinks of water within a system (i.e. precipitation, runoff, evapotranspiration) and calculating groundwater discharge through an assumed mass imbalance (Burnett et al., 2006). Hydraulic conductivity can be used in conjunction with Darcy's Law to calculate groundwater input (Freeze and Cherry, 1979). However, these techniques are designed to solely measure fresh groundwater discharge and are therefore inadequate for quantitatively deciphering the amount of recirculated brackish and saline waters that also move through the STE (Burnett et al., 2006). Recirculated seawater typically accounts for more than 90% of the total water cycled through a subterranean estuary (Li et al., 1999). Seepage meters are a direct way of measuring the volume of SGD that includes the discharge of both fresh groundwater and recirculated seawater. Seepage meters measure SGD by enclosing an area of submerged sediment with a flexible container and analyzing volume displacement over a set length

of time (Lee, 1977; Burnett et al., 2006). Seepage meters can also be used to analyze the chemical constituents present in SGD through longer meter deployment and accounting for headspace dilution (Burnett et al., 2006). The use of seepage meters works well in calm waters but in areas with strong wave action the precision of the instrument may drop significantly (Shinn et al., 2002; Corbett and Cable, 2003). The anisotropic nature of coastal sediments also makes it difficult to scale up seepage meter measurements to even basin wide estimates let alone global estimates (Burnett et al., 2006).

Tracers may also be used to assess and quantify SGD. Tracers are advantageous as they are typically able to smooth out the heterogeneity found along coastlines which are difficult to capture through direct measurement with seepage meters (Burnett et al., 2001). An ideal tracer of SGD is enriched in groundwater, behaves conservatively in seawater, and is easy to measure (Burnett et al., 2006, Charette et al., 2008). In homogenous media, it is ideal to use a vertical profile of the tracer in pore waters and use a one-dimensional advection-diffusion model (Cornett et al., 1989; Moore, 2000; Schwarzenbach et al., 2003). A second and more universally acceptable method follows the specific tracer through the system, which necessitates understanding all of the sources and sinks of that tracer within the system. Some common tracers include ^{226}Ra and methane gas, but a wide variety of compounds including radioisotopes (tritium, uranium-thorium series isotopes), stable isotopes (carbon, strontium), and anthropogenic compounds (CFCs) have been used trace groundwater (Burnett et al., 2006). In order to further understand the wide variety of physical, chemical, and biological processes occurring within the subterranean estuary, it is ideal to use a variety of tracers and if possible a use these in conjunction with more traditional (Michael et al., 2011). Further

discussion of methods of qualitatively and quantitatively measuring SGD is found in several review papers (Burnett et al., 2001, Burnett et al., 2006, Gallardo and Marui, 2006).

Use of radioactive elements to examine water column processes

Fresh groundwater and recirculated brackish and saline waters flow through a complex geologic environment enriched with a variety of elements. Members of the uranium-thorium decay series are present in many sediments types in varying proportions where they are physically and chemically weathered and enter groundwater (Chabaux et al., 2003). Uranium and thorium are known to be compatible in a variety of minerals but in general it is difficult to predict their distribution or release rates in host rocks without direct analysis (Porcelli, 2008). Nuclides in the uranium-thorium decay series have different solubilities, physical behaviors, and undergo a variety of chemical reactions in coastal oceans and sediments. In **Table 1**, the behaviors of uranium, thorium, radium, and radon in fresh and saline waters are summarized.

The variety of short- and long-lived isotopes in this series can be described as being in secular equilibrium, that is the long-lived parent and short-lived daughter isotope have the same activity. Disequilibrium that exists between the parent and daughter can be used to trace water masses and ocean processes (Swarzenski, 2007). The use of water column disequilibrium as an oceanographic tool first appeared in the literature nearly half a century ago. Early measurements of $^{238}U/^{234}Th$ disequilibrium in shallow water shed light on the particle reactivity of thorium and the processes of scavenging and remineralization (Bhat et al., 1969). The disequilibrium of ^{227}Ac and its parent ^{231}Pa have been used to look at diapycnal ocean mixing (Geibert et al., 2002).

Based on the behavior of these individual radionuclides and their varying half-lives, individual isotopes and comparative ratios may be used to look at a variety of processes in the aquatic environment. Individual isotopes are often used as chronometers of processes occurring in estuarine and oceanic water. Due to its short half-life, ^{210}Pb has been used extensively to measure sedimentation rates in estuarine environments (e.g. Nittrouer et al., 1979; French et al., 1994, Bellucci et al., 2007). ^{234}U can be used to analyze weathering patterns and can trace SGD in reducing environments (Chabaux et al., 2003; Charette et al., 2008). Radon can be used to qualitatively and quantitatively study estuarine mixing and gaseous exchange with the overlying air, and is likewise used extensively as a tracer of groundwater and estuarine mixing rates (McKee, 2008).

Radium as a tracer of submarine groundwater

Radium is an ideal tracer of SGD: its dominant source is groundwater and it is therefore enriched in groundwater relative to surface waters, its contribution from other sources is minimal, it behaves conservatively in seawater, and it is relatively easy to measure (Burnett et al., 2006; Charette et al., 2008; Moore, 2010). As with other radioactive U-Th series isotopes, radium acts as an environmental chronometer and the suite of individual radium isotopes are on time scales that correlate to a variety ocean processes: ^{224}Ra (3.66d), ^{223}Ra (11.4d), ^{228}Ra (5.75y), ^{226}Ra (1599y) (Swarzenski et al., 2001). The suite of radium isotopes has been used for over a decade to trace groundwater as it discharges into the marine environment (Moore and Arnold, 1996; Rama and Moore, 1996; Moore, 2010).

Salinity controls the partitioning of radium to particles in surface estuaries and subterranean estuaries, and radium behaves non-conservatively in estuarine mixing (Li

and Chan, 1979). Radium is produced by the alpha decay of four thorium parents (^{234}Th, ^{232}Th, ^{228}Th, and ^{227}Th). Thorium is strongly particle bound and when alpha decay occurs, radium and its corresponding alpha particle undergo recoil and may be expelled to the surface of the particle or directly in to the surrounding water. In freshwater, the dissolved radium is highly particle reactive and remains particle bound or quickly associates with particulate matter. In saline water, radium on the surface of particles is desorbed and high dissolved phase activities are observed (Li and Chan 1979; Moore, 1999). Radium concentrations are enriched in brackish groundwater relative to surface water because groundwaters are closely associated with thorium enriched sediments (Moore, 1999).

The ratios of radium isotope activities have been used in a variety of applications from deciphering the geologic origin of groundwater and aquifer type (Al-Masri, 2006; Charette and Buesseler, 2004) to estimating the extent of riverine influence on the ocean (Moore et al., 1986; Moore and Krest, 2004). **Table 2** shows several common applications of various radium activity ratios. The longer-lived radium isotopes (^{226}Ra and ^{228}Ra) have been used to provide models of long term coastal mixing extending offshore tens to hundreds of kilometers (Li et al., 1977; Moore, 2000; Moore, 2010). Evidence for a groundwater source of radium to coastal systems was first acknowledged by observations that these long-lived radium isotopes in coastal waters exceeded input from rivers; subsequent findings have observed the same concepts using the short-lived radium isotopes (Moore, 1996; Rama and Moore, 1996).

Nutrients in submarine groundwater discharge

Shallow aquifers are susceptible to anthropogenic contamination and may ultimately discharge this contamination to surface waters via SGD (Simmons, 1992; Valeila et al., 1992; Heywood and Pope, 2009). Coastal aquifers are consistently enriched in nitrogen, which is correlated with human activity (e.g. Valeila et al., 1992; Simmons, 1992; Gallagher et al., 1996; Reay, 2004). High levels of ammonium have been observed in shallow pore water in the York River estuary (I. Anderson, VIMS, unpublished; Salisbury, 2011; Kellum et al., in progress), and the discharge of these nutrients in non-Redfield ratios (Redfield, 1934) may impact phytoplankton and bacterial communities and ultimately affect higher trophic levels dependent upon these (Slomp and van Capellen. 2004). Accurate estimates of SGD nutrient fluxes are imperative for proper nutrient management in the increasing number of eutrophied estuarine systems worldwide (Diaz, 2001).

Trace metals in submarine groundwater discharge

As with nutrients, SGD may be a significant source of trace metals to coastal regions. In studies of global metal budgets, groundwater has been proposed as a possible contributor that could solve many metal budget imbalances (Basu et al., 2001; Milliman, 1993; Bone et al., 2007). Metals such as mercury and copper may have significant regional inputs to coastal systems via SGD (Bone et al., 2007, Charette and Buesseler, 2004). Tracing radium isotopes from their groundwater source through mixing has also provided insight for a groundwater source of elevated iron observed in phytoplankton blooms in the Southern Ocean (van Beek et al., 2008). Significant potential for trace

metal input via groundwater exists along the York River estuary. Military operations such as those along the York River estuary have repeatedly contaminated groundwater (USGAO, 2005; VaDEQ, 2005). The movement of metals associated with fossil fuels are of particular interest due to the heavy fuel reliance of military operations and as well as fuel spills associated with shipping (Everett 1998; USGAO, 2005). Sea level rise may alter the behavior of certain metals that may have previously been stable in aquifers but with exposure to higher salinities an increase in metal desorption and subsequent input to coastal waters may occur (Moore, 1999; Moore, 2010).

Organic contaminants in submarine groundwater discharge

Because industry often lines waterways, this interface of SGD from current and historic industrial sites could be important to the cycling of organic contaminants through estuarine systems. Because the subterranean estuary has a long residence time, it may be an important long-term source of contamination sequestered in sediments to the surrounding waters (Moore, 1999; Robinson et al., 2009). The Chesapeake Bay and its rivers have been used as shipping channels and their shorelines for agriculture and industry for hundreds of years and the long-term impacts on land and water quality is evident (Helz, 1976; Mitra et al., 1999). All groundwater samples collected in Phillips Creek (Virginia) had detectable levels of agricultural contaminants, while many seepage meters samples collected nearby detected these same compounds (Gallagher et al., 1996). In addition to agriculture, the York River watershed has a significant amount of industrial and military presence, especially along its coastline. There are multiple sites along the York River estuary with sediments heavily contaminated with PCBs that have been remediated to varying extents (VaDEQ, 2005). The Yorktown Naval Weapons Station

located on the south bank has contaminated groundwater and the nearby surface waters with a variety of contaminants including TNT and PCBs (VaDEQ, 2005; Bromage et al., 2007). The Department of Defense has acknowledged their repeated contamination of groundwater within military bases and is working on mitigation efforts in some areas (USGAO, 2005).

Only one study thus far has field data examining the movement of fossil fuel derived contaminants through the STE, tracking a dissolved hydrocarbon plume from its origin through groundwater flowing in to a nearby estuary. Measurements of benzene, toluene, ethyl benzene, and xylene, (BTEX) and napthalene were collected and helped show this plume dominated flow only in the 10m nearest shore (Westbrook et al., 2005). Another study modeled the potential input of BTEX through SGD and demonstrated that tidal flushing may increase attenuation in the subterranean estuary (Robinson et al., 2009). A few other studies have illuminated the potential for organic contaminant movement through SGD. A handful of seepage meter measurements were made in Sarasota Bay [FL, USA] to analyze for sewage infiltration and caffeine was identified in some samples (Peeler et al., 2006). Karst aquifers located several kilometers inland that drain in to the Caribbean Sea were contaminated with a variety of personal care products, pharmaceuticals, and industrial and agricultural products. However, the movement of these organic compounds from the inland aquifer to the Caribbean Sea was not investigated so this pathway is only hypothesized (Metcalfe et al., 2011).

The industrial history and the continued input of similar compounds via SGD suggests that a strong potential exists for PAHs and other organic contaminants to be present in shallow groundwater and may ultimately be discharged to surface water

through SGD. Long-term monitoring in the York River estuary suggest that studies on the input of contaminants such as PAHs and PCBs via groundwater are vital for understanding the long term health of Chesapeake Bay and the implementation of successful management strategies (Reay, 2009). Understanding how a diverse group of organic compounds moves through the subterranean estuary is inadequately understood and clearly necessitates further study.

Table 1: Summarized behavior of U/Th series nuclides in seawater and freshwater (Chabaux et al., 2003; Swarzenski et al., 2003).

Element	Behavior in Seawater	Behavior in Freshwater
Uranium	conservative in oxygenated water	associated with particles (40-90%) and dissolved phase in oxygenated water
Thorium	highly particle reactive	highly particle reactive
Radium	some particle reactivity, conservative in seawater	highly particle reactive
Radon	noble gas, unreactive	noble gas, unreactive

Table 2. Summary of applications of radium isotope ratios (Porcelli and Swarzenski, 2003; Porcelli, 2008; Charette et al., 2008, and sources therein).

Radium Isotope Ratio	**Applications**
223/228	water residence time (weeks)
223/226	aquifer recharge rate
224/228	water residence time (days)
224/228	source lithology
224/228	thorium sorption rate
226/228	relative recoil rates, source lithology

Radium budget of the York River estuary (VA, USA) dominated by submarine groundwater discharge with a seasonally variable groundwater end-member

Abstract

Submarine groundwater discharge (SGD) is a major source of biogeochemically important compounds to the coastal environment. Naturally occurring radium (Ra) has been successfully used to trace SGD because it is enriched in sediments and desorbs from particles in saline environments. In the York River estuary (YRE), Ra was measured seasonally in surface water and shallow groundwater during 2012 (Jan. – Mar. and Jul. – Sept.) and other Ra sources including desorption and diffusion from sediments were also quantified. The flux of SGD to the YRE was then determined by quantifying each source and sink within the system for several radium isotopes (^{223}Ra, ^{224}Ra, ^{226}Ra). In the YRE, a major source of Ra that could only be satisfied by SGD was determined using the Ra mass balance. SGD estimates (6-118 L/m^2/d) made by season were similar, suggesting that Ra fluxes are driven by seasonality in the pore water end member rather than SGD volume variability. Short-lived Ra isotopes are regenerated more rapidly that long-lived Ra isotopes, indicating that short-lived Ra isotopes are best able to account for a variety of different flow paths including shallow flushing. This study provides evidence that the York River subterranean estuary cycles and discharges a significant quantity of water as SGD.

1. Introduction

Submarine groundwater discharge (SGD) may be a major contributor to the budget of a wide variety of compounds important to the biogeochemical cycling of the global oceans (Moore 2010). Global estimates of SGD rates are on the order of 0.01-10% of surface water runoff rates, with more estimates in the higher end of this range (Taniguchi et al., 2002). In some estuarine systems, such as Jamaica Bay [NY, USA], groundwater is the only natural freshwater input (Beck et al., 2007). A salinity gradient occurs across the STE similarly to surface estuaries and processes such as adsorption and flocculation, ion exchange, and chemical precipitation occur. The STE therefore acts as a source for some compounds and a sink for others (Charette et al., 2008; Moore, 1999).

SGD can be quantified either directly by collecting benthic fluxes of water or indirectly by using tracers of SGD (Lee, 1977; Moore 2010; Burnett et al., 2006). SGD flux estimates are extremely variable within a system as well as between systems and estimated fluxes often depend on the quantification method. The use of seepage meters for understanding SGD in large scale coastal environments is not practical for several reasons, including the high number of units required to understand natural variability, the intensive manual labor required, and artifacts associated with their use (Burnett et al., 2006 and sources therein).

Radium (Ra) has been successfully used to trace SGD and coastal mixing processes (Moore, 2000; Moore, 2003, Moore et al., 2006). Radium is produced in sediments from the decay of its thorium (Th) parent and is bound to particles in fresh water. Both fresh and saline groundwaters are enriched in radium relative to surface waters that have low levels of the parent thorium. When surface bound radium in

sediments is exposed to saline waters, radium desorbs from the particle and enters the dissolved phase (Li and Chan, 1979). The varied half-lives of individual radium isotopes (^{223}Ra=11.4 d, ^{224}Ra=3.6d, ^{226}Ra=1600y, ^{228}Ra=5.75y) allows radium to be used as a conservative geochronometer in the coastal ocean over day to millennial time scales (Rama and Moore, 1996).

This study investigates SGD to the York River Estuary [VA, US] using a mass balance of Ra. Neither radium nor SGD in the York River estuary (YRE) have been investigated previously. Accurate estimates of SGD are crucial for understanding the role submarine groundwater discharge may play in the input of nutrients and other compounds of interest to the YRE and ultimately to the Chesapeake Bay. SGD has been determined a crucial part of the mass balance YRE was selected as a study site because these findings may be expanded to other sub-estuaries of the Chesapeake Bay as well as the Chesapeake Bay as a whole, and because a significant body of descriptive research has been collected within the YRE which improve the precision of calculations and provide broader spatial and temporal context for these results.

A box model for Ra was selected that encompasses the YRE from its head at the confluence of the Mattaponi and Pamunkey Rivers to its mouth where it enters the Chesapeake Bay. Radium enters the YRE through a) the Mattaponi and Pamunkey tributaries b) tidal flushing of salt marshes c) desorption from suspended sediments d) input from exchange with the Chesapeake Bay, e) diffusion from sediment and f) advection through sediments (SGD). Additionally, Ra also enters from industrial deep groundwater discharge at West Point, near the confluence of the Mattaponi and Pamunkey. Losses of radium from the YRE were calculated from exchange with the

Chesapeake Bay and loss of Ra to radioactive decay. The input of radium from advection through sediment (SGD) was estimated as the net difference between all other quantified sources and sinks. Additionally, this study provides improvements on estimates of inlet exchange, desorption, diffusive fluxes, and the pore water end member over previous Ra box models (Beck et al., 2007; Beck et al., 2008; Garcia-Solsona et al., 2008a). This study suggests that the distribution of Ra across the subterranean estuary is variable but is not random. Further, this study provides evidence that the SGD Ra end member is seasonally variable while SGD fluxes to the YRE are not. The residence time of the entire York-Mattaponi-Pamunkey systems ranges (**Fig. 1**) from <20 to > 200 days so both short-lived (^{223}Ra, ^{224}Ra) and long-lived isotopes of radium (^{226}Ra) were individually used to calculate the input of radium from the SGD and ultimately calculate the flux of water passing through the STE.

2. Methods

2.1. Site description

The YRE drains about 6900 km^2 of land in the lower portion of the Chesapeake Bay, and has two major tributaries, the Mattaponi and Pamunkey Rivers (Reay, 2009). The YRE is microtidal, with a mean tidal range of 0.7 m to 0.85 m but has significant tidal currents that are strongest in the channel and weaker on the shoals (Sisson et al., 1997; Huzzey and Brubaker, 1998). The residence time of the YRE from West Point (head of estuary) to the YRE mouth can range from 20 days to more than 200 days under high and low flow conditions, respectively, and is typically approximately 40 days (Shen and Haas, 2004).

The YRE experiences a range of salinities; surface water collected during sampling ranged between fresh water and salinity 25 annually while bottom waters were likely approximately 1.1 units more saline (Jian Shen, personal communication). During 2012, surface water salinities ranged between 2 at the head of the estuary (WP) during winter to 23 near the mouth of the estuary during summer. The York River watershed receives a generally constant rate of precipitation year round, but high evapotranspiration rates in summer set up maximum salinity conditions in the YRE during late summer (VECOS, 2013). Similarly, low evapotranspiration rates in winter result in minimum salinity conditions during the winter months. Minimum salinity conditions were observed during January-March 2012 (herein referred to as winter) and maximum salinity conditions were observed from July-September 2012 (herein referred to as summer). Surface and pore water were sampled in winter and summer to represent the variation in radium activity across a range of salinities. Input from salt marshes, desorption from suspended sediments, and diffusion from sediments were measured without regard to season. During sampling, surface water salinity did not exhibit a continuous along-estuary gradient, but rather a local salinity maximum was found several kilometers upriver from the mouth. This is regularly observed and is caused by reverse estuarine circulation that often occurs during regionally wet years when fresher Chesapeake Bay water is advected in to the mouth of the YRE (Hayward et al., 1982).

2.2. Radium in YRE surface water

Surface water dissolved radium was measured seasonally in the YRE at 9 sites in winter and 10 sites in summer (**Figure 1).** Additionally, surface water Ra was sampled

monthly at the GP site. Sites were distributed along the YRE from the head at West Point (WP) to the estuary mouth, and included a mixture of nearshore and open water sites. Samples were collected at three sites at the mouth of the York River to characterize water that exchanges with Chesapeake Bay (GI, CM, GM). The YRE receives the majority of its fresh water input from the Mattaponi (USGS, 2013: 02080105) and Pamunkey Rivers (USGS, 2013: 01673000), located about 52km upstream from the mouth of the York River estuary. Surface water samples were collected in the tidal fresh regions of the Mattaponi and Pamunkey tributaries (MA, PM) as well as at their confluence at West Point (WP). The lower reaches of these tributaries are brackish during most of the year, with salinities below 5 in winter months and upwards of 11 during summer. The transition from brackish to freshwater typically occurs upstream of West Point, between 60 and 90km upstream of the mouth of the YRE (Lin and Kuo, 2001; Shen and Haas, 2004). Seasonal input from these tributaries varies but long-term mean stream flows are 1.41×10^6 m^3/d and 2.65×10^6 m^3/d for the Mattaponi and Pamunkey, respectively (Reay, 2009). Stream flow for the Mattaponi and Pamunkey is gauged upstream at the fall line more than 40km upstream of their confluence at the head of the YRE. Combined stream flows from the Mattaponi and Pamunkey were 6.70×10^6 m^3/d and 6.79×10^5 m^3/d during the winter and summer of 2012, respectively.

Dissolved radium was extracted from large-volume (20-40 L) water samples by passing through manganese fiber columns at a maximum flow rate of one liter per minute (Moore and Reid 1973; Moore and Scott, 1986; Moore, 2008). Fibers were then rinsed with deionized water (~500 mL) to remove salt, and manually squeezed to remove excess water and maintain an ideal water to fiber ratio (Sun and Torgerson, 1998; Kim et al.,

2001; Moore, 2008). Radium activity was measured by radon emanation using a radium delayed coincidence counter (RaDeCC) (Scientific Computer Instruments) (Moore and Arnold, 1996). Measurements were made immediately after sample collection for ^{224}Ra and ^{223}Ra isotopes (Moore, 2008). A subset of manganese fiber samples selected for ^{226}Ra determination were capped and sealed for 3+ days to allow ingrowth of ^{222}Rn, and analyzed using the RaDeCC total counts category (Waska et al., 2008; Peterson et al., 2009).

The extraction efficiency of the manganese fibers was calculated by repeated measurements of field samples with two columns in series and measuring the activity on both columns. The extraction efficiency of dissolved radium on to the manganese fibers was 94±5% (n=10). The efficiency of the RaDeCC instrument was measured with an IAEA standard (n=20 counts) as described by Scholten and colleagues (2010), and background activity (^{223}Ra= 0.00125±0.0056; ^{224}Ra= 0.0396±0.0706; ^{226}Ra=0.602±0.390 cpm, n=10) was determined for each system by averaging long counts (20+ hours) of each empty circulating cell (Garcia-Solsona et al., 2008b). Uncertainty in replicate Ra samples was 14.8% for ^{223}Ra (n=7); 13.8% for ^{224}Ra (n=7), and 10.1% for ^{226}Ra (n=3), which included an approximate counting error of 10% for ^{223}Ra and 5% for both ^{224}Ra and ^{226}Ra.

2.4. Ra input from salt marshes

Salt marshes are known to be a source of radium to the coastal ocean as tidal waters flood the marsh with higher salinity waters (Bollinger and Moore, 1984; Bollinger and Moore, 1993). The flux of radium across a fixed point at the outlet of Taskinas Creek

was measured over twelve hours on 3 August 2012. Taskinas Creek is a brackish tidal marsh creek system flowing into the YRE that is continuously monitored for physical and chemical parameters (Moore and Reay, 2009; VECOS, 2013). Surface water radium samples were collected continuously over 75 minute periods resulting in integrated samples, and processed as described above. Water quality parameters were measured every 30 minutes using a handheld YSI, and water flow rate estimated using a neutrally buoyant drifter. An onsite stationary YSI run by CBNERRVA (VECOS, 2013) provided tidal height data at 15-minute intervals approximately 5 m upstream from the sampling site. Water fluxes were estimated by flow speed at the surface (multiplied by a correction coefficient of 0.9 to account for the muddy bottom drag) (EPA, 2013 http://water.epa.gov/type/rsl/monitoring/vms51.cfm) and cross-sectional area, which ranged from 12 m^2 to 27 m^2 over the tidal cycle. Because sampling occurred over a span just shy of a full tidal cycle, the radium activities and fluxes for the final time point were estimated as the average of the first measurement of radium on the previous rising tide and the last measurement. Salinity in the surface water was ~5 units lower at low tide than high tide, indicating input from fresh runoff or groundwater in the Taskinas. An enrichment approach was used to determine the quantity of radium supplied over the tidal cycle, and therefore represents an upper limit because fresh discharge is included in the estimate.

2.5. Ra diffusion from sediments

Radium input by diffusion from sediments was measured over timed intervals by incubating sediment cores and measuring the radium content in overlying water (Bird et

al., 1999; Beck et al., 2007). Diffusion of radium from sediments was measured in both fine- and coarse-grain sediments. Coarse sediment cores (n=6, 0.0346 m^2) were collected from the intertidal zone at the GP site. Fine sediment cores (n=2, 0.055 m^2) were collected by box core from the CB site at a water depth of ~18 m. Radium-free YRE water (salinity ~18, pre-extracted over two manganese fiber columns placed in line) was carefully added to the individual cores so as to not disturb the sediment, and overlying water was gently bubbled with air to stir and oxygenate the water. The sediment-water interface of the CB site cores was disturbed during transfer from the box core to sample box, and sediments were smoothed and allowed to sit for 72 hours to equilibrate with the Ra-free water. Overlying water was drained from cores at varying times (1-600 hours) for Ra measurement as discussed in Sec. 2.2, and replaced with Ra-free water. Radium flux from the sediment to the overlying water (J_{diff}) was calculated using **Equation 1** (adapted from Beck et al., 2007),

$$I_t = [(J_{diff}A_{surf}) / \lambda] (1 - e^{-\lambda t}) + A_o e^{-\lambda t} \quad (1)$$

where I_t is the inventory of radium in the overlying water (dpm) at time, t (d), J_{diff} is the diffusive flux of radium to the overlying water (dpm/m^2/d), A_{surf} is the sediment surface area of the core, λ is the decay constant of each isotope (λ_{223} = 0.0608 d^{-1}; λ_{224} = 0.189 d^{-1}), and A_o is the initial radium activity of the surface water likely resulting from initial desorption upon Ra-free water addition (Beck et al., 2007). Parameters and uncertainties for J_{diff} and A_0 were calculated by least-squares fitting of **Equation 1** using SigmaPlot.

2.6. Desorption from suspended sediments

Radium is produced from Th adsorbed on particles, and may be released by desorption or recoil to the dissolved phase when sediments are resuspended. This input was determined using shallow sediments (<2 cm depth) from four sites, including both the nearshore (GP, FL, CP) and offshore sediments (CB). Sediments were characterized visually as either mostly fine or mostly coarse, and then known masses of each sediment type were added to 20 L of radium-free YRE water (salinity ~18). These mixtures were then shaken for 5 minutes and dissolved radium extracted and analyzed as described in Sec. 2.2. A portion of each sediment type was dried overnight in a warm oven (90 ^{o}C) to measure dry weight.

2.7. Radium in near shore pore water

Pore water (groundwater) samples were collected using a drive point piezometer (Charette and Allen, 2006). Sample sites (**Figure 1**) were selected to include a range of salinities, and samples were collected from both the North and South banks to account for differences in sediment types on each bank (Nichols et al., 1991). Pore water samples were collected from five sites during winter and six sites during summer. Additionally, pore water was sampled monthly at the GP site from January 2012 through March 2013. At each site, a groundwater profile in the intertidal region was attempted at 50cm intervals from 0-200 cm. The full 200 cm profile was not collected at all sites when impermeable clay layers were encountered. At sites where sediments were impermeable at depths >50 cm (CP, BB), samples were collected at shallower depths. Pore water samples were collected for water quality parameters and radium analysis (4L). Radium

samples were oxygenated to prevent reduction of Mn fibers then extracted and analyzed as described previously.

3. Results

3.1 Pore water salinity

Salinity in the York River subterranean estuary was not constant with depth over the study period implying that the position of the mixing interface varied (**Table 3**). Surface water and shallow pore water salinity varied seasonally at the GP site, reflecting seasonal patterns in the water year (**Figure 2**). At shallow depths (<1 m), salinity and dissolved Ra were significantly higher during summer compared with winter (Student's t-test, $p<0.05$). Deep groundwater (>150 cm) salinity remained relatively constant over the course of the year. Across sites, the same distribution of salinity was present with respect to both season as well as depth. Pore waters collected below a depth of one meter were significantly fresher than samples collected above one meter (Student's t-test, $p<0.01$). Similarly, pore water collected during winter was significantly fresher across all depths than samples collected during the summer (Student's t-test, $p<0.01$).

3.2. Surface water dissolved Ra

Samples collected in the tidal fresh region of the Mattaponi and Pamunkey Rivers had low radium activity (average ± standard deviation: ^{223}Ra = 0.3±0.0 dpm/100L; ^{224}Ra = 4.8±2.1 dpm/100L; ^{226}Ra =11.3 dpm/100L) (**Table 1**). Although the Mattaponi and Pamunkey Rivers were not sampled during the winter of 2012, Ra activities were

assumed to be similarly low because these tributaries are even fresher during winter months.

Mean surface water Ra activity for the YRE was calculated as the site-weighted average of all samples collected downstream of WP and upstream of the mouth of the YRE (winter, n=7 sites; summer, n=8 sites). Mean surface water Ra activities for the YRE were generally higher in summer (^{223}Ra = 5.1±1.3, ^{224}Ra = 51±14, ^{226}Ra = 31±11 dpm/100 L) compared with winter (^{223}Ra = 3.3±3.2, ^{224}Ra = 26±8.5, ^{226}Ra = 11±6.4 dpm/100 L). ^{224}Ra and ^{226}Ra were significantly higher in surface water during summer than winter (Student's t-test, $p<0.001$ and $p<0.01$, respectively). The lowest surface water radium activities (^{223}Ra = 0.1, ^{224}Ra =2.1 dpm/100L) were collected during a precipitation event at the GP site that was preceded by several days of heavy rain. All other surface water collections were made during fair weather. The highest surface water ^{223}Ra activity (12.5 dpm/100L) was observed at the BB sample site, coincident with high pore water Ra thought to be associated with low pore water pH. When the two outliers from the BB site are removed because surface water from BB was not samples during the summer, ^{223}Ra activity in surface water was also significantly lower (Student's t-test, $p<0.001$) during winter than summer.

Surface water was collected from three sites at the mouth of the YRE (GI, CM, and GM). During the winter of 2012 these samples had very low dissolved Ra activities (^{223}Ra = 0.2±0.18, ^{224}Ra = 1.7±1.5; ^{226}Ra = 3.97±0.59 dpm/100L). Samples were collected over multiple dates, at multiple sites spanning the shoals and the channel, and on both incoming and outgoing tides, during which the surface water radium activity remained consistently low. The low radium activities found at the mouth of the YRE

were significantly lower than bulk YRE Ra (Student's t-test, ^{223}Ra, $p<0.01$; ^{224}Ra, $p<0.01$; ^{226}Ra, $p=0.05$), suggesting samples collected at the mouth represented different waters than the York River estuary, likely representing Chesapeake Bay water. In the summer, the mouth of the YRE was sampled only during outgoing tides, and ^{223}Ra and ^{226}Ra activity in surface waters collected at the mouth and in bulk YRE waters were not significantly different (Student's t-test, $p=0.46$, $p=0.10$, respectively). ^{224}Ra in surface water was lower at the mouth than bulk YRE water (Students t-test, $p<0.001$), suggesting again that these surface water samples collected at the mouth during summer months are representative of the Chesapeake Bay. Differences in isotope half-life are likely why differences between the York and its mouth are observed between with the ^{224}Ra isotope but not ^{223}Ra and ^{226}Ra. ^{223}Ra and ^{226}Ra are longer-lived than ^{224}Ra, so discharge in to the Chesapeake Bay carries proportionally more of the longer-lived isotopes than ^{224}Ra.

Non-conservative addition of ^{223}Ra, ^{224}Ra, and ^{226}Ra was observed during both summer and winter across the YRE (**Figure 3**). The ratio of Ra entering the YRE at WP relative to YRE surface water was highest for ^{226}Ra. Although the majority of ^{226}Ra is particle bound rather than dissolved in fresh waters, the long residence time of aquifers allows more time for ingrowth of the long-lived ^{226}Ra. A substantial portion of fresh water river flow is derived from terrestrial groundwater drainage, carrying ^{226}Ra-enriched water. The activity of ^{226}Ra should be (and was) highest during dry periods (e.g., summer) when the largest fraction of tributary input is derived from terrestrial aquifers.

High ^{226}Ra measured at WP is likely influenced by the RockTenn pulp and paper processing plant located in West Point, where $6x10^4$ m^3 of deep groundwater is withdrawn for processing daily from the multiple aquifers, including the Potomac (44

dpm/100L; USGS, 2010) (VaDEQ, 2012). No measurements of short-lived Ra isotopes have been made in the Potomac aquifer but their activity is likely low due to the low salinity of the Potomac aquifer and their rapid removal via decay. After use, this Potomac-derived processing water is discharged to Pamunkey River surface waters, likely still enriched in ^{226}Ra (USGS, 2010). The processing water therefore provides negligible quantities of the short-lived Ra isotope but provides approximately $2.6x10^7$ dpm/d of ^{226}Ra. However, this ^{226}Ra from processing water makes up only about 5% of the tributary input (measured at WP) and is likely included in the WP surface water samples. Therefore, this input is not counted separately for ^{226}Ra.

3.3. Taskinas Creek time-series

Surface water ^{224}Ra activities were lowest in the tidal marsh creek during the flood tide and remained low just past high tide, representing Ra-poor YRE surface water entering Taskinas Creek (**Table 2**). The lowest ^{224}Ra activities (55-62 dpm/100 L) were coincident with the highest salinities (salinity 16-17) and water fluxes into Taskinas Creek. The highest ^{224}Ra activities (80 dpm/100 L) were observed midway between high and low tide, indicating Ra input from tidal flushing of the marsh. In subsequent samples collected during the ebb tide, ^{224}Ra activity in Taskinas Creek remained elevated over flood tide activities (>70 vs. <60 dpm/100 L) (Student's t-test, $p<0.001$). ^{223}Ra was correlated with ^{224}Ra, and although the same clear trend with salinity and tidal height was not observed (Student's t-test, $p=0.29$), its enrichment through channelized flow through marsh sediments was likely driven by the same controls. However, enrichment of ^{223}Ra but may occur on a smaller scale due to slower rate of regeneration (a function of half-

life). Although the behavior of ^{223}Ra was not as clear as ^{224}Ra, marsh inputs of ^{223}Ra were treated using the same calculations. Radium tidal marsh (F_{marsh}) inputs to the Taskinas Creek were calculated as the product of the net water flux and the difference in radium activity between flood tide and ebb tide (C_{enrich}), and normalized to the known tidal marsh area of Taskinas Creek (Moore, 1980) (**Equation 2**).

$$F_{marsh} = F_{in} * C_{enrich} * A_{Taskinas}^{-1} \quad (2)$$

3.4. Diffusive input of Ra from sediments

The flux of Ra from diffusion over time was estimated in waters overlying undisturbed sediment cores. From coarse sediment, the diffusive flux of ^{223}Ra and ^{224}Ra from coarse sediment was 0.9 and 23 dpm m^{-2} d^{-1}, respectively. The ^{223}Ra and ^{224}Ra flux from fine sediment was 0.7 and 26 dpm m^{-2} d^{-1}, respectively (**Figure 4**). The diffusive flux rates are similar in both fine and coarse-grain sediments and are applied to their respective percent coverage of YRE bottom sediments (Nichols et al., 1991).

3.5. Ra input from suspended sediments

Ra was desorbed by suspending fine-grain sediments in brackish YRE waters and was strongly correlated with the mass of sediment added ($R^2 > 0.8$). The Ra release rate from fine-grain sediments was 0.18±0.03 and 1.6±0.3 dpm/g for ^{223}Ra and ^{224}Ra, respectively. Desorbed Ra activity from coarse-grain sediments was not correlated with the sediment mass added ($R^2 < 0.05$). Coarse-grain sediments have lower surface area than fine-grain sediment so the desorption rate for these may have been too small to detect.

3.6. Pore water (groundwater) dissolved Ra

Pore water samples from the YRE (n=150) were collected and analyzed for the short-lived Ra isotopes and a subset of these were analyzed for ^{226}Ra (**Table 3**). During summer, pore water Ra (^{223}Ra = 24.3±24.7, ^{224}Ra = 396±320, ^{226}Ra = 129±105 dpm/100L) was significantly higher (Student's t-test, $p<0.05$) than pore water Ra during winter (^{223}Ra = 9.7±8.7, ^{224}Ra = 133±94, ^{226}Ra = 72±31 dpm/100L). The lowest pore water Ra activity (^{223}Ra = 1.9, ^{224}Ra = 0.7 dpm/100L) corresponded with low salinity (0.17). Pore water Ra activity correlated with salinity for all isotopes. ^{226}Ra was most strongly correlated ($R^2 = 0.34$) while ^{223}Ra had the weakest correlation with salinity ($R^2 = 0.23$) and ^{224}Ra fell between the two ($R^2=0.32$). Individual ^{223}Ra and ^{224}Ra activities that clearly deviated from the bulk sample pool had a pH more than two standard deviations below the mean pore water pH (5.4 and 4.4 vs. 6.88±0.54). Pore water pH is known to affect radium availability, increasing desorption with decreasing pH (Szabo et al., 2012). Pore water samples collected where the pH was above 7 had significantly lower ^{223}Ra and ^{224}Ra activity ($p<0.01$). However, these pH values fell within two standard deviations from the mean and were therefore included in the regression calculations.

4. Discussion

The YRE Ra budget was determined using a simple box model approach adapted from Beck et al. (2007). The YRE was defined from West Point (WP) to the mouth of the York upriver of Guinea Marsh (GM) and Goodwin Island (GI) (**Figure 1**). The mass balance of Ra in the YRE is given by **Equation 3**,

$$J_{inlet} + J_{decay} = J_{trib} + J_{diff} + J_{marsh} + J_{desorb} + J_{SGD} \quad (3)$$

where sinks of Ra are on the left-hand side of the equation and sources are on the right-hand side. J_{inlet} is the net exchange of Ra with the Chesapeake Bay, J_{decay} is the loss of Ra via radioactivity decay, J_{trib} is the flux of Ra to the YRE from the Mattaponi and Pamunkey tributaries, J_{diff} is the diffusive flux of Ra from sediments, J_{marsh} is the Ra flux from tidal flushing of salt marshes, J_{desorb} is the flux of Ra from suspended and resuspended sediments, J_{SGD} is the advective flux of Ra from sediments (SGD), and all fluxes are in activity per unit time. J_{SGD} was calculated by difference after accounting for all other known sources and sinks, as described in the following sections (4.2-4.6), using literature constants in **Table 4**. Ra input via SGD (J_{SGD}) was calculated as a minimum value by maximizing all other Ra input source terms. Because the half-life of ^{226}Ra is very long (1600 y), the diffusive flux, marsh flux, and desorption from resuspended sediment which occur over short time periods were assumed to be negligible and were not included in the mass balance for this isotope (Beck et al., 2007; Porcelli et al., 2008).

4.1. Exchange with Chesapeake Bay

Ra exchange between the YRE and the Chesapeake Bay is a function of surface water Ra activity and the return flow factor. Net loss of Ra from the YRE to the Chesapeake Bay (J_{out}, dpm/d) is calculated using an exponential loss model which considers all exchange terms at the inlet as part of a hydrodynamic model residence time estimate (e.g. tidal prism, estuarine circulation, advective mixing) (Monson et al., 2002). Exponential loss of Ra as a function the residence time (RT) is calculated using **Equation 4**, where

$$C_1 = C_o e^{-1/RT} \quad (4)$$

$$J_{inlet} = V_{YRE} * C_o * 1-(C_1/C_o) \quad (5)$$

where C_o is the Ra enrichment in YRE water relative to that in the Chesapeake Bay, C_1 is the concentration of Ra in surface water remaining in the same quantity of water after one day assuming no inputs, and RT is the residence time of the YRE within the model boundaries (Monson et al., 2002; Shen and Haas, 2004). The percent loss per day ($1-(C_1/C_o)$) is scaled to a loss per volume of YRE using the YRE volume (V_{river}) and calculated using **Equation 5** (Monson et al., 2002).

USGS gaging station data was used to compare water flow rates during sampling to modeled residence times to accurately determine the appropriate residence time (RT) for each sampling period (Shen and Haas, 2004). Average residence time for the model domain was calculated as the volume-weighted mean of the residence time in each of nine sub-units in the model of Shen and Haas (2004). During the summer study period, USGS gaging station water flow rates most closely matched the "low flow" rate (RT= 150 days), while they most closely matched the "mean flow" rate during winter (RT=41 days) (USGS, 2013; Shen and Haas, 2004). Because surface water Ra activity was higher in the YRE than in the Chesapeake Bay, the exchange of all three Ra isotopes with the Bay represented a net loss from the estuary during both summer and winter. A large Ra sink was observed during all seasons by exchange with the Chesapeake Bay (^{223}Ra: $7.0\pm8.0\times10^8$ dpm/d, winter; $2.9\pm3.4\times10^8$ dpm/d, summer; ^{224}Ra $5.4\pm2.3\times10^9$ dpm/d, winter; $2.9\pm6.0\times10^9$ dpm/d, summer ^{226}Ra: $2.2\pm1.4\times10^9$ dpm/d, winter; $1.8\pm4.0\times10^8$ dpm/d, summer) (**Table 5**). The loss of the short-lived Ra isotopes via exchange with the Chesapeake Bay contributed 3-28% of the overall Ra sinks. Because ^{226}Ra is long-lived

relative to the residence time of the YRE, exchange with the Chesapeake Bay was the only significant loss of Ra in the system. Errors associated with each of these inlet exchange fluxes large relative to the calculated values, which are driven by the error on the C_o term, the initial Ra concentration in YRE surface water. The C_o term, which was calculated as a difference between mean YRE surface water dissolved Ra and mean Bay water dissolved Ra. Because the associated errors with each of these terms overlaps for most isotopes and seasons, the propagated error of the difference was driven up significantly.

Previous studies have calculated separate estimates for the input and removal terms (J_{out} and J_{in}) via inlet exchange; for comparison, we calculate a J_{inlet} as the net difference between these. These studies (Beck et al., 2007; Beck et al., 2008; Garcia-Solsona et al., 2008a) calculate the net inlet exchange of Ra from a coastal estuary to an external body of water using the tidal prism. This method of using solely the tidal prism as an exchange vector assumes that any water that enters the estuary over the course of a tidal cycle is fully mixed with the water column, obtains the Ra signature of the estuary, and leaves with this Ra signature. The tidal prism method further assumes that this body of water is advected away from the mouth of the estuary once it reaches the coastal ocean, and new, Ra-deplete water enters. This method neglects processes that return outflow to the estuary, and may be inappropriate for most coastal systems unless the residence time is the same as the ratio of estuary volume to tidal prism and the tidal volume is equally mixed across the length and width of the estuary. Using the tidal prism method to calculate exchange could be improved by constraining the return flow factor (Moore et al., 2006). The exponential loss model employed here may be more appropriate

for most systems because it accounts for the amount of time it takes for the YRE to physically flush over the full length of the estuary. In the current study system, this method also allowed consideration of seasonal variability in residence time.

4.2. Radioactive Decay of Radium

Ra loss via radioactive decay (J_{decay}) was calculated as the product of the mean Ra concentration in surface water (C_{YRE}), York River estuary volume (V_{YRE}), and the decay constant for each individual isotope (λ_{Ra}) (**Equation 6**) (Beck et al., 2007).

$$J_{decay} = V_{YRE} * C_{YRE} * \lambda_{Ra} \quad (6)$$

During the winter, $4.2\pm1.8\times10^{10}$ dpm/d of ^{224}Ra were lost through radioactive decay; during the summer months, overall higher surface water Ra activity led to proportionally higher loss by decay ($8.2\pm1.9\times10^{10}$ dpm/d). The longer-lived ^{223}Ra isotope followed the same seasonal trends, with $1.8\pm1.8\times10^{9}$ dpm/d lost by decay during winter and $2.6\pm0.9\times10^{9}$dpm/d in summer (**Table 5**). Radioactive decay represented the greatest loss term by an order of magnitude for both ^{223}Ra and ^{224}Ra (72-97%).

The amount of dissolved Ra present in surface water at any given point is affected by residence time, which therefore also drives the importance of the decay term in a mass balance of Ra. For example, if a system is supplied with some amount of Ra daily but all of the water is flushed out over the same period of time, the importance of decay decreases as the half-life of the isotope increases. Residence time, therefore, must be considered when making comparisons of decay rates among systems. The importance of inlet exchange calculated using tidal prism exchange may be significantly overestimating inlet exchange and consequentially underestimating the importance of decay. In Venice

Lagoon, residence time was shorter than the half-lives of ^{223}Ra and ^{224}Ra, and exchange at the inlet was not surprisingly the most importance loss for these isotopes because the residence time was shorter than the Ra half-lives (Garcia-Solsona et al., 2008a). In most large systems this is not the case. Previous estimates of Ra loss in estuaries have typically been made in systems with smaller ratios of volume to tidal prism (e.g. Jamaica Bay, 2.8 [Beck et al., 2007]; Great South Bay, 4.8 [Beck et al., 2008]) where rapid flushing is assumed and a greater focus placed on estimates of exchange at the inlet, J_{out} and J_{in} (Garcia-Orellana et al., 2010). These studies argue that >50% of the Ra loss was due to exchange at the inlet (>30% net flux at the inlet). It is clear that when a higher concentration of Ra is present in surface water coincident with long residence times, the importance of decay in short-lived Ra isotope budgets increases.

4.3. Input from tributaries

Combined tributary input from the Mattaponi and Pamunkey was 6.70×10^6 m^3/d during the winter and 6.79×10^5 m^3/d during summer of 2012 (USGS, 2013). The winter discharge from both rivers was higher than the long-term annual mean river flow, while summer river flows were slightly below the long-term annual mean flow for each river (USGS, 2013; Reay, 2009). Combined, 2012 represents a typical seasonal water flow trend where maximum river flow occurs during the winter and minimal flows occur during summer (USGS, 2013). The contribution of Ra via tributaries (J_{trib}) was calculated as the product of tributary volume flux (V_{trib}), a factor of 1.35 to account for ungaged flow (Seitz, 1971), and the mean radium activity in water collected at the confluence of

the Mattaponi and Pamunkey at WP (C_{trib}). The amount of ungaged flow, 1.35 times higher than the gaged flow rates, was selected to maximize possible tributary inputs.

$$J_{trib} = C_{trib} * V_{trib} * 1.35 \quad (7)$$

Tributaries contributed less than 4% of short-lived radium isotope input to the YRE during both the winter and summer of 2012 (**Table 5**). Although higher activities were observed during the summer at WP, tributaries were relatively unimportant in the mass balance because water flow rates were lower during the summer. Despite the fact that the head of the YRE Ra box model was designated at a brackish water interface (up to salinity 13 during summer 2012), this input from the Mattaponi and Pamunkey tributaries was still relatively unimportant; suggesting that if only fresh tributary inputs were considered calculated fresh water fluxes would be even lower. However, input of ^{226}Ra from tributaries was comparable to the input from SGD during winter (22%) and contributed 35% of radium input during the summer. Tributaries are likely a significant source of ^{226}Ra because fresh aquifers with long residence times are sources of substantial quantities of dissolved Ra in base flow, which is higher during summer than winter as was observed.

4.4. Input from tidal marshes

Peak Ra activity in the tidal marsh creek (^{223}Ra = 7, ^{224}Ra = 80 dpm/100L) occurred midway between high tide and low tide, as the tidal creek drained the surrounding marsh. This suggests tidal flushing of the marsh creek was a source of Ra to the Taskinas Creek and the YRE. The areal input of Ra from the Taskinas Creek tidal marsh ($3.5x10^5$ m^2) (F_{marsh}) was calculated in **Equation 2,** and scaled to the total tidal

marsh area in the YRE ($2.2x10^7$ m^2; Moore, 1976; Doumlele, 1976; Moore, 1980; Priest et al., 1987) (**Equation 8)**. This estimate of total tidal marsh area in the YRE includes salt, brackish, and fresh tidal marshes, maximizing this estimate.

$$J_{marsh} = A_{marsh} * F_{marsh} \quad (8)$$

The input of Ra from marsh creeks during the summer was $4\pm2x10^7$ dpm/d and $8\pm3x10^8$ dpm/d for ^{223}Ra and ^{224}Ra, respectively. The maximum Ra activity in the Taskinas was observed during ebb tide when salinity was slightly lower than the minimum Ra activity during flood tide (16.1 vs. 14.6, respectively). Therefore, the estimate of Ra input from marsh creeks potentially includes some amount of Ra from fresh creek water, and represents a maximum estimate of input from marshes. This estimate made during summer was also used for the marsh creek radium source during winter. Marsh creeks comprised a maximum of 2% of the radium input to the YRE during winter and summer.

Per square meter, the input of Ra from marsh creeks to the YRE was 1.6±0.8 dpm/d for ^{223}Ra and 37±12 dpm/d ^{224}Ra. Marshes represent a larger component of the budget for ^{223}Ra (16-17%) than ^{224}Ra (3-5%) in the YRE. This may be due to the large variability in ^{223}Ra measurements at low activities- there is not a clear trend between high and low tide as observed for ^{224}Ra. Fluxes of Ra from the YRE marshes are lower than those measured in Jamaica Bay (11.2 and 176 dpm/m^2/d for ^{223}Ra and ^{224}Ra, respectively). This may be due to higher salinities in Jamaica Bay marshes relative to York River estuary tidal marshes, which may desorb higher quantities of Ra. Marshes comprised less than 5% of the total Ra source for both short-lived isotopes in Jamaica

Bay, NY, which has little fresh water input, and was not considered a source in Great South Bay, NY (Beck et al., 2007; Beck et al., 2008).

4.5. Diffusive Flux

The diffusive flux of Ra from sediment cores was calculated as the flux per sediment surface area (**Equation 1**). The diffusive flux of Ra from fine sediments (F_{diff}) to the YRE was $1.5\pm0.4x10^8$ dpm/d and $4.7\pm1.2x10^9$ dpm/d for ^{223}Ra and ^{224}Ra, respectively, by using the total area of fine sediment in the YRE and solving for J_{diff} (**Equation 9**). Some scatter was observed among the data, which can be attributed to errors in sample collection such resuspension of sediments while adding and removing overlying waters. Diffusive flux rates measured in the YRE (^{223}Ra, 0.7-0.9; ^{224}Ra, 23-26 dpm/m^2/d) were similar to those measured elsewhere (^{223}Ra 1.68-3; ^{224}Ra 30-52.8 dpm/m^2/d) (Bird et al., 1999; Beck et al., 2007; Beck et al., 2008). The relative importance of diffusion to the Ra budget in the YRE (5-10%) is comparable to its importance in other systems (<1-8%; Beck et al., 2007; Beck et al., 2008).

$$F_{diff} = J_{diff} * A_{sed} \quad (9)$$

4.6. Ra input from resuspended sediments

Suspended sediment concentration is highly variable within the YRE, and maximum suspended sediment concentration near the sediment-water interface can reach 1 g/L during peak flow (Friedrichs et al., 2000). During repeated surveys in 1996-1998 bottom water TSS ranged from <25 mg/L at the lower and upper reaches of the YRE, to >300 mg/L at the primary and secondary estuary turbidity maxima (ETM; Lin and Kuo,

2001). During the same time span, surface water TSS ranged from <25 mg/L to >75 mg/L at the ETM (Lin and Kuo, 2001). Long-term means of TSS by salinity zone (e.g. oligohaline, mesohaline) of the YRE (Ches. Bay Program, as reported in Reay, 2009) were averaged to determine a mean TSS concentration of 44 mg/L. This concentration is similar to the range reported previously (Lin and Kuo, 2001; Friedrichs et al., 2000; Friedrichs et al., 2009). To maximize desorbable input from resuspended sediment, a TSS value overestimation was selected to be 100mg/L.

The input of radium by desorption from resuspended sediments was estimated using **Equation 10**,

$$J_{desorb} = S_{sed} * V_{YRE} * C_{sed} \quad (10)$$

where S_{sed} is the concentration of suspended sediments, V_{YRE} is the volume of the YRE, and C_{sed} is the activity of radium available for release from a given mass of suspended sediment. The experiment employed in the current work to evaluate Ra release from sediments used shallow fine sediments where Ra was likely at equilibrium with parent Th (i.e., $A_{Ra} = A_{Th}$). Therefore, the experimental results reflect the maximum potential particulate Ra, which is an unrealistic source because this quantity is not regenerated daily. A more accurate estimate of Ra input from suspended sediments is that produced daily from Th decay, which is given by **Equation 11**.

$$C_{sed} = \lambda_{Ra} * A_{Th} * (1-e^{-\lambda_{Th} t}) \quad (11)$$

Results from the desorption experiment indicate release of 0.18±0.03 and 1.6±0.29 dpm/g fine-grain sediment for ^{223}Ra and ^{224}Ra, respectively. No measureable release of Ra correlated with sediment added was observed from coarse-grained sediment (**Figure 5**). Because of these low desorption rates from coarse-grained sediments and the

fact that >80% of suspended sediment is fine (Lin and Kuo, 2001), desorption of Ra from suspended sediments was calculated using only the desorption rate from fine-grained sediments.

Previous estimates of Ra desorption from suspended sediments evaluated effects of exposing fresh water sediments to saline waters (Moore, 1981; Webster, 1995). In the current model, Ra desorption from riverine sediments at the head of the estuary are included in the tributary Ra flux because water at the upstream boundary of the model (WP) is saline (>2.3). Resuspended sediments in the YRE produced $5.6\pm3.6\times10^{6}$ and $4.5\pm2.8\times10^{8}$ dpm/d ^{223}Ra and ^{224}Ra, respectively. Suspended particulate matter accounted for less than 1% of the Ra input to the YRE, consistent with estimates from other systems (Beck et al., 2008, Garcia-Solsona et al., 2008a; Garcia-Orellana et al., 2010). In systems with high suspended sediment concentration, e.g. where small mountainous rivers carry heavy sediment loads (Milliman and Syvitski, 1992), desorption may be much more important.

4.7 Submarine groundwater discharge

By accounting for all known sources and sinks of Ra using **Equation 3**, the Ra budget in the YRE is not balanced. The sinks of Ra in the YRE are much lower than the measured sources. This source of unaccounted Ra during winter provides $2.2\pm2.0\times10^{9}$ (^{223}Ra), $4.0\pm1.9\times10^{10}$ (^{224}Ra), and $1.8\pm1.4\times10^{9}$ dpm/d (^{226}Ra) and during summer provided $2.7\pm1.0\times10^{9}$ (^{223}Ra), $7.9\pm1.9\times10^{10}$ (^{224}Ra), $5.5\pm4.1\times10^{8}$ dpm/d. Presumably, the source of this Ra is submarine groundwater discharge (Rama and Moore, 1996; Hussain et al., 1999; Krest et al., 2000; Kelly and Moran, 2002; Moore, 2003; Beck et al., 2007;

Beck et al., 2008). Saline submarine groundwater discharge desorbs Ra from sediment, enriching pore water with Ra that can then be advected in to surface waters. For all isotopes and during both seasons SGD was the most important source of Ra to the YRE, contributing 65-93% of total inputs.

The volume flux of submarine groundwater discharge (F_{SGD}) can be calculated by dividing the excess Ra flux (J_{SGD}) by pore water Ra activity (C_{GW}) (**Equation 12**)

$$F_{SGD} = J_{SGD} * C_{GW}^{-1} \quad (12)$$

While the flux imbalance of Ra (J_{SGD}) was determined through a mass by difference approach, the pore water Ra activity was estimated using direct measurements of pore water Ra across the YRE. An accurate Ra end member concentration is critical for calculating SGD volume flux. Pore water Ra measured at <1m to 8m and from nearly fresh groundwater to surface water salinities have been used as pore water end members, with the presumption that the statistical mean or median adequately represents the SGD end member and that no significant changes occur in sediments near the sediment-water interface (Charette and Buesseler, 2004; Beck et al., 2007; Beck et al., 2008; Garcia-Solsona et al., 2008a). These estimates made at depth do not account for the changes in radium behavior (e.g. sorption) between what is measured tens to hundreds of centimeters below the sediment-water interface and what is actually discharged. "SGD" comprises a combination of flow mechanisms that operate on widely varying time and length scales (e.g., Moore, 2010; Santos et al., 2011), and geochemical tracers can only reflect the SGD components that transport the tracer (King et al., 2009; King, 2012).

In the YRE, each Ra isotope behaved conservatively with respect to salinity (**Figure 6**). Scatter among the data may represent variability in sediment pH or flushing

rates between sites. The scatter could also be attributed to different sediment types desorbing variable quantities of Ra, but this is unlikely (Beck and Cochran, 2013). Ra measured in seepage meters in the YRE is lower than pore water Ra (^{223}Ra 4-16, ^{224}Ra 60-230 dpm/100L; GP site, Kellum et al., in progress), falling along a mixing curve of pore water Ra at high salinity with surface water at similar salinity. As Ra undergoes further desorption as salinities in the top few centimeters of sediment as pore water salinity approaches bottom water salinity, it can be assumed that this Ra desorption rate remains constant. However, flushing at these very shallow depths likely increases relative to deeper sediments, decreasing Ra activities measured at very shallow depths or through seepage meters (**Figure 6**) (Bollinger and Moore, 1984; Bollinger and Moore, 1993). For this reason, the non-conservative relationship between Ra and salinity that occurs in very shallow sediments can be bypassed using the regression of Ra and salinity to estimate large-scale flushing through sediments. Using the Ra activity measured in seepage water or at the sediment water interface addresses rapid flushing occurring on small scales at the sediment-water interface, which may not represent the larger SGD flow mechanisms (Santos et al., 2012) of geochemical concern. To adequately determine the pore water Ra activity representative of non-shallow flushing, the correlation between Ra and salinity was extrapolated to the salinity at the sediment-water interface, which can be approximated as bottom water salinity.

During winter, the range of pore water salinities was <1-10, while during summer pore water salinities ranged from <1 to 19. Ra pore water end member activity was also seasonally variable because Ra activity in pore water was correlated with salinity. ^{224}Ra activity in shallow pore water was significantly lower in the winter than summer at the

same depths (e.g. at 50cm, Student's t-test, p=0.002 for ^{224}Ra). The mean Ra activity in pore water was estimated using the observed Ra-salinity relationship in pore water and calculated for winter and summer using the volume weighted bottom water salinity mean for the entire YRE (**Figure 6**). The mean salinity of discharge was estimated using long-term bottom water salinities in the YRE during for winter and summer from 1995-2008 (Jian Shen, personal communication). Mean volume-averaged bottom water salinities during winter were 13.8 and 17.4 during summer. The pore water end member activities (C_{GW}) were therefore calculated using the regression of Ra and salinity to be 28±7 (^{223}Ra), 490±90 (^{224}Ra) and 116±32 dpm/100L (^{226}Ra) during winter. During summer, the pore water end members were higher, at 35±8 (^{223}Ra), 570±105 (^{224}Ra), and 132±36 dpm/100L (^{226}Ra).

By using **Equation 12**, SGD estimates ranged from 6±4 to 120±61 L/m^2/d (**Table 6**). Other Ra sources in the budget represent maximum estimates, so the relative contribution of SGD to the radium mass balance of the YRE is likely higher than calculated. SGD fluxes vary depending on the Ra isotope used to make the estimate. The rate of desorption is known to be rapid (Aaron Beck, personal communication) and is likely very similar across isotopes, with differences only due to slight kinetic differences between isotopes. However, because each Ra isotope is regenerated at a different rate as a function of half-life, each isotope is produced at a different rate. This hypothesis is supported by measurements made in coastal South Carolina where the isotope-specific Ra supply from a coastal marsh was measured (Bollinger and Moore, 1984). Here, it was found that flushing of the upper 25cm of ^{228}Ra was required to adequately supply the marsh while the upper 5cm supplied three times as much ^{224}Ra as needed (Bollinger and

Moore, 1984; Bollinger and Moore, 1993). This difference in isotope regeneration rate is likely driving the differences in SGD flux rates observed across isotopes. This suggests that each isotope provides a flux estimate representing a different flow mechanism or combination of mechanisms (Santos et al., 2012). For example, because the variability of ^{226}Ra across pore water salinities does not vary much relative to the variability of ^{224}Ra, this suggests that the long-lived isotope-derived flux is representative of longer or larger term flow mechanisms, during which time the ^{226}Ra isotope is able to sufficiently be regenerated. ^{226}Ra may also be able to be used as a tracer of fresh groundwater input of SGD, indicated by its enrichment in nearly fresh pore waters. However, the time scales of ^{226}Ra regeneration and STE flushing must be better understood to accurately develop this.

^{226}Ra-derived flux rates (6-20 L/m^2/d) are similar to flux estimates made in the Elizabeth River using long-lived Ra isotopes (19-23 L/m^2/d; Charette and Buesseler, 2004) (**Table 7**). Estimates made using ^{223}Ra and ^{224}Ra account for shallower flushing (or flushing occurring on shorter time scales) than ^{226}Ra and are nearly an order of magnitude larger than estimates made by ^{226}Ra in both the Elizabeth River and the YRE (Charette and Buesseler, 2004). In a study at Cherrystone Inlet (Eastern Shore, VA) seepage meters were used to estimate maximum hourly submarine groundwater discharge rates (scaled to 0.4-80 L/m^2/d) (Reay et al., 1992). These rates may be lower than short-lived ^{223}Ra and ^{224}Ra estimates because seepage meters cut off some amount of shallow flushing that occurs near the surface of the sediment by design (Burnett et al., 2006 and sources therein). In a study using ^{222}Rn as a tracer of SGD, estimates of Chesapeake Bay SGD were 1.7x10^7 m^3/d, which translates to less than 3 L/m^2/d depending on the Chesapeake

Bay estimate (Hussain et al., 1999). This estimate of SGD is likely low as well because ^{222}Rn also likely does not account for very shallow flushing (King et al., 2009).

Across seasons, SGD fluxes made by the short-lived Ra isotopes were similar. SGD fluxes made using a hydrodynamic model detected a slight difference between seasons, but more importantly a strong seasonal change in SGD composition was observed (Gonneea et al., 2013). SGD estimates made using ^{226}Ra vary seasonally, which may indicate (summer, 6±4 $L/m^2/d$; winter, 20±17 $L/m^2/d$) differences in fresh water input. Because ^{226}Ra is regenerated slowly, this may suggest that supplied ^{226}Ra mostly originated in fresh groundwater that has a long residence time relative to the subterranean estuary. Therefore, higher ^{226}Ra input during winter suggests that the portion of SGD derived from terrestrial groundwater was higher during winter than summer. Recent work has suggested that SGD composition (e.g., salinity) varies seasonally, and these findings support this argument (Gonneea et al., 2013). Strong seasonal changes in pore water salinity are observed in the YRE (**Figure 2**), indicating a variable pore water end-member and consequentially seasonally variable SGD composition. There may be a seasonal difference in SGD water fluxes, but the error propagated through the extensive Ra mass balance process reduces the ability of this method to detect small seasonal differences. A seasonal difference in SGD fluxes was observed in the Pettaquamscutt estuary (Kelly and Moran, 2002); however, the results of this study suggest that their conclusion is an artifact of sampling design. In the Pettaquamscutt estuary (Kelly and Moran, 2002), surface water samples were collected monthly but pore water samples were only sampled in August. Surface water salinity in the Pettaquamscutt estuary (volume-weighted average) during winter was lower than during summer (10-20 vs. 15-25, respectively)

(Kelly and Moran, 2002). It is therefore highly likely that the pore water end member salinity and consequentially Ra activity are also lower during winter than summer in the Pettaquamscutt Estuary. The seasonal cycle observed in their study suggested the lowest SGD flux during winter. By not sampling the pore water end member during each season, this study overestimates the pore water end member Ra during winter, causing SGD during winter (and likely during spring and fall) to be underestimated (Kelly and Moran, 2002). It is clear that measuring both the surface water and pore water end member at the same time is needed for accurate SGD estimates.

4.8 Hydraulic head as a function of water table height and sea level

The pressure of land-derived drainage (hydraulic head) can alter pore water Ra availability due to changes in salinity. Between January 2012 and March 2013, gaging of the Pamunkey and Mattaponi Rivers showed a typical seasonal water cycle (**Figure 7**) with low discharge during the summer and high discharge during the winter. Compared to previous years, the monthly discharge rates to the Mattaponi and Pamunkey were slightly lower than the long-term average. Shallow groundwater height was measured in a nearby well monitored by the USGS located in Suffolk, Virginia (USGS, 2013: VA 58B-13) (**Figure 7**). Seasonal trends of recharge to the shallow unconfined aquifer at this site also followed a somewhat seasonal cycle of higher groundwater levels of recharge from January through March 2012, followed by depletion during summer and recharge from November 2012 to March 2013. River discharge of the Mattaponi and Pamunkey tributaries and water table height in Suffolk, VA suggest that water table height near the YRE would have been highest during the late winter and lowest during the summer.

YRE surface height corrected for astronomical tides was measured at the Yorktown USCG Training Center (NOAA, 2013) and varied by 0.29m during the study period (January 2012 – March 2013). Sea surface height was lowest in January of 2012 (0.33m above MLLW), remained high from June to November (>0.5m above MLLW), and returned to low levels in January 2013 **(Figure 7).** Increasing sea level increases saline intrusion to the coastal aquifer (Gonneea et al., 2013), resulting in a seawater-dominated subterranean estuary. Under these conditions, Ra activity increases in pore water as salinity increases and which is then discharged to surface waters causing high Ra activities in surface waters as well when sea level is high. Ra in surface water was significantly higher during summer than winter ($p<0.05$ for all isotopes). This observation supports the hypothesis that sea higher pore water salinity drove higher Ra in fluxes, but does not exclude the possibility that higher SGD rates occurred during summer. However, because a difference in SGD rates was not detected via the Ra mass balance but a difference in end members was, it is more likely that more Ra is released due to high pore water end member salinity when sea level is high rather than a large seasonal SGD water flux.

The cycles of sea level height and water table height occur on seasonal time scales. During summer, these oceanic and terrestrial forces controlling SGD have a similar directional affect on the Ra behavior in pore water and in surface water. When sea level is higher, this decreases the hydraulic head difference between the water table and sea level, and ultimately decrease the influence of terrestrial water during times when sea level are high (Gonneea et al., 2013). Similarly, when water table height is low during summer, this allows for increased saline intrusion in pore water regardless of sea surface

height variability. These competing controls have also been hypothesized by Charette (2007) but not directly tested. Winter pore water salinities were lower than during summer, indicating a stronger terrestrial force when sea surface height was low and sea surface was high. Ra in surface water and pore water are therefore affected by sea surface height and water table height, but which is the stronger control could not be separated in the YRE due to their seasonal overlap. Several other controls on SGD other than sea level and water table height (e.g., storms, waves, buoyancy) were not investigated as potential seasonal factors, but may be important (Moore, 2010).

5. Conclusions

In the YRE, a major source of Ra that could only be satisfied by SGD was determined using a Ra mass balance. Pore water was enriched in Ra relative to surface water and behaved conservatively with respect to salinity. As salinity in surface and pore water varied with respect to sea level and hydraulic head (as first demonstrated by Gonneea et al., 2013), Ra activity observed in pore water and surface water varied. SGD estimates made by season were similar, suggesting that Ra fluxes are driven by seasonality in the pore water end member rather than SGD volume.

As estimated by Ra, up to 120 $L/m^2/d$ of SGD are cycled through the YRE. Short-lived Ra isotopes are regenerated more rapidly than long-lived Ra isotopes, indicating that short-lived Ra isotopes are best able to account for a variety of different and small-scale flow paths including shallow flushing. This hypothesis is supported by the range of SGD flux rates calculated by isotope which negatively correlate with isotope half-life and therefore regeneration rate.

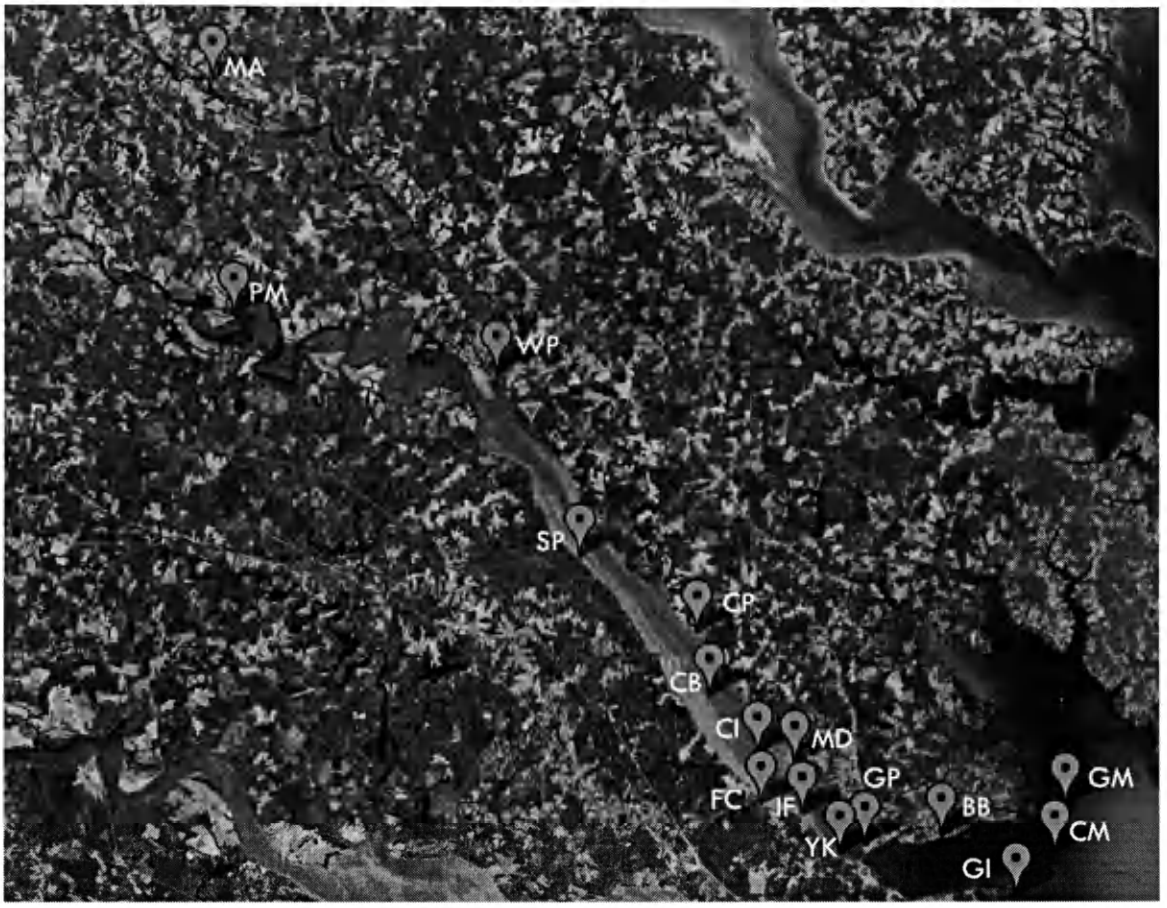

Figure 1. York River estuary [VA] surface water dissolved Ra sampling locations.

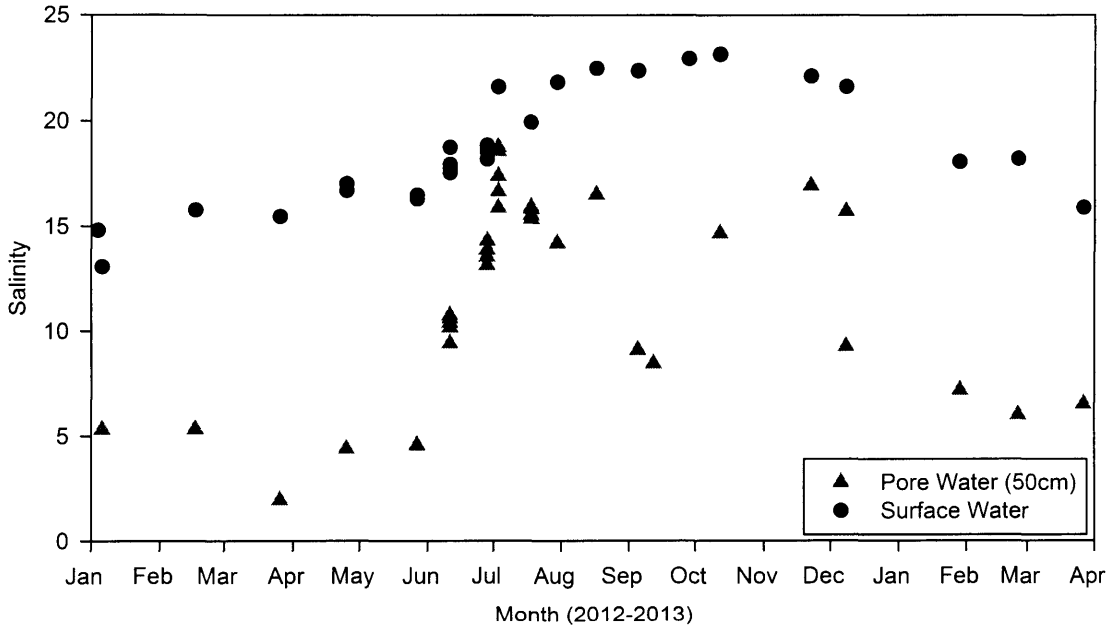

Figure 2. Salinity of surface (black circle) and 50cm pore water (red triangle) at the GP site in the YRE.

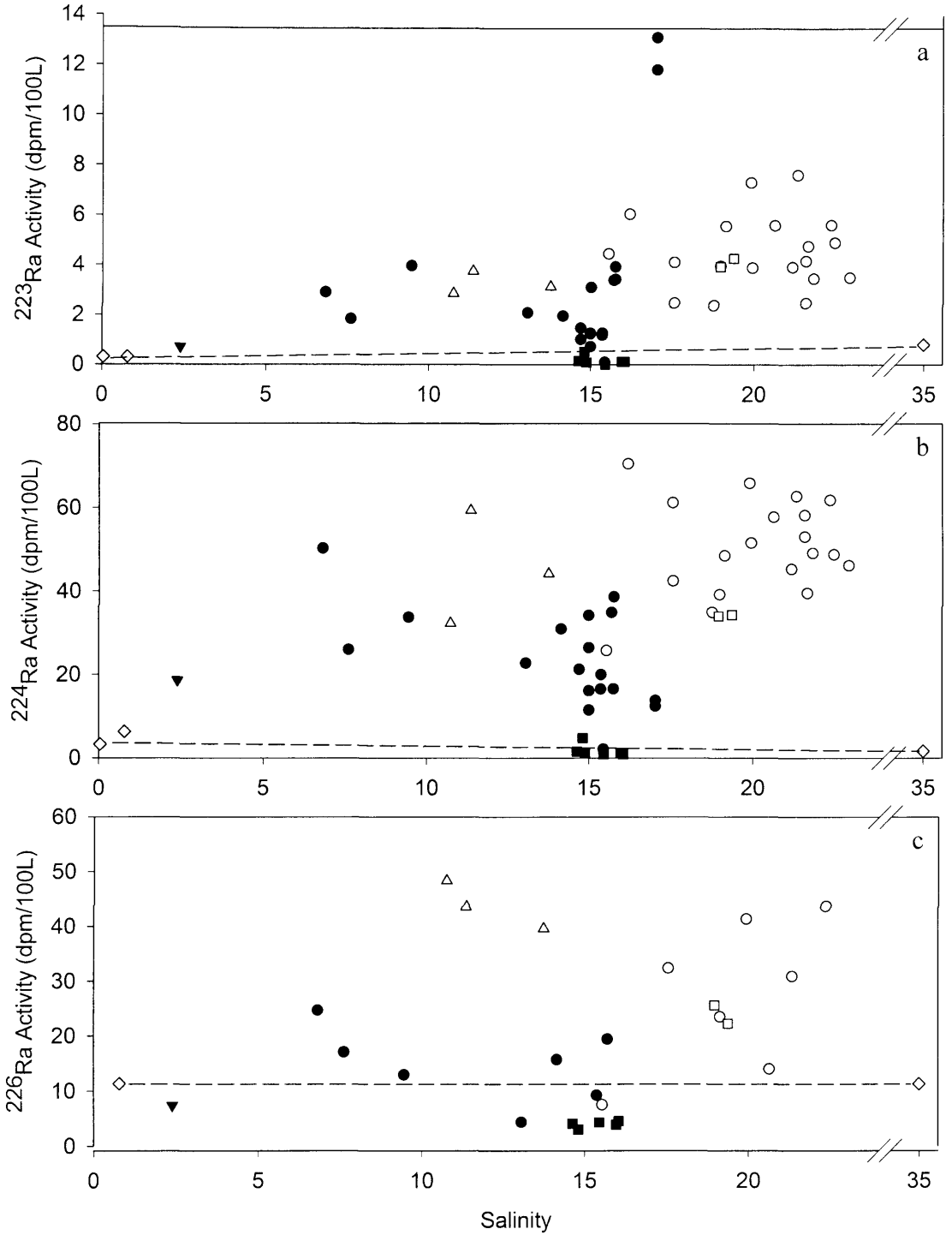

Figure 3. Radium activity in surface waters as a function of salinity a) ^{223}Ra b) ^{224}Ra c) ^{226}Ra. Winter (closed), summer (open), WP, head of box model (triangle), YRE surface waters (circle), YRE mouth-end of box model (square), fresh and ocean (Moore et al., 1998) end members (diamond).

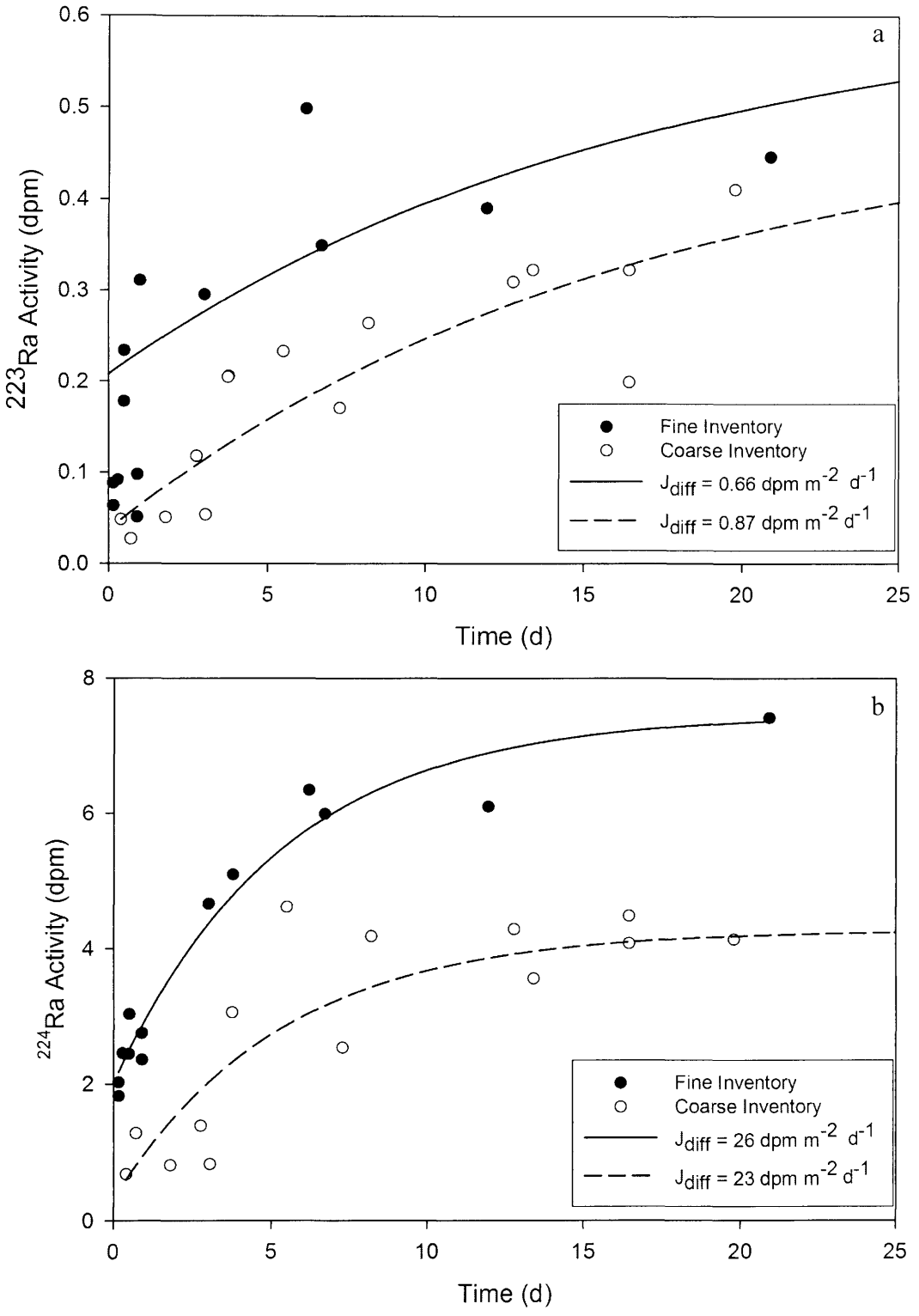

Figure 4. Diffusive flux of Ra from fine and coarse-grain sediments (circles). a) ^{223}Ra b) ^{224}Ra. Curves fitted and the diffusion rate calculated using **Equation 1**.

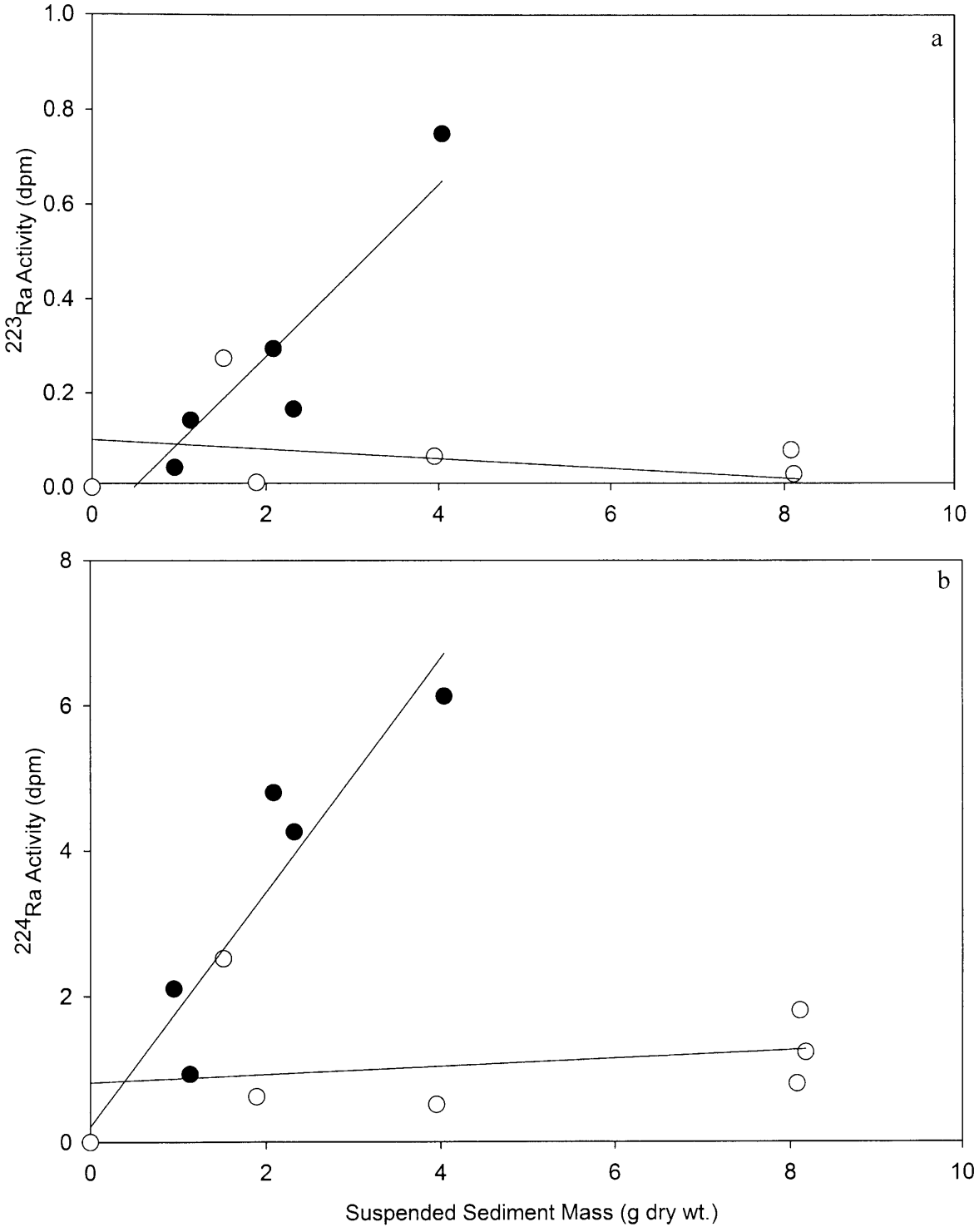

Figure 5. Release of radium from suspended sediment with fine-grain sediments (filled circles) and coarse-grain sediments (open circles) a) ^{223}Ra b) ^{224}Ra.

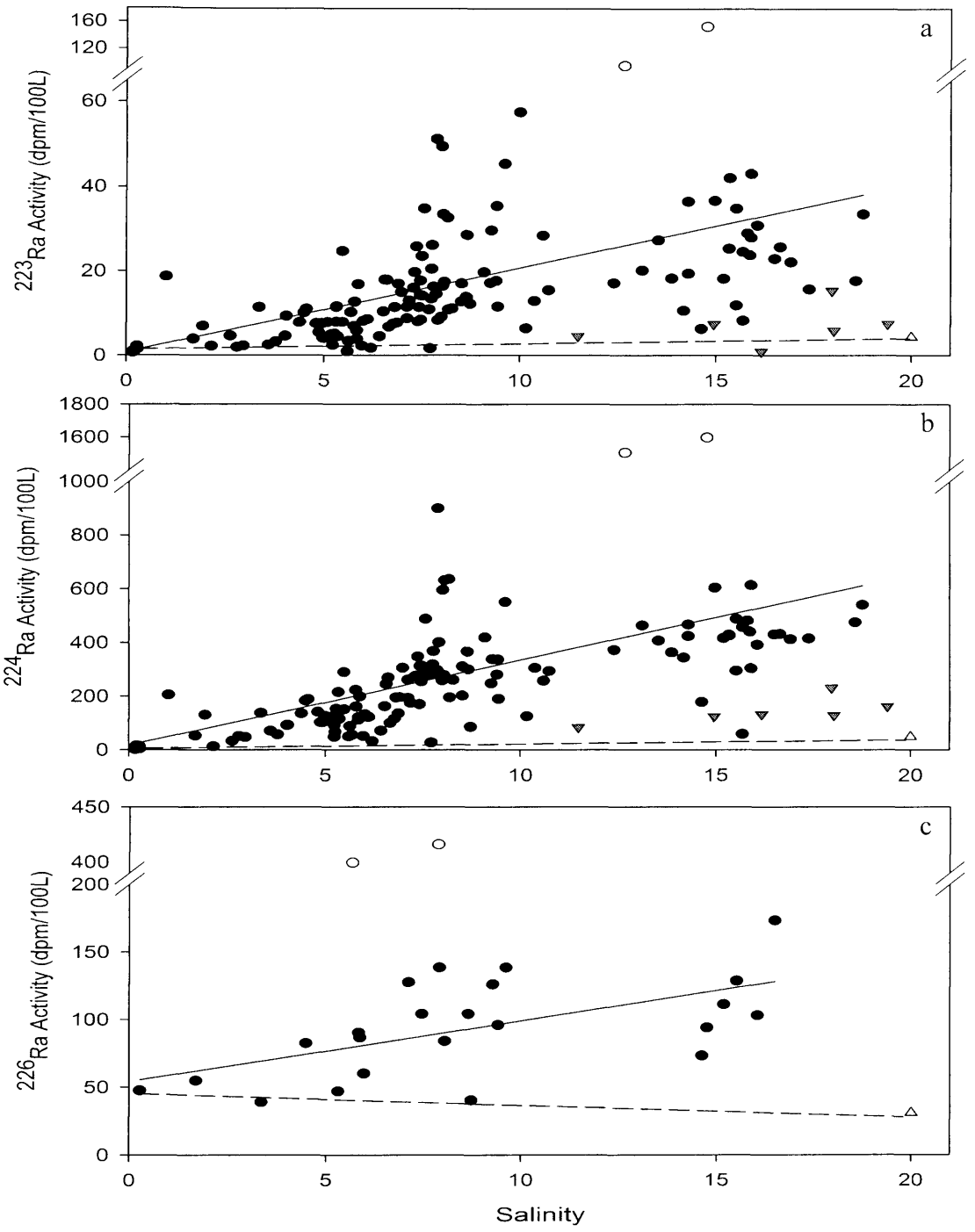

Figure 6. Combined summer and winter pore water radium activity in the YRE. a) ^{223}Ra b) ^{224}Ra c) ^{226}Ra. Solid line represents regression of pore water samples (filled circles) against salinity, dashed line represents conservative mixing between fresh pore water and the ocean end member. Outliers (open circles) were removed from regression. Dark triangles are seepage meter measurements (Kellum et al., in prep.) (dark triangles) and YRE surface water are also shown as open triangles.

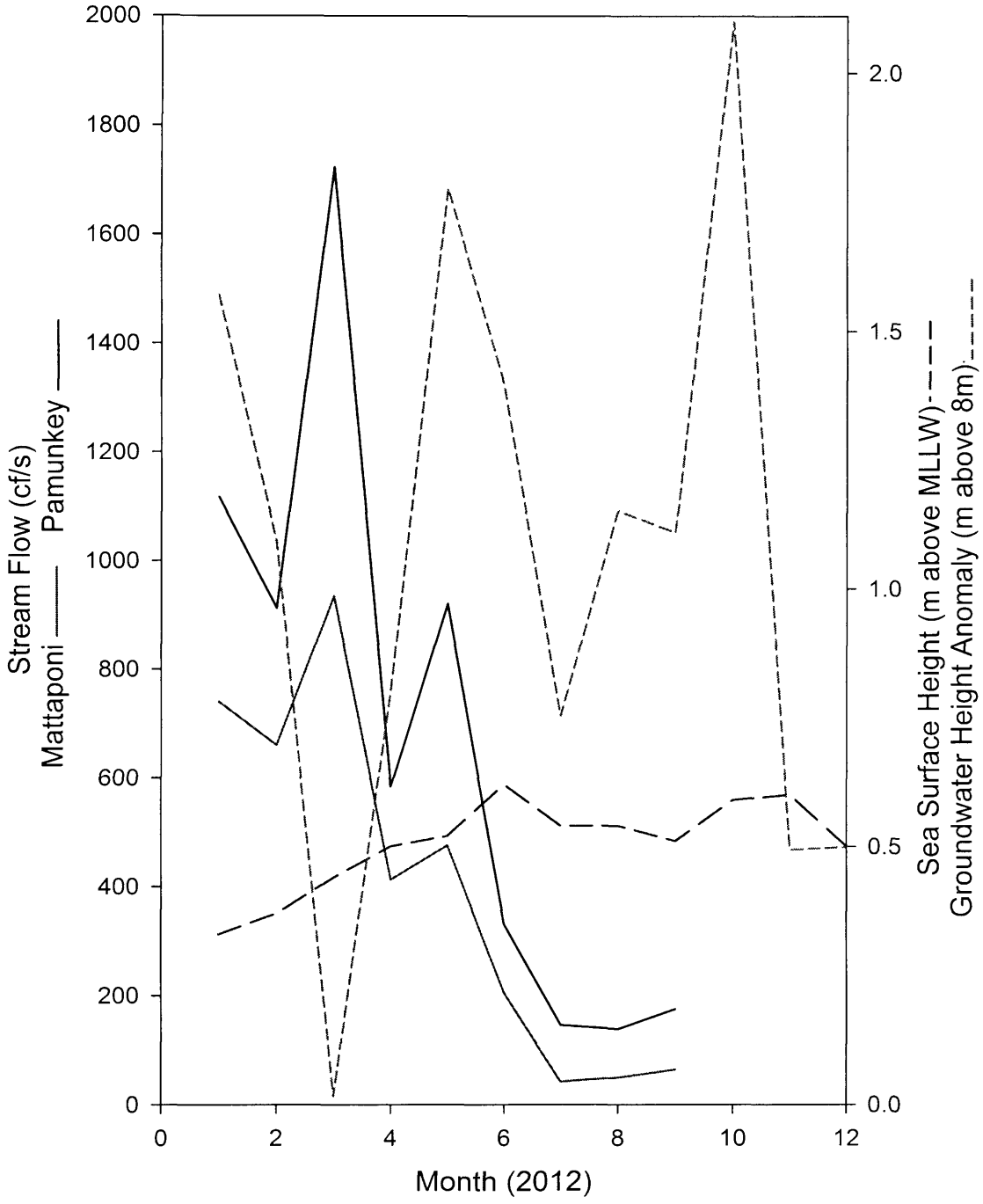

Figure 7. YRE water data for the year 2012 including stream flow from the Mattaponi (red) and Pamunkey (black), water table height in Suffolk VA (pink), and sea surface height (blue).

Table 1. York River estuary surface water sample salinity and radium activity by site and date.

Site	Date	Salinity	^{223}Ra (dpm/100L)	^{224}Ra (dpm/100L)	^{226}Ra (dpm/100L)
GP	01/06/12	14.80	0.98	13.80	
GP	01/06/12	13.06	2.08	22.77	4.37
CB	01/20/12	14.70	1.24	21.23	
CI	02/08/12	15.36	1.18	16.50	
GI	02/08/12	14.81	0.51	4.76	
GM	02/08/12	14.88	0.08	1.22	4.56
BB	02/12/12	17.03	12.48	13.09	
GP	02/17/12	15.75	3.67	27.61	
CI	02/22/12	15.37	1.26	19.97	
GI	02/22/12	15.45	0.00	0.87	4.30
GM	02/22/12	14.63	0.14	1.54	4.06
CB	02/27/12	15.00	2.18	30.32	
SP	03/04/12	7.61	1.83	25.97	17.10
WP	03/04/12	2.39	0.71	18.63	7.40
CM	03/07/12	15.97	0.11	1.01	4.24
SP	03/09/12	6.81	2.90	50.26	24.72
CP	03/19/12	9.45	3.96	33.74	12.98
BB	03/25/12	15.70	3.38	34.88	19.44
IF	03/25/12	14.15	1.95	30.94	15.72
GP	03/26/12	15.44	0.09	2.11	
GP	07/03/12	21.60	3.79	50.31	
CI	07/11/12	18.77	2.37	34.95	9.23
GI	07/11/12	19.37	4.25	34.28	22.28
GM	07/11/12	18.96	3.92	33.97	25.64
YT	07/11/12	19.13	5.55	48.53	23.52
CB	07/12/12	17.56	3.29	51.87	32.40
MD	07/12/12	18.97	3.95	39.20	
GP	07/18/12	19.92	5.59	58.78	41.37
CP	07/19/12	16.19	6.03	70.55	
SP	07/23/12	15.54	4.44	25.76	7.51
WP	07/23/12	11.05	3.30	45.80	45.95
MA	07/24/12	0.04	0.31	3.28	
IF	07/25/12	20.63	5.58	57.82	14.03
GP	07/30/12	21.82	3.45	49.19	
FL	07/31/12	21.33	7.61	62.81	30.92
GP	08/17/12	22.47	4.89	48.87	
CB	08/21/12	21.17	3.91	45.32	
GP	09/05/12	22.36	5.60	61.90	43.69
PM	09/10/12	0.78	0.31	6.32	11.32

WP	09/25/12	13.75	3.12	44.20	39.60
GP	09/28/12	22.93	3.49	46.22	
CI	02/05/13	14.41	1.35	19.18	
CM	02/05/13	19.49	1.48	15.07	
GI	02/05/13	19.56	1.06	12.00	
GM	02/05/13	19.48	0.69	14.73	
WP	02/06/13	5.32	1.42	24.53	
WP	03/02/13	7.97	1.09	34.61	

Table 2. Surface water radium activity, salinity, and tidal height in the Taskinas Creek on 3 August 2012.

Time Midpoint	Salinity	Tidal Height (m)	^{223}Ra dpm/100L	^{224}Ra dpm/100L
8:43	15.68	1.85	2.8	58
9:55	16.18	2.10	6.2	55
11:03	16.99	2.19	2.2	57
12:20	17.47	2.10	3.0	62
13:41	17.28	1.83	2.8	58
14:55	16.48	1.54	7.1	67
16:14	14.57	1.33	2.6	80
17:29	12.54	1.27	4.6	72
18:29	12.36	1.32	2.5	71
19:25	12.63	1.50	3.3	71

Table 3. York River estuary pore water radium activity and water quality parameters by site, date, and depth.

Site	Date	Depth (cm)	Salinity	pH	^{223}Ra (dpm/ 100L)	^{224}Ra (dpm/ 100L)	^{226}Ra (dpm/ 100L)
GP	01/06/12	50	5.31	7.45	11	114	47
GP	01/06/12	100	6.8	6.59	11	195	
GP	01/06/12	150	4.02	6.81	5	92	
GP	01/06/12	210	5.09	6.67	8	123	
GP	01/06/12	300	2.63	7.19	5	33	
GP	01/06/12	400	3.78	7.13	3	57	
GP	02/17/12	50	5.32	7.51	12	215	
GP	02/17/12	100	6.89	6.97	17	196	
GP	02/17/12	150	5.47	7.01	8	151	
GP	02/17/12	200	4.94	6.93	8	104	
SP	03/09/12	25	4.49	6.52	10	183	87
SP	03/09/12	50	5.87	6.31	17	199	83
WP	03/09/12	50	1.69	6.27	4	53	55
CP	03/19/12	25	9.27	6.39	30	338	126
CP	03/19/12	40	9.41	7.47	35	337	96
IF	03/25/12	50	0.27	7.54	2	14	48
IF	03/25/12	100	0.18	7.55	1	12	
IF	03/25/12	150	0.19	7.69	1	14	
IF	03/25/12	200	0.17	7.63	1	2	
GP	03/26/12	50	1.93	7.02	7	131	
GP	03/26/12	100	1	7.29	19	205	
GP	03/26/12	150	9.43	6.47	12	190	
GP	03/26/12	250	5.27	6.71	5	153	
GP	03/26/12	300	3.6	6.76	2	71	
GP	04/25/12	50	4.38	6.83	8	135	
GP	04/25/12	100	8.86	6.80	17	310	
GP	04/25/12	100	4.04	6.76	9	93	
GP	04/25/12	150	7.36	6.70	26	348	
GP	04/25/12	250	5.23	6.70	2	48	
GP	04/25/12	300	6.20	6.70	2	32	
GP	05/27/12	50	4.55	6.67	11	188	
GP	05/27/12	100	9.07	6.79	14	366	
GP	05/27/12	100	5.78	6.73	13	162	
GP	05/27/12	166	7.40	6.82	8	170	
GP	05/27/12	200	6.66	6.89	7	100	
GP	05/27/12	250	5.31	6.87	8	124	

GP	06/11/12	50	10.59	6.93	28	257	
GP	06/11/12	50	9.39	7.07	18	280	
GP	06/11/12	50	10.73	6.84	15	293	
GP	06/11/12	50	10.37	7.04	13	305	
GP	06/11/12	50	10.16	7.07	6	125	
GP	06/11/12	100	7.31	6.82	20	275	
GP	06/11/12	100	7.28	6.71	16	272	
GP	06/11/12	100	6.97	6.87	15	306	
GP	06/11/12	100	7.42	7.26	11	312	
GP	06/11/12	100	7.46	6.90	8	313	
GP	06/28/12	50	14.29		36	467	
GP	06/28/12	50	13.53	6.84	27	407	
GP	06/28/12	50	13.12	6.81	20	464	
GP	06/28/12	50	14.29	6.81	19	424	
GP	06/28/12	50	13.87	6.88	18	363	
GP	06/28/12	100			23	286	
GP	06/28/12	100	7.74	6.87	20	318	
GP	06/28/12	100	7.45	6.45	14	255	
GP	06/28/12	100	7.73	6.85	13	290	
GP	06/28/12	100	7.71	6.8	2	27	
GP	07/03/12	50	18.75	6.60	33	541	
GP	07/03/12	50	16.63	6.60	26	432	
GP	07/03/12	50	15.86	6.87	24	441	
GP	07/03/12	50	18.56	6.62	18	475	
GP	07/03/12	50	17.37	6.57	16	416	
GP	07/03/12	100			18	306	
GP	07/03/12	100	8.51	6.81	17	310	
GP	07/03/12	100	8.02	6.79	16	278	
GP	07/03/12	100	8.63	6.73	14	366	
GP	07/03/12	100	8.5	6.73	13	202	
GP	07/18/12	50	15.89	6.76	43	615	
GP	07/18/12	50	15.34	6.92	42	426	
GP	07/18/12	50	15.52	6.84	35	488	
GP	07/18/12	50	15.8	6.85	29	483	
GP	07/18/12	50	15.33	6.79	25	429	
GP	07/18/12	100	7.56	6.83	35	488	
GP	07/18/12	100	7.76	6.79	26	368	
GP	07/18/12	100	8.06	6.71	17	270	
GP	07/18/12	100	7.79	6.85	16	286	
GP	07/18/12	100	7.85	6.86	15	297	
CP	07/19/12	15	15.19	6.52	18	416	111

CP	07/19/12	20	15.51	6.45	12	295	129
CP	07/19/12	25	16.05	6.6	31	392	103
SP	07/23/12	25	15.68	7.13	8	59	
SP	07/23/12	50	8.72	6.82	12	86	40
SP	07/23/12	75	8.15	6.51	33	636	
SP	07/23/12	200	2.15	7.41	2	13	
IF	07/25/12	50	0.19	8.32	1	15	104
IF	07/25/12	200	0.28	7.75	2	5	
IF	07/25/12	25*	14.97	7.3	37	605	399
IF	07/25/12	25*	8.65	7.28	29	300	
IF	07/25/12	25*	5.68	7.7	10	56	
GP	07/30/12	50	14.17	6.8	11	344	
GP	07/30/12	100	7.5	6.77	23	287	
GP	07/30/12	150	7.9	6.78	8	401	138
GP	07/30/12	200	5.23	6.88	4	92	
GP	07/30/12	250	5.97	6.83	2	51	60
BB	08/01/12	50	14.76	5.44	153	1599	94
BB	08/01/12	50	12.67	4.41	95	1507	
FL	08/09/12	25	3.35	6.94	11	138	39
FL	08/09/12	50	9.61	6.91	45	551	138
FL	08/09/12	100	5.47	6.92	25	289	
FL	08/09/12	150	7.87	6.9	51	900	416
FL	08/09/12	200	10	6.92	58	1211	
GP	08/17/12	50	16.49	6.84	23	431	173
GP	08/17/12	100	7.67	6.92	11	278	
GP	08/17/12	150	7.11	6.76	11	261	128
GP	08/17/12	200	5.84	6.75	6	122	90
GP	09/05/12	25	11.01	6.71			
GP	09/05/12	50	9.08	6.77	20	419	
GP	09/05/12	100	8.26	6.79	11	260	
GP	09/05/12	140	7.46	6.92	18	268	104
GP	09/05/12	190	5.84	6.75	4	112	

BB	09/12/12	10	13.72	6.93			
CP	09/12/12	50	15.42	6.43			
GP	09/12/12	50	8.42	7			
FL	09/19/12	50	16.08	6.79			
IF	09/19/12	50	8.47	7.59			
SP	09/19/12	50	15.46	6.57			
WP	09/25/12	20	8.04	6.29	33	632	84
WP	09/25/12	50	8	6.48	50	596	
GP	10/12/12	40	14.63	6.95	6	178	73
GP	10/12/12	75	6.42	7.07	5	72	
GP	10/12/12	140	7.11	6.81	9	193	
GP	10/12/12	200	5.77	6.83	7	223	
GP	11/22/12	25	17.93	6.44			
GP	11/22/12	50	16.9	6.73	22	413	
GP	11/22/12	90	12.4	7.02	17	373	
GP	11/22/12	130	7.5	6.81	14	277	
GP	11/22/12	200	5.6	6.86	1	50	
GP	12/08/12	25	17.06	6.33			
GP	12/08/12	50	15.68	6.84	24	457	
GP	12/08/12	70	9.24	7.07	17	248	
GP	12/08/12	130	8.17	6.81	11	195	
GP	12/08/12	200	5.63	6.89	3	89	
GP	01/29/13	30	15.89	7.03	28	304	
GP	01/29/13	50	7.17	7.34	13	175	
GP	01/29/13	80	6.76	7.21	7	116	
GP	01/29/13	110	7.98	7.01	9	258	

GP	01/29/13	150	5.25	6.8	4	67	
GP	01/29/13	190	4.88	6.78	5	102	
GP	02/25/13	50	6	7.14	8	133	
GP	02/25/13	75	6.1	6.77	9	123	
GP	02/25/13	110	6.6	6.98	18	269	
GP	02/25/13	155	5.2	6.78	5	119	
GP	02/25/13	200	4.8	6.79	8	141	
GP	02/25/13	310	2.8	7.44	2	51	
GP	03/27/13	50	6.51	7.28	10	162	
GP	03/27/13	75	6.86	7.22	8	136	
GP	03/27/13	110	6.55	7.07	18	245	
GP	03/27/13	155	5.35	6.93	4	114	
GP	03/27/13	200	4.98	6.95	4	127	
GP	03/27/13	310	2.96	7.51	2	47	

Table 4. Physical parameter values used to calculate radium fluxes in the York River estuary.

Term	Parameter	Value	Source
A_{marsh}	YRE tidal marsh area	2.2×10^7 m^2	County Tidal Marsh Inventory*
A_{sed}	Subtidal surface area	1.90×10^8 m^2	Jian Shen, personal communication
$A_{Taskinas}$	Taskinas tidal marsh area	3.5×10^6 m^2	Moore, 1980
C_{enrich}	Taskinas Ra tidal enrichment	5.7×10^5 dpm d^{-1} (^{223}Ra) 1.3×10^7 dpm d^{-1} (^{224}Ra)	Measured
F_T	Taskinas water flux	9.3×10^4 m^{3}d^{-1}	Measured
λ_{Ra}	Decay constant	0.0608 d^{-1} (^{223}Ra) 0.1894 d^{-1} (^{224}Ra) 0.0000012 d^{-1} (^{226}Ra)	
RT	Residence time of the YRE	41 d (winter) 150 d (summer)	Shen and Haas, 2004
S_{sed}	Suspended sediment concentration	100 mg L^{-1}	Lin and Kuo, 2001; Reay, 2009
V_{trib}	Input from tributaries	6.70×10^6 m^3 d^{-1} (winter 2012) 6.79×10^5 m^3 d^{-1} (summer 2012)	USGS, 2013
V_{YRE}	YRE volume	8.65×10^8 m^3	Jian Shen, personal communication

Table 5. Radium fluxes (in 10^8 dpm/d) and *percent contribution* to Ra budget in the York River estuary during summer and winter 2012. Percentages are rounded so may not add to 100%.

	Winter						**Summer**					
	^{223}Ra		^{224}Ra		^{226}Ra		^{223}Ra		^{224}Ra		^{226}Ra	
Sinks of Radium												
Loss to Chesapeake Bay	**7±8**	*28%*	**54±23**	*11%*	**22±14**	*100%*	***2.9±3.4***	*10%*	***29±60***	*3%*	***1.8±4.0***	*100%*
Loss to decay	**18±2**	*72%*	**420±180**	*89%*	-		***26±19***	*90%*	***821±192***	*97%*	-	
Sources of Radium												
Input from tributaries	**0.8±0.2**	*3%*	**19±3.8**	*4%*	**1.9±1.0**	*22%*	***0.2±***	*1%*	***3.1±0.9***	*0%*	***3.0±0.3***	*35%*
Diffusive flux from sediments	**1.5±0.4**	*6%*	**47±12**	*10%*			***1.5±0.4***	*5%*	***47±12***	*5%*		
Input from marsh creeks	**0.4±0.2**	*1%*	**8±3**	*2%*			***0.4±0.2***	*1%*	***8±3***	*1%*		
Desorption from particles	**0.06±0.04**	*2%*	**4.5±2.8**	*1%*			***0.06±0.04***	*3%*	***4.5±2.8***	*1%*		
Input from SGD	**22±20**	*89%*	**400±190**	*84%*	**18±14**	*78%*	**27±10**	*93%*	**790±190**	*93%*	**5.5±4.1**	*65%*

Table 6. Submarine groundwater discharge fluxes as a function of season and radium isotope.

	m^3/d ($x10^6$)	**$L/m^2/d$**
F_{SGD} ^{223}Ra Winter	7.7±7.3	106±99
F_{SGD} ^{224}Ra Winter	8.8±4.4	120±61
F_{SGD} ^{226}Ra Winter	1.5±1.3	20±17
F_{SGD} ^{223}Ra Summer	6.2±2.8	84±37
F_{SGD} ^{224}Ra Summer	7.0±2.2	96±29
F_{SGD} ^{226}Ra Summer	0.4±0.3	6±4

Table 7. SGD estimates in Chesapeake Bay made by various methods.

SGD Study Location	Method	10^6 m^3/d	$L/m^2/d$	Study
York River Estuary	Ra Mass Balance (^{223}Ra, ^{224}Ra, & ^{226}Ra)	0.4-8.8	6-120	This study
Cherrystone Inlet [VA]	Seepage Meters	-	0.4-80	Reay et al., 1992
Chesapeake Bay	^{222}Rn tracer	17.0	1.47	Hussain et al. (1999)
Elizabeth River	$^{226/228}Ra$ mixing model	1.0	18.9	Charette and Buessler (2004)

Control of subterranean estuary geochemistry on groundwater chemical fluxes to the York River estuary, VA (USA)

Abstract

The subterranean estuary is enriched in many metals and nutrients with respect to surface water, acting as a source for some and sink for others. The behavior and distribution of various pore water constituents, including nutrients (DOC, TDN, NH_4, TDP), selected trace metals (Ra, U, Ba, Fe), and PAHs, were investigated in the York River estuary from January 2012-March 2013. The behavior of these constituents varied with respect to salinity and of these, only Ba was positively correlated with salinity and Ra in the subterranean estuary. The regeneration rates of each of the remaining compounds varied with respect to the Ra tracers used to derive submarine groundwater discharge (SGD) fluxes, and again only Ba was regenerated at a similar rate as Ra. Using a ^{224}Ra tracer, Ba fluxes were estimated at 11-12 nmol/m^2/d and therefore provide a large source of Ba to surface waters. Because no positive correlations were drawn between the remaining constituents and salinity or Ra, flux estimates calculated using Ra-derived fluxes and constituent concentrations measured near the sediment-water interface only provide minimum (^{226}Ra) and maximum (^{224}Ra) constituent flux estimates. Findings suggests that in order to accurately determine the flux of many of these compounds, tracers are needed whose behaviors in the subterranean estuary match their own.

1. Introduction:

Submarine groundwater discharge (SGD) to the coastal ocean is controlled by a variety of physical forcing mechanisms that are closely tied to hydrologic changes in terrestrial and oceanic end members (Moore, 1999). Recent work argues that sea level may be a stronger control on SGD than groundwater table height, and each typically varies through the year (Gonneea et al., 2013). The compounds present in shallow pore water and their SGD fluxes can also vary as function of these forces. For example, in the Pamet estuary [MA, US] the presence of nutrients was inversely correlated to salinity over all seasons, suggesting that the source of nutrients is SGD and that its discharge to the coastal ocean is closely related to hydrological factors controlled by climate (Charette, 2007). Other constituents of SGD may be controlled seasonally by the salinity of both surface water and pore water, which can impact the particle reactivity for compounds like radium (Moore et al., 1981). Dissolved organic matter may also be controlled by seasonal changes because the presence of these compounds is influenced by fresh groundwater (Santos et al., 2009). The variability of dissolved organic matter in the Gulf of Mexico is not related to changes in groundwater table height or tidal variability, but rather factors like temperature (impacts uptake rates) and feedback from primary production exhibits seasonality and are thought to influence the fluxes of these SGD constituents over the course the year (Santos et al., 2009). Overall, a variety of physical, hydrological, chemical, and biological forces may play a role in controlling fluxes of SGD and its biogeochemical constituents.

Radium (Ra) is enriched in the subterranean estuary (where fresh and salt water mix in coastal aquifers) and can be used as a tracer of SGD. Ra activity in pore water and

surface water can vary seasonally, and Ra tracers suggest variability in the volume of water and its contents flowing through subterranean estuary (STE) on a seasonal basis (Kelly and Moran, 2002; Loveless et al., 2008; Crotwell and Moore, 2003; Nozaki et al., 2001). In Port Royal Sound [SC, US], no seasonal variability was observed in the fluxes of Ra from the sound to the coastal ocean (Crotwell and Moore, 2003); however, salinity was strongly correlated with Ra activity. In the Chesapeake Bay, Ra was also strongly correlated with salinity (Moore, 1981). In contrast, when Ra was analyzed in the Chao Phraya River [Thailand] over a salinity range similar to that of the YRE, a comparison of wet and dry seasons found no significant differences in Ra activity in surface water across the estuary (Nozaki et al., 2001; Dulaiova et al., 2006).

To investigate seasonal variability in SGD fluxes of pore water constituents, shallow pore water and surface water samples were collected monthly at Gloucester Point, VA [US], from January 2012 - March 2013. Spatial variability in the pore water end member was also measured through sampling at five additional sites across the York River estuary during September of 2012. The goals of this study were to 1) examine the behavior of pore water constituents including nutrients, selected trace metals, and polycyclic aromatic hydrocarbons (PAHs), across the STE in coastal VA [US], 2) infer controls on the pore water distribution of these constituents, and 3) use Ra-derived SGD fluxes to estimate seasonal fluxes of these constituents from the STE to surface waters.

2. Methods

2.1 Subterranean estuary sampling

In the winter and summer of 2012, shallow pore water (groundwater) profiles (0-200 cm) were sampled using a drive point piezometer (Charette and Allen, 2006) at six sites in the York River estuary (YRE) in the intertidal zone (**Figure 1**). Pore water could not be collected from some depths at different sites due to the presence of impermeable layers, likely clay lenses. Above a depth of 2m, sediment at all sites was a mixture of sands and muds. The BB site had the finest sediment makeup at all attempted sampling depths. Following piezometer well installation, the system was flushing via peristaltic pumping for a minimum of 5 minutes prior to sampling to help clarify any sediment disturbed caused by well installation and reduce the suspended particulate load. Water quality parameters (salinity, pH, dissolved oxygen, ORP) were measured using a handheld YSI-556. Large volume samples (4 L) were collected for Ra analysis. Pore water samples were collected in September 2012 at these sites at the low tide line (50 cm depth) for inorganic nutrients (NO_x and NH_4), trace metals, and PAHs.

Shallow pore water samples were collected monthly from January 2012 – March 2013 at Gloucester Point, VA [GP]. Pore water samples were collected using a drive point piezometer at the low tide line. A groundwater profile was attempted from 0-200 cm at 50 cm intervals, and 4 L samples were collected for radium analysis and water quality parameters. Additional pore water samples for various chemical analyses (DOC, TDN, NO_x NH_4, trace metals, and PAHs) were collected on some dates coincident with the radium samples.

2.2 Radium analysis

Dissolved Ra was extracted by passing water samples through manganese fiber columns at a maximum flow rate of one liter per minute (Moore and Reid 1973; Moore and Scott, 1986; Moore, 2008). After extraction, fibers were rinsed with deionized water (~500 mL) to remove salt and manually squeezed to achieve an ideal water to fiber ratio (Sun and Torgerson, 1998; Kim et al., 2001; Moore, 2008). Ra activity was measured using a radium delayed coincidence counter (RaDeCC) (Scientific Computer Instruments) (Moore and Arnold, 1996). Initial RaDeCC measurements were made for the ^{224}Ra and ^{223}Ra isotopes (Moore, 2008). A subset of samples was selected for ^{226}Ra analysis. Samples for ^{226}Ra analysis were placed in glass flasks fitted with rubber stoppers and valves, sealed for 3+ days to allow ingrowth of ^{222}Rn, and analyzed using the RaDeCC total counts category (Waska et al., 2008; Peterson et al., 2009).

The extraction efficiency (94±5%) of the manganese fibers was calculated by repeated measurements (n=10) using two columns connected in series. Counting efficiency of the RaDeCC was calibrated using a standard Mn-fiber (Scholten et al., 2010), and background activities (^{223}Ra=0.003cpm; ^{224}Ra= 0.063cpm; Total counts=0.725 cpm) were determined using long counts (20+ hours) on the empty circulating cells (Garcia-Solsona et al., 2008). Ra measurement uncertainty calculated from replicates averaged 13.8% for ^{224}Ra and 14.3% for ^{223}Ra (n=7) and 10.1% for ^{226}Ra (n=3).

2.3 Chemical Analyses

Pore water samples for DOC (60 mL) were collected in duplicate and were syringe filtered into acidified polycarbonate bottles using 0.7μm nominal pore-size GFF filters (preashed 450C for 4h) and frozen (-20C) until analysis. Samples were analyzed for TDOC and TDN using a Shimadzu TOC-V with TN capabilities. Additional pore water (60mL) replicate samples for inorganic nitrogen were collected and filtered in to acid-washed LDPE bottles using a 0.45 μM capsule filter. Dissolved NH_4 and NO_x were measured by the manual hypochlorite method and spongy cadmium method (Koroleff, 1983), respectively, and analyzed using a Shimadzu UV-1601 spectrophotometer. Dissolved organic nitrogen (DON) was estimated by subtracting the tDIN ($NH_4 + NO_x$) from TDN (Sharp, 2002). Total dissolved phosphorous (TDP) was analyzed by ICP-MS alongside trace metal samples as discussed below.

Trace metal samples were collected and filtered through 0.45 μM capsule filter into acid-cleaned LDPE bottles, and acidified immediately after collection to pH<2 with concentrated HCl (trace metal grade). Samples were stored for a minimum of one month prior to analysis to ensure that all metals were in the dissolved phase. Samples were diluted 11-fold with 1% Optima-grade HNO_3, spiked with In as an internal standard, and analyzed by direct injection on an Element 2 ICP-MS (Beck et al., 2007). Samples were analyzed for a suite of trace metals but only P, U, Ba, and Fe are reported here.

Replicate samples of unfiltered pore water were collected in 1L pre-cleaned glass bottles (baked at 400°C, solvent rinsed) during September at all pore water sampling sites and April, May, and June at the GP site. Samples were immediately placed on ice for transport back to the lab where they were refrigerated at 4°C until extraction within 24

hours of collection. Extractions were done in groups of two to eight samples, and one laboratory blank was extracted with each set of extractions. Samples were combined with a deuterated PAH surrogate standard mixture (d_4-dichlorobenzene, d_8-naphthalene, d_{10}-acenaphthene, d_{10}-phenanthrene, d_{12}-chrysene, and d_{12}-perylene) and were extracted using pre-cleaned separatory funnels with three 40mL additions of dichloromethane. Samples were then reduced under nitrogen using a TurboVap evaporator (Zymark) and stored at -20°C until further processing. Excess water in the samples was removed using a sodium sulfate column and samples were further reduced to 1mL. An internal standard containing *p*-terphenyl was added and the samples were further reduced to 100 μL. Samples were analyzed using gas chromatography/tandem mass spectrometry (Varian CP-3800/Saturn 2000) and analyzed using selected ion monitoring using Varian software. PAH concentrations were corrected for recovery (d_4-dichlorobenzene = 9±3%, d_8-naphthalene = 23±6%, d_{10}-acenaphthene =56±14%, d_{10}-phenanthrene = 48±8%, d_{12}-chrysene = 38±3%, d_{12}-perylene =34±4%) (Spier et al., 2011). Low recovery may be related to the nature of groundwater samples (low pH, sulfidic, rich in organic carbon). The limit of detection was approximately 0.01 μg/L per analyte.

3. Results

3.1 Radium

Radium activity in shallow pore water (groundwater) was highest during the summer and lowest during winter (**Table 1**). Pore water ^{223}Ra, ^{224}Ra, and ^{226}Ra were positively correlated with salinity (R^2 = 0.23, 0.34, and 0.32, respectively, $p<0.01$ for all

regressions) when outliers were removed (**Figure 2**). Radium behavior in pore water is discussed further in Chapter 1.

3.2 Nutrients

Dissolved organic carbon concentrations in pore water collected at the GP site ranged from 258 to 2770 μM (820±410 μM; **Table 1**). DOC exhibited non-conservative addition with respect to salinity, and peak concentrations were observed at mid-range salinities (8-14) at depths of 25-100cm (**Figure 3, Figure 4**). The highest DOC concentrations (>1800 μM) observed were collected at the shallowest depths in September 2012 when surface and pore water salinities were high. These concentrations are much higher than most DOC measurements but also indicate non-conservative addition of DOC with salinity. Pore water was enriched relative to surface water DOC in the YRE (200-500 μM) (Raymond and Bauer, 2001).

Total dissolved nitrogen (TDN) ranged from 63 μM to 382 μM and was negatively linearly correlated with salinity ($R^2 = 0.44$) (**Figure 4**). Only a limited number of samples were collected at salinities below 5 (n=2), but TDN appears to be enriched at low salinities. The most abundant inorganic nitrogen species was ammonium, which made up of the largest fraction of tDIN in all samples and contributed >90% of tDIN in most samples. Pore water was generally reducing (ORP< -200mV) at most depths, indicating why most inorganic nitrogen is found in the reduced form (Slomp and Van Cappellen, 2004). NH_4 was strongly negatively correlated with salinity ($R^2 = 0.51$) when one outlier was excluded (BB site, 9/12/12) (**Figure 4**). Similar to TDN, NH_4 appears to be highly enriched at low salinities and at depth, indicating a fresh groundwater source.

NO_x was below 1 μM in all groundwater samples, and is omitted from subsequent discussion because it typically represented less than 5% of the TDN. This is consistent with previous observations in the YRE, where substantial NO_x (up to 23 μM) was only observed in a few shallow samples (Kellum et al., in prep.; I. Anderson, VIMS, unpublished; Salisbury, 2011). DON calculations were made for October 2012 and February 2013 and made up >50% of the TDN on each sample, similar to previous investigations (Kroeger et al., 2007). No relationship of DON was observed with respect to salinity, although this may be related to the small number of observations (n=9).

TDP was highly variably but appears to be added non-conservatively with respect to salinity in the STE (**Figure 4**). TDP concentrations peaked between salinities of 6 and 10 and the maximum TDP concentration of 45 μM, as did NH_4. The minimum TDP was 2.0±0.1 μM. Similar TDP and DIP concentrations were observed in the GP area previously (Salisbury, 2011; I. Anderson, VIMS, unpublished).

3.3 Trace Metals

Uranium (U) in pore water ranged from 0.08 to 8.12 nM and was removed non-conservatively with respect to salinity in nearly all samples **(Figure 4**). U is removed under anoxic conditions in pore waters (e.g. Barnes and Cochran, 1993), but where U was higher than expected relative to conservative mixing (n=2), oxygen levels were similar to most pore water samples (<5% below 50cm).

Pore water Ba was lowest at low salinities, ranging from 10.8 nM in nearly fresh pore water to >450 nM at high salinities. Ba was strongly correlated with pore water

salinity (R^2= 0.47) (**Figure 4**), and was enriched relative to surface waters, indicating that the STE is a source of Ba to surface waters.

Pore water Fe was consistently low (<1 μM) at depths greater than 150 cm and enriched in most samples collected at 50 cm (1.7-72 μM), coincident with an observed layer of Fe-oxides in sediment (Kellum et al., in prep.). Fe at 50cm depth was enriched relative to surface waters (<1 μM, Kellum et al., in prep). No clear distribution of Fe was observed with respect to salinity (**Figure 4**); samples appear to be distributed more clearly with respect to depth, with the highest of observed Fe near 50 cm.

3.4 PAHs

Shallow pore water collected from April 2012 - September 2012 had PAH concentrations that ranged from below detection limit (10 ng/L) to greater than 1000 ng/L for individual PAHs (e.g., 1546 ng/L fluoranthene) (**Figure 4**). Thirty PAHs (Absolute Standards, Inc. #93462) were searched for in samples, however, relatively few of these congeners were consistently found in samples (**Table 2**). PAHs were only present in shallow samples (≤50 cm depth), and fluoranthene was generally the most abundant compound. A different mixture of PAH congeners (acenaphylene, acenaphthene, 1-methyl-phenanthrene, and perylene) were observed in April 2012, compared with other pore water samples. Fluoranthene was quantified at four of five sites, and had a mean concentration of 259 ng/L. The second most abundant sample was pyrene, which was quantified at three of five sites and had a mean concentration of 154 ng/L. Because sample concentrations of individual PAHs were extremely variable, PAH concentrations

are reported as the sum of 30 PAH congeners (ΣPAH_{30}). The range for ΣPAH_{30} was from below detection to 2580 ng/L (BB), and the median was 90 ng/L.

4. Discussion

4.1 Behavior of constituents in pore water

Dissolved organic carbon

DOC is non-conservatively added with respect to salinity, indicating an autochthonous source within the subterranean estuary. The source of DOC in shallow pore water is likely particulate organic matter (e.g. sea grasses, benthic diatoms) on the sediment surface that is physically and biologically degraded and advected in to the shallow pore water (Santos et al., 2009). DOC has been shown to behave both conservatively and non-conservatively in pore waters with respect to salinity (Beck et al., 2007; Santos et al., 2008; Santos et al., 2009). This relationship may be a function of the physical mixing processes and rate of biological production and consumption in the pore waters, which are variable between sites and seasons (Santos et al., 2009). DOC has been suggested as an electron donor for denitrificiation along steep redox potential gradients (Addy et al., 2005; Santos et al., 2008). Oxygen availability steeply dropped off where peak DOC in the pore water was measured and therefore may be an electron donor for denitrification.

High concentrations of DOC in the pore water relative to the surface waters indicates that SGD represents a source of DOC to the YRE. DOC entering YRE surface water has a predominately terrestrial source with an approximate age of a few decades,

but the stable carbon signature of DOC leaving is much more marine in origin (Raymond and Bauer, 2001). Autochthonous DOC represents as much as 38-56% of the DOC present in surface water at the YRE mouth, an input of 1.2 μM/L/d (Raymond and Bauer, 2001). Non-conservative DOC addition to YRE surface waters as estimated by Raymond and Bauer (2001) is equivalent to an area-normalized rate of 5.5 mmol C/m^2/d. Known DOC production mechanisms such as photo-oxidation and bacterial degradation were unable to account for the observed excess DOC measured in surface waters mid-estuary in the YRE (Raymond and Bauer, 2001). Additionally, many of these sources do not remain constant through seasonal changes in temperature and light availability, but the amount of mid-estuary enrichment remained constant throughout the seasons suggesting a constant source of these compounds. Therefore, DOC-enriched SGD may be able to supply DOC to the surface water.

Nitrogen

High concentrations of TDN and NH_4 at low salinities indicate a fresh groundwater source for these compounds. TDN and NH_4 concentrations in shallow pore water were comparable to estimates made during the summers of 2008 and 2009 in the YRE near the GP site (Salisbury, 2011; I. Anderson, VIMS, unpublished). TDN in YRE surface water is high when freshwater input is low, suggesting base flow (groundwater input) provides substantial TDN (Reay, 2009). The north shoreline of the YRE is largely residential with high septic tank use, which can contribute high TDN loads (e.g. 5000 μM) (Reay, 2004). However, the south bank is mostly green spaces, military and industry, each of which can also contribute substantial N to shallow groundwater **(Figure**

5). Additionally, N may be supplied to the STE through the degradation of organic matter advected in to pore water or occurring in situ (Santos et al., 2009) and removed through denitrification (Addy et al., 2005; Santos et al., 2008).

Positive correlation of N with depth and negative correlation with salinity have been observed in shallow subterranean estuaries globally, including Cherrystone Inlet [VA], Hasaki Beach [Japan], Jamaica Bay [NY], and the Gulf of Mexico (Reay et al., 1992; Uchiyama et al., 2000; Beck et al., 2007; Santos et al., 2009). In the Gulf of Mexico, N at mid depths (~50cm) was strongly negative correlated with salinity, but deeper depths were not (Santos et al., 2009). In Jamaica Bay, Hasaki Beach, and Cherrystone Inlet, regeneration of N with depth was observed, and this behavior in Jamaica Bay was attributed to remineralization of organic matter (Reay et al., 1992; Uchiyama et al., 2000; Beck et al., 2007).

There were no clear seasonal changes in the distribution of TDN in the STE at the GP site. Seasonal variability of nitrogen in the shallow STE has been observed previously in temperate environments due to variable remineralization rates (Rutkowski et al., 1999; Uchiyama et al., 2000; Jahnke et al., 2005; Ullman et al., 2003; Santos et al., 2009). In previous studies, DIN concentrations in shallow groundwater (<2m) were very high in late summer (Aug., Sept.) but decreased 5-fold to reach a December minimum (Uchiyama et al., 2000). Seasonal changes in groundwater nutrient concentrations in the nearby South Atlantic Bight and Delaware Estuary were hypothesized to be related to sedimentary remineralization rates, and this likely also caused the seasonal differences observed on Hasaki Beach [Japan] (Uchiyama et al., 2000; Jahnke et al., 2005, Ullman et al., 2003). Seasonal differences in nitrogen uptake rates by phytoplankton as well as

differences in microbial remineralization rates have also been suggested as factors affecting nutrient variability in the shallow subterranean estuary (Santos et al., 2009). The lack of observed seasonality in N species at the GP site may be due to the deep, meteoric source of groundwater that is less likely to show strong seasonality compared to surface POM production and microbial remineralization rates.

Phosphorous

TDP is highly variable and appears to be added non-conservatively with respect to salinity, indicating an autochthonous source. Previous phosphate measurements in the shallow pore water (<20 cm) at the GP site varied from 4.6 to 21.5 μM, though salinities were not reported (Salisbury, 2011). The high variability in TDP distributions with respect to depth and salinity suggests that a combination of factors may be affecting TDP distribution. A similar trend where TDP peaks at mid-depths was observed in Hasaki Beach [Japan] (Uchiyama et al., 2000). Inorganic phosphate is typically rapidly removed from groundwater through sorption to iron oxides (Slomp and Van Capellen, 2004; Charette and Sholkovitz, 2002), which are visually evident at the GP site between 25 and 50cm. However, no correlation is observed between dissolved Fe and P in pore water at the GP site (**Figure 6**). Additionally, this sorption process is less efficient under anaerobic conditions (Slomp and Van Cappellen, 2004). Recently, it has been suggested that the sulfate oxidizing bacteria, *Beggiatoa*, may act as mediators of P movement in STE, providing a substantial source of TDP to overlying surface water (Dale et al., 2013). *Beggiatoa* bacteria are present at the GP site (Beck et al., unpublished), indicating that

their presence may provide a TDP source which may explain why such low N:P ratios are observed in discharge (~3:1).

Uranium

Dissolved U was depleted by as much as 4 nM relative to conservative mixing and complete depletion was observed within 1 m of the surface (**Figure 4**). U is removed from solution by precipitation following the reduction of U(VI) to U(IV) (Lovely et al., 1990; Barnes and Cochran, 1993; Windom and Niencheski, 2003; Charette and Sholkovitz, 2006). Removal of dissolved U in the STE due to reducing conditions is consistent with the low oxygen concentrations and reduced N-species observed in pore water. Sulfate reducing microbes have been identified to mediate U reduction (Barnes and Cochran, 1993), and hydrogen sulfide gas was evident at depths below 1 m at most sites in the York River STE. A lack of sulfate-reduction at the IF site may explain why U levels were higher than expected from conservative mixing. Substantial removal of U in the STE is consistent with observations from numerous other sites (e.g. Shaw et al., 1994; Duncan and Shaw, 2003; Moore and Shaw, 2008; Charette and Sholkovitz, 2006; Santos et al., 2011).

Barium

Dissolved Ba was enriched in the shallow STE (up to 440 nM) relative to surface water (191 nM), and concentrations were higher than could be explained by conservative mixing. Multiple mechanisms have been proposed as sources of Ba within the STE. Previously, Ba has been associated with Fe- and Mn-oxides, co-precipitating and

adsorbing to these metal oxides during their reductive dissolution (Shaw et al., 1998; Charette and Sholkovitz, 2006; Moore and Shaw, 2008; Santos et al., 2011). However, Ba was not correlated with Fe in pore waters (**Figure 6**) so this mechanism is unlikely to be the controlling mechanism. More likely, enrichment is due to Ba desorption from sand surfaces during saline intrusion. Ba is strongly correlated with salinity ($R^2 = 0.56$) as well as ^{224}Ra ($R^2 = 0.67$) and ^{223}Ra ($R^2 = 0.47$) (**Figure 7**). Ra is known to be controlled by desorption as a function of salinity (Moore, 1981; Webster et al., 1995) and this strong correlation with both salinity and Ra suggests that the distribution of Ba in pore water is also a function of increased desorption across the STE salinity gradient.

Iron

Dissolved iron was consistently highly enriched at mid-depths (50 cm) with shallower depths lower but still enriched relative to surface waters (Kellum et al., in prep.). Similarly, in Great South Bay, dissolved iron peaked at a depth near 50 cm. Here, it was suggested that Fe precipitation at these depths was caused by changes in pH (Beck et al., 2010; Spiteri et al., 2006). However, there is no clear relationship of Fe with pH in the YRE (**Figure 6**). In Waquoit Bay, sediment cores revealed the oxidative precipitation of Fe to form Fe-oxide rich sediments at depth (Charette and Sholkovitz, 2002). In the Waquoit Bay system, fresh groundwater was enriched in dissolved Fe and was the proposed Fe source; in the YRE samples collected at depth had low levels of dissolved Fe (Charette and Sholkovitz, 2002). In both Waquoit Bay and Great South Bay, pore water Fe was consistently an order of magnitude or more higher than was measured in the YRE (Charette and Sholkovitz, 2002; Beck et al., 2010). There is no clear surface water or

deep groundwater source of Fe in the YRE so it is likely that the Fe-oxide rich sediment is continuously oxidized and reduced within the STE.

Polycyclic aromatic hydrocarbons

High spatial variability was observed for PAH congeners and their concentrations in pore water. PAH concentrations in pore water were much higher than York River surface water (Countway et al., 2003), suggesting that SGD is a source of PAHs to the YRE. PAHs were not correlated with salinity (**Figure 4**), indicating that salinity did not control the distribution of PAHs. Rather, PAH distribution in pore water may be associated with current and legacy land use. Sample sites encompassed a variety of adjacent land use types, including forested, residential, military, and mixed use (**Figure 5**). The most rural and pristine site was the SP site, located within the York River State Park, an extensive reserve that is primarily forested and protected wetlands. This site had no PAHs above the limits of detection (10 ng/L) in pore water samples. The FL and IF sites are both generally rural, but have major military operations near shore (Camp Peary, Yorktown Naval Weapons Station) and a highway 50 m or less from the shoreline. Vehicular traffic on the military bases and nearby highway may also represent local sources of PAHs via atmospheric deposition and runoff. Low PAH concentrations were observed at these sites in shallow pore water. High PAH concentrations have been observed in storm water runoff from highways, pulsing from <300 ng/L to >4000 ng/L (3-5 ringed PAHs) during two rain events (Spier et al., 2011). Some portion of storm water runoff is likely to percolate in to shallow groundwater and may be transported to the YRE via SGD. The highest PAH concentrations were observed at the BB site, which

is residential in nature. High PAH concentrations here may be related to creosote-soaked pilings, which are extremely high in PAHs (Wendt et al., 1996). Additionally, this PAH site may be related to atmospheric deposition of PAHs originating from the industrial south shore.

4.2 Using Ra SGD fluxes for chemical constituents

Flux estimates by isotope (F_C) are calculated by **Equation 1.** Surface water constituent concentrations (C_S) (from samples collected at the GP site and literature values from the YRE) were subtracted from pore water samples concentration (C_P) to ensure estimates limited simple recirculation of these constituents from discharge estimates (Santos et al., 2008). Pore water concentrations at discharge were estimated as the constituent concentration measured at the mean salinity of YRE bottom waters (winter, 13.8; summer, 18.4; **Table 3**). Ra-derived SGD fluxes (F_{SGD}) for summer and winter were calculated in Chapter 1. Seasonal fluxes of chemical constituents are averaged to determine an approximate "annual" flux. Because all constituent flux estimates are based on the same salinity distribution and rely on the same water flux data, all estimates are largest when the ^{224}Ra isotope is used and smallest when calculated by the ^{226}Ra estimate.

$$F_C = (C_p - C_s) * F_{SGD} \quad (1)$$

Nutrients

Annual DOC fluxes range from 11-78 mmol/m^2/d (**Table 4**). This quantity represents a significant source of DOC to surface waters. The input of DOC from SGD

has been estimated in other basins to range from 21-34 mmol/m^2/d (Australia, Florida) (Santos et al., 2008; Santos et al., 2012). Raymond and Bauer (2001) estimated an autochthonous DOC input of 1.2 umol C/L/d to the YRE surface waters. Scaled to an average YRE depth of 4.55m, this is equivalent to an SGD source of 5.5 mmol/m^2/d. These estimates suggest that SGD can account for at least half of this input of DOC to the YRE, and may account for nearly an order of magnitude.

Estimated annual fluxes for TDN and NH_4 range from 1-7 and 1-7 mmol/m^2/d, respectively. DON fluxes are not calculated due to limited data at high salinities, but are likely similar in magnitude to NH_4 fluxes as NH_4 and DON concentrations were similar in magnitude. Scaled up to basin-wide estimates, TDN from SGD represents between one tenth and twice as much of the input of TN (dissolved+particulate) entering the YRE via the Mattaponi and Pamunkey Rivers (0.3-7.5 10^3 kg/d vs. $3x10^3$ kg/d) (Langland et al., 2007). SGD may supply up to 75% of the TN entering the entire YRE by all sources ($1x10^4$ kg/d) (Dauer, 2005). Sources of N to the Mattaponi and Pamunkey are mostly agriculture, urban areas, and forest (Sprague et al., 2000). In addition to near shore septic systems (Reay, 2004), the aforementioned sources are also likely the dominant sources of N to YRE surface water as well as fresh groundwater in the YRE watershed that eventually enters the STE and discharged via SGD. Direct discharge near septic systems in coastal Virginia had DIN fluxes that averaged 2.0 mmol/m^2/d with a maximum of 36 mmol/m^2/d (Reay, 2004). Estimates of DIN fluxes as high as 56 mmol/m^2/d have been made in coastal Virginia [Chingoteague] (Simmons, 1988). Because SGD does not exhibit significant seasonality, TDN from SGD is more important during dry periods than

wet because TN via fresh tributaries is largest during periods of groundwater saturation (e.g. winter).

Annual TDP fluxes through the STE range from 0.3-2.5 mmol/m^2/d. This flux is larger than the inorganic P measured in direct discharge by seepage meters in coastal Virginia, which averaged 0.03 mmol/m^2/d (Reay, 2004). This difference may be influenced by 1) a low ratio of PO_4^{-3} :TDP, 2) changes in P behavior near the sediment-water interface that are not captured by the Ra-mass balance technique or 3) system disruption caused by seepage meters deployment. SGD represents, at minimum, a source equivalent to one third of the Mattaponi and Pamunkey River input of TDP (290 kg/d) (Langland et al., 2007). At maximum, SGD provides more than twice the input of TDP to the entire YRE from river input (930 kg/d) (CWVa, 2005). The ratio of TDN:TDP at the sediment-water interface is low, approximately 3:1 regardless of isotope used. The ratio of TDN:TDP in SGD has been used to correlate SGD-derived N with a HAB outbreak in the southern sea of Korea (Lee and Kim, 2007). Without understanding how these ratios change near the sediment-water interface as well as how calculated fluxes vary depending on the half-life of the Ra isotope tracer, it is difficult to track and ultimately manage the impact of SGD-derived nutrients on surface waters.

Trace Metals

On an annual basis, uranium was removed non-conservatively at a rate of 0.06-0.5 μmol/m^2/d. Regardless of the Ra tracer used, the U content of water that passes through the STE is significantly altered and U removed. These removal rates are similar to those found along the Florida gulf coast (1 μmol/m^2/d), Waquoit Bay, MA (0.4 μmol/m^2/d) and

South Carolina (0.2 μmol/m^2/d) (Santos et al., 2011; Charette and Sholkovitz, 2006; Duncan and Shaw, 2003). Alternatively, some studies have observed U addition via SGD (Swarzenski and Baskaran, 2007). In the karstic Tampa Bay, an area about half the area of the Chesapeake Bay, U was added via SGD at a rate 83 to 203 mol/d (compared to losses in the York River estuary of 3.6- 47 mol/d). However, in some sampling locations U removal was observed in Tampa Bay (Swarzenski and Baskaran, 2007). Two pore water samples in the YRE fell above the conservative mixing line, suggesting U may have been added at these sites during sampling (>7.4 nM at salinities <16). Similarly, a handful of samples were collected where the addition of U was observed in the northern Florida gulf while U-removal in SGD dominated the system (Santos et al., 2011). The variability in addition versus removal of U observed between sites and systems is likely a function of the physical mixing that occurs and the underlying sediment type of the sampling sites. The presence of Fe- and Mn- oxides in sediments can control U availability (Barnes and Cochran, 1993). If the underlying sediments are enriched in U and are flushed rapidly, shallow pore water may remain oxic and SGD may ultimately be a source of U to surface waters. Alternatively, if the rate of flushing by oxic seawater through sediments is slower, anoxia may develop and U removal will subsequently occur. Similarly, the amount of organic material available can contribute to anoxia and subsequently contribute to U removal by controlling the dissolved oxygen availability. The combination of these controls is a possible explanation as to why differences are observed within systems as well as between systems.

Unlike all other measured pore water constituents, Ba is positively correlated with Ra, indicating that the flux rate calculated using either ^{223}Ra or ^{224}Ra is not a minimum or

maximum but rather a reasonable estimate of the Ba flux through SGD. Ba was added non-conservatively across the subterranean estuary at a rate of 1-13 μmol/m^2/d. Similar rates of Ba addition were observed along the northern FL gulf coast (8 μmol/m^2/d) and the South Atlantic Bight (10 umol/m^2/d) (Santos et al., 2011; Moore and Shaw 2008).

Fe is known to be redox sensitive, which may control its distribution. However, because Fe had no clear distribution across the STE with respect to salinity or Ra, fluxes via SGD were not calculated.

Polycyclic aromatic hydrocarbons

Because of the variability in the individual PAH congeners present in any given sample, 30 congeners were summed (ΣPAH_{30}) for the purpose of calculating fluxes. The distribution of ΣPAH_{30} was not related to salinity ($R^2 = 0.01$) and therefore, a median ΣPAH_{30} was used to determine fluxes to account for the limited sample number and a single highly enriched sample. The SGD-derived ΣPAH_{30} flux was calculated to be 1.2-9.7 ng/m^2/d, which is much lower than atmospheric deposition measured in the Chesapeake Bay measured in the early 1990s (1-16 μg/m^2/d; Leister and Baker, 1994). PAH concentrations in direct runoff from a local major highway (up to 2-4.7 μg/L; Spier et al. 2011) and maximum concentrations observed in pore water in the current study (2.6 μg/L) were similar. This suggests that the pore water and the STE may not represent efficient removal routes for PAHs originating in surface runoff. PAHs in pore water have not previously been measured, so other organic compounds with similar behavior in groundwater are provided for comparison. High pesticides fluxes were measured near agricultural sites in the Chesapeake Bay, ranging from 7.7 to 26.9 μg/m^2/d. (Gallagher et

al., 1996). Pharmaceuticals and pesticides have been found in coastal groundwater around Long Island and the Yucatan peninsula (Zhao et al., 2011; Metcalfe et al., 2011). Robinson et al. (2009) suggested that tides significantly enhance BTEX attenuation in the near-shore aquifer. SGD may provide a long-term source of PAHs to surface waters, acting as a source for PAHs long after their initial deposition.

4.3 Variability and Sources of Error

Flux estimates are provided for a variety of compounds as discussed in Section 4.2. However, these flux estimates have large associated errors due to measurement techniques as well as variability among samples and across sites (**Table 4**). Although the majority of constituent samples were collected at the GP site, samples collected across sites were distributed similarly with respect to salinity, suggesting similar sources and controls across sites.

Even if errors on estimates made using Ra-derived SGD fluxes for individual isotopes were small, the variability suggested by comparing estimates made using ^{224}Ra and ^{226}Ra-derived SGD flux rates are in most cases an order of magnitude apart (**Table 4**). As discussed previously in Chapter 1, what exactly Ra-derived SGD fluxes represent is unclear. Each Ra isotope provides a different flux estimate of SGD, which is related to their rate of regeneration. The short-lived ^{224}Ra in-grows from its parent thorium much more rapidly than the long-lived ^{226}Ra isotope, and therefore accounts for higher rates of flushing occurring near the sediment-water interface. Therefore, when constituent concentrations are applied to these Ra-derived SGD fluxes, the calculated constituent fluxes are by definition variable, but how exactly they compare to one another is unclear.

To accurately be able to use Ra as an SGD tracer for various constituents, the relationship between the two must be better understood. For example, Ra is an ideal tracer for Ba because the two are correlated in pore water (**Figure 7**). It is understood that these two compounds behave similarly pore water, where they are both released by cation exchange. However, it is still unclear which isotope of Ra provides the most accurate SGD flux for this compound because it is not clear what SGD flow paths are a) releasing Ba and b) represented by each Ra isotope SGD flux. SGD fluxes determined using an Ra tracer are only ideal for those compounds whose reaction rates occur at the similar rates as a given Ra isotope tracer, which are unknown for the compounds measured in this study for the YRE.

Although the remaining measured pore water constituents are not correlated with Ra, SGD-derived fluxes are made to point to draw the reader's attention to the large variability associated with these methods. Based on comparisons of these fluxes against literature values made using Ra-, Rn-, derived fluxes and direct measurements, this suggests that ^{224}Ra and ^{223}Ra provide high end estimates of fluxes, while ^{226}Ra fluxes provide low end estimates. Extrapolating Ra fluxes to across the board constituents appears to be a largely inaccurate way to. Direct measurements likely provide more accurate estimates for compounds that are not affected by changing redox conditions that occur when installing benthic chambers. In the case of redox-sensitive compounds, other tracers with more similar behavior to the compounds of interest should be used as tracers until the flow mechanisms of Ra-derived SGD fluxes are better understood.

5. Conclusions

Nutrients, trace metals, and PAHs were measured in pore water in the YRE. The distribution of each element across pore water depth and salinity gradients were investigated and each measured constituent (except PAHs and Fe) had a clear distribution with respect to salinity. Each measured constituent was added non-conservatively in the subterranean estuary except U, which was non-conservatively removed. The relationship between the behaviors of these constituents with respect to a Ra tracer was investigated and only Ba was positively correlated with both ^{223}Ra and ^{224}Ra in pore water. Because nutrients, U, and PAHs were not correlated with the short-lived Ra isotopes, it is unlikely that their rates of production and removal occur on the same time scale as Ra. Therefore, Ra-derived SGD fluxes are imprecise estimators of the input rates of these compounds in the YRE. Ra-derived SGD fluxes were calculated for summer, winter, and annually using pore water concentrations at near-surface water salinities using three Ra isotopes. The combination of short-lived and long-lived Ra isotopes provides minimum (^{226}Ra) and maximum (^{224}Ra) estimates of SGD fluxes for DOC, nutrients, U, and PAH compounds.

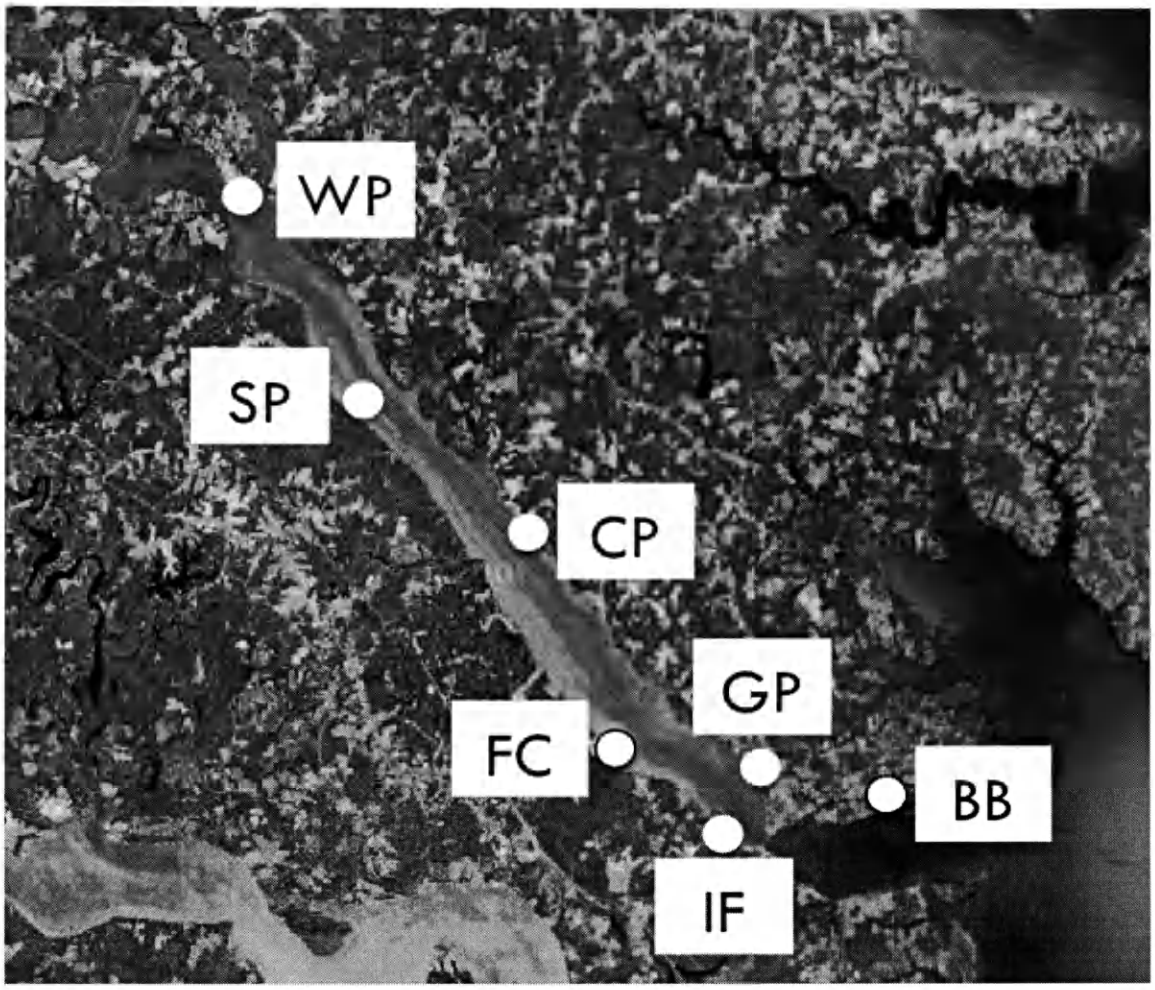

Figure 1: Pore water sampling locations along the YRE.

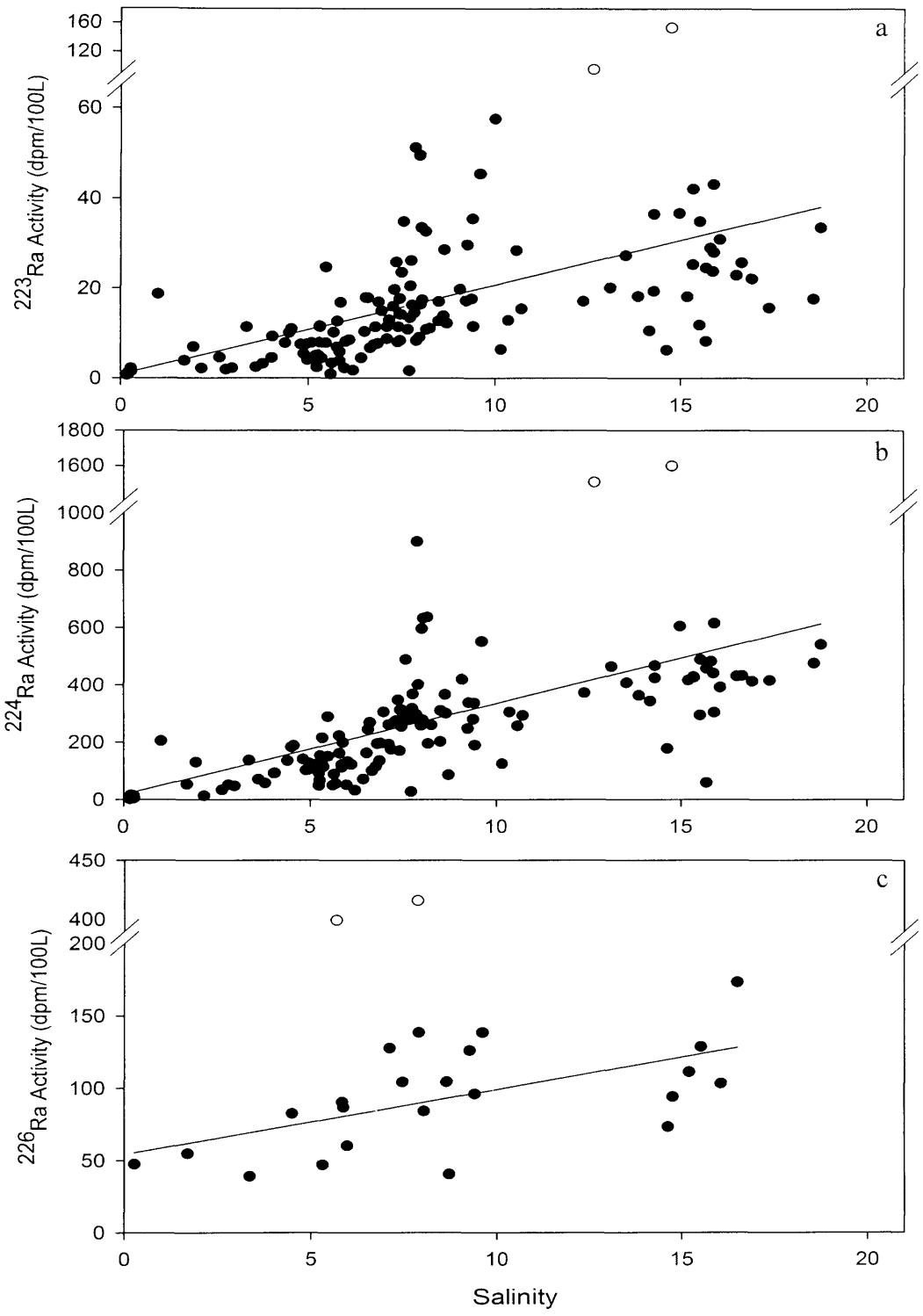

Figure 2. Pore water radium activity in the York River estuary. Solid line represents regression of pore water samples (filled circles) against salinity; outliers (open circles) were removed from regression. a) ^{223}Ra b) ^{224}Ra c) ^{226}Ra

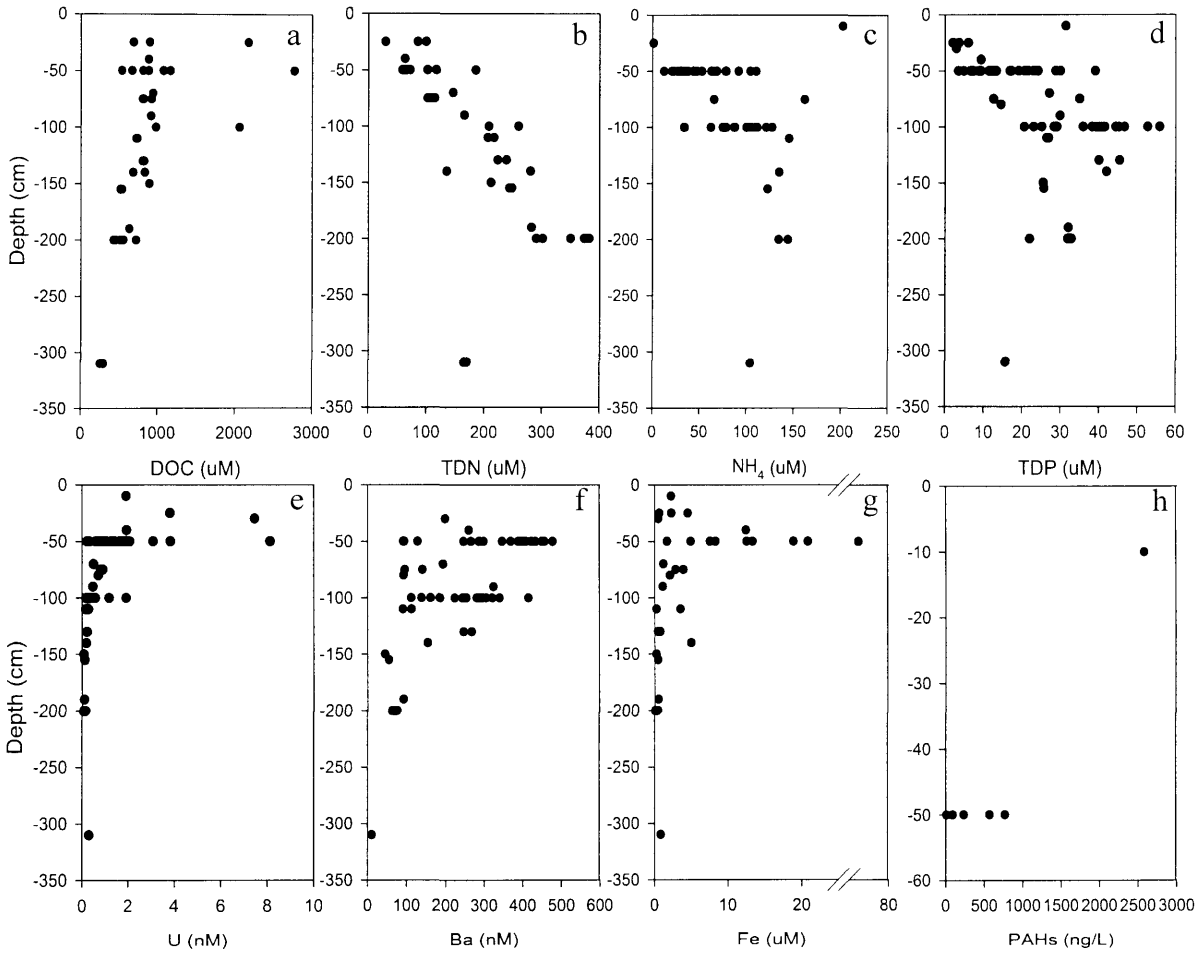

Figure 3. Depth profiles of nutrients in pore water a) Dissolved organic carbon (DOC) b) total dissolved nitrogen (TDN) c) ammonium (NH_4) d) total dissolved phosphorous (TDP) e) barium (Ba) f) uranium (U) g) iron (Fe) h) PAHs. *Note: depth scale of PAH plot is not consistent with all other plots in figure.*

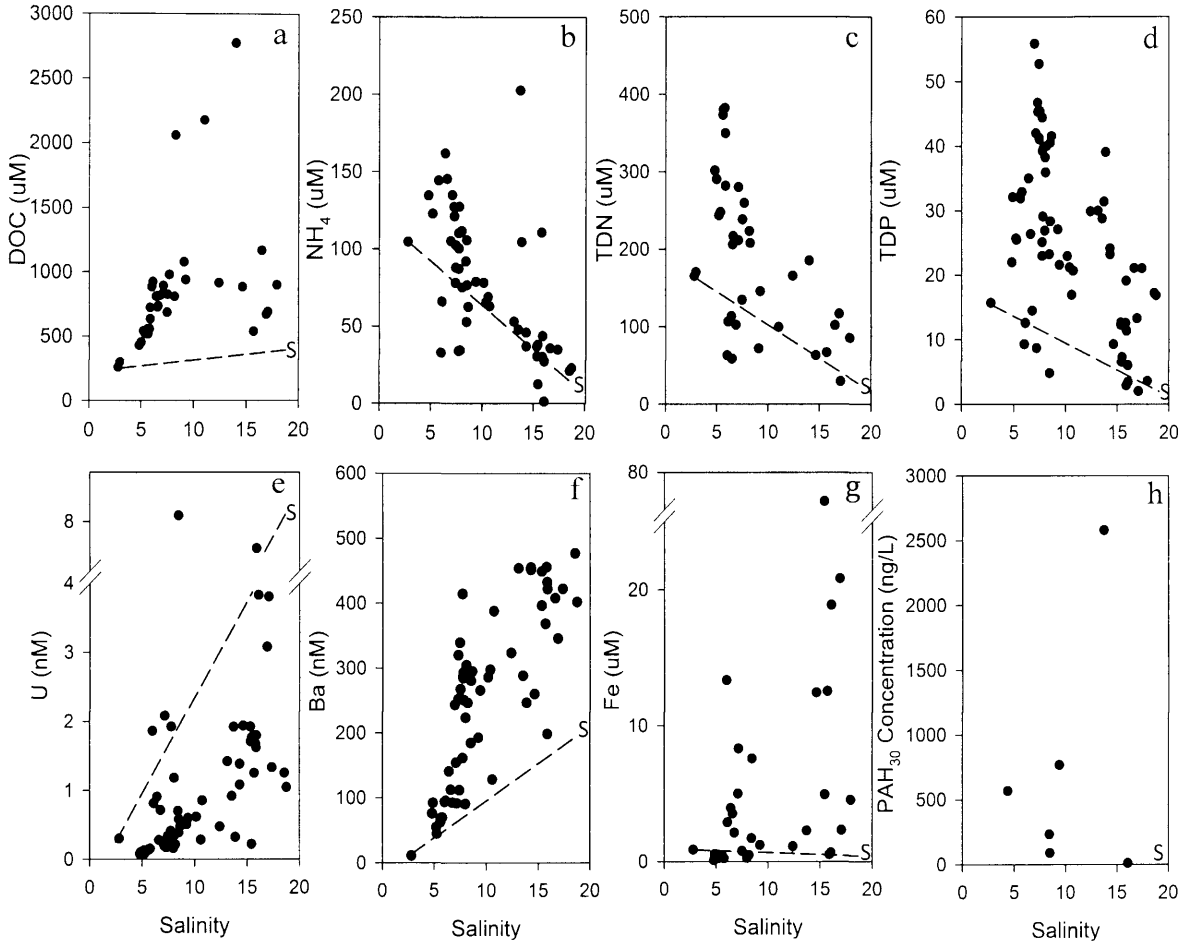

Figure 4. Dissolved organic nutrients in pore water as a function of salinity. A conservative mixing line is drawn between the freshest pore water sample and the approximate surface water concentration, "S". a) Dissolved organic carbon (DOC) b) ammonium (NH_4) c) total dissolved nitrogen (TDN) d) total dissolved phosphorous (TDP) e) uranium (U) f) barium (Ba) g) iron (Fe) h) sum of 30 polycyclic aromatic hydrocarbons (PAH_{30}). Surface water "S" concentration sources: [a]Raymond and Bauer, 2001; [b,c,d]Reay, 2009; [e]Epstein and Zander, 1978; [f]Moore and Shaw, 2009; [g]Kellum et al., in prep.; [h]Countway et al., 2003.

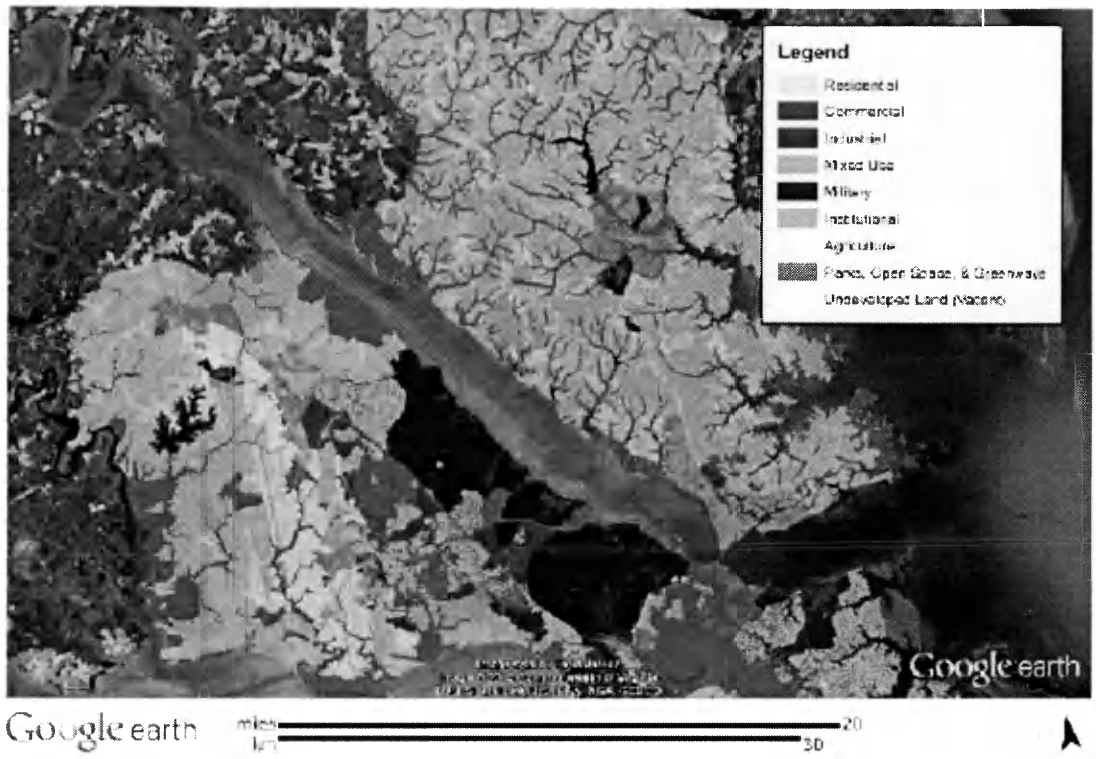

Figure 5. Land use map in the lower York River Estuary watershed and surrounding lands.

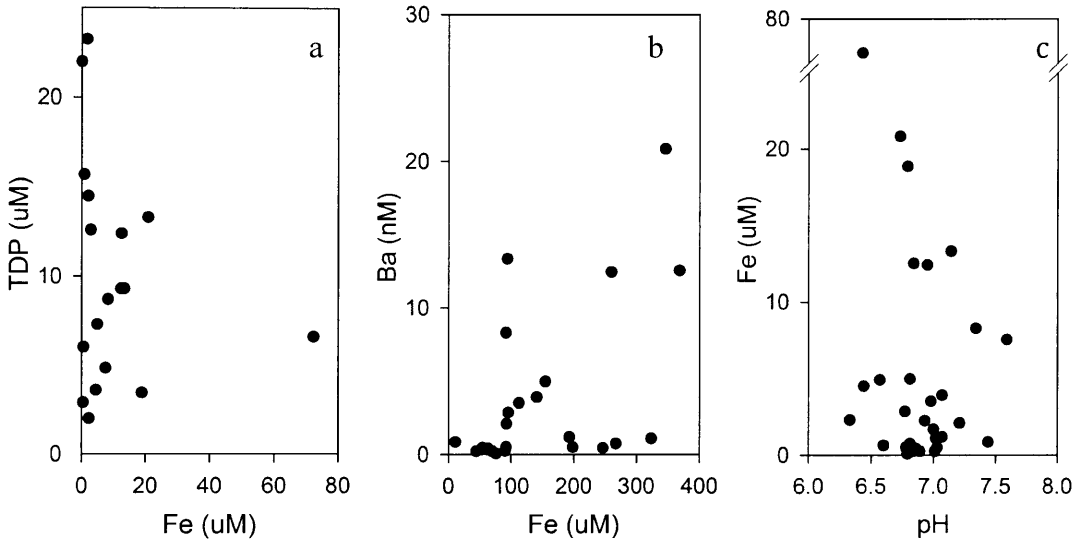

Figure 6. Distribution of a) total dissolved phosphorous (TDP) b) barium (Ba) c) pH with respect to iron.

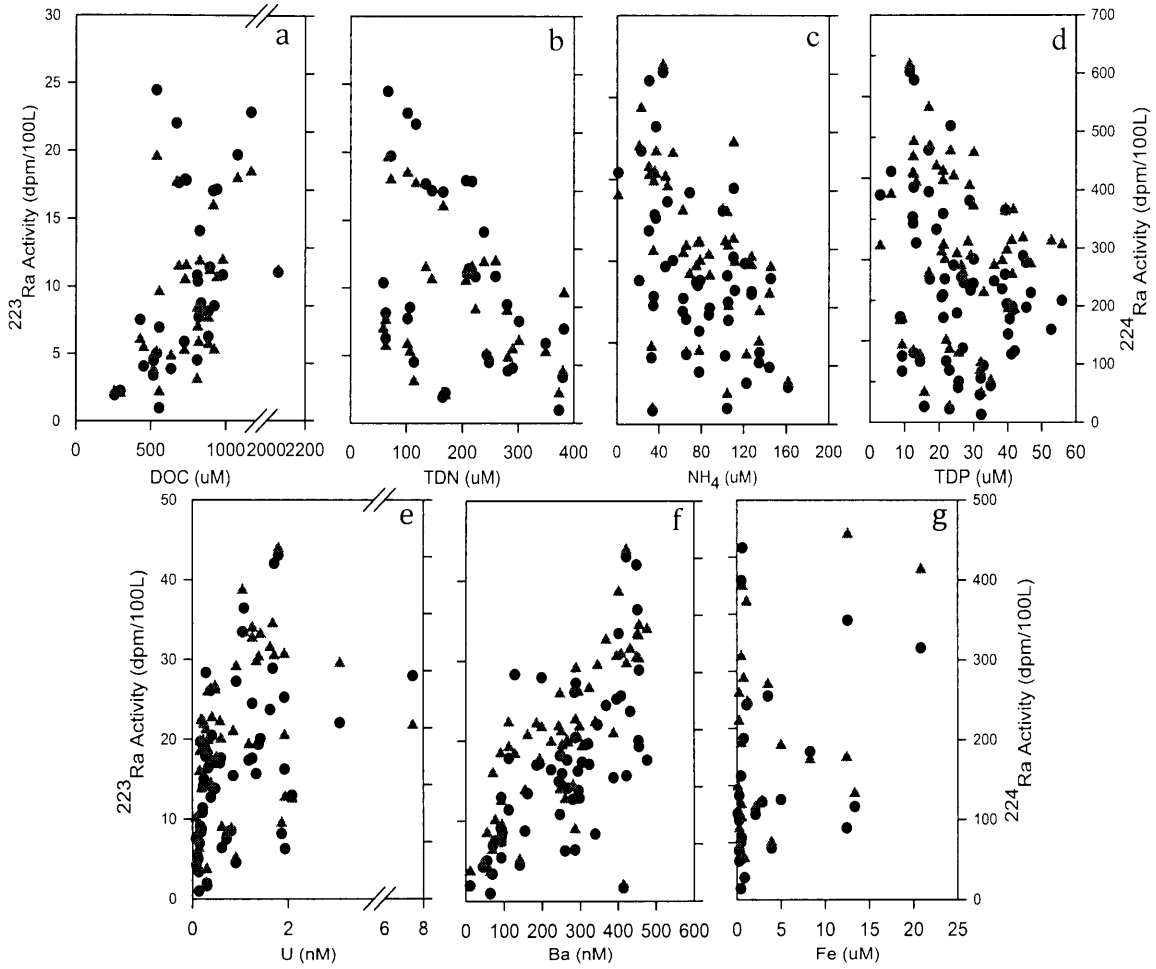

Figure 7. Pore water constituent distributions with respect to ^{223}Ra (black circles) and ^{224}Ra (red triangles). a) Dissolved organic carbon (DOC) b) ammonium (NH_4) c) total dissolved nitrogen (TDN) d) total dissolved phosphorous (TDP) e) uranium (U) f) barium (Ba) g) iron (Fe)

Table 1. Pore water geochemical parameters by site and sampling date. *Samples were collected from the same depth 5m apart perpendicular to the shoreline. ND= not detected. ±Average error of replicates is: ^{223}Ra=14.8%; ^{224}Ra= 13.8%; ^{226}Ra=10.1%; DOC=6.4%; TDN=2.8%; NH_4 =6.8%; TDP=7.7%; U=11.7%; Ba=8.3%; Fe=14% ΣPAH_{30} =16.3%

Site	Date	Depth (cm)	Sal.	pH	^{223}Ra dpm/ 100L	^{224}Ra dpm/ 100L	^{226}Ra dpm/ 100L	DOC uM	TDN uM	NH_4 uM	DON uM	TDP uM	U nM	Ba nM	Fe nM	ΣPAH ng/L
GP	01/06/12	50	5.31	7.45	11	114	47									
GP	01/06/12	100	6.8	6.59	11	195										
GP	01/06/12	150	4.02	6.81	5	92										
GP	01/06/12	210	5.09	6.67	8	123										
GP	01/06/12	300	2.63	7.19	5	33										
GP	01/06/12	400	3.78	7.13	3	57										
GP	02/17/12	50	5.32	7.51	12	215										
GP	02/17/12	100	6.89	6.97	17	196										
GP	02/17/12	150	5.47	7.01	8	151										
GP	02/17/12	200	4.94	6.93	8	104										
SP	03/09/12	25	4.49	6.52	10	183	87									
WP	03/09/12	50	1.69	6.27	4	53	55									
SP	03/09/12	50	5.87	6.31	17	199	83									
CP	03/19/12	25	9.27	6.39	30	338	126									
CP	03/19/12	40	9.41	7.47	35	337	96									
IF	03/25/12	50	0.27	7.54	2	14	48									
IF	03/25/12	100	0.18	7.55	1	12										
IF	03/25/12	150	0.19	7.69	1	14										
IF	03/25/12	200	0.17	7.63	1	2										
GP	03/26/12	50	1.93	7.02	7	131										
GP	03/26/12	100	1	7.29	19	205										

GP	03/26/12	150	9.43	6.47	12	190										
GP	03/26/12	250	5.27	6.71	5	153										
GP	03/26/12	300	3.6	6.76	2	71										
GP	04/25/12	50	4.38	6.83	8	135										568
GP	04/25/12	100	4.04	6.76	9	93										ND
GP	04/25/12	100	8.86	6.80	17	310										
GP	04/25/12	150	7.36	6.70	26	348										
GP	04/25/12	250	5.23	6.70	2	48										
GP	04/25/12	300	6.20	6.70	2	32										
GP	05/27/12	50	4.55	6.67	11	188										
GP	05/27/12	100	5.78	6.73	13	162										
GP	05/27/12	100	9.07	6.79	14	366										
GP	05/27/12	166	7.40	6.82	8	170										ND
GP	05/27/12	200	6.66	6.89	7	100										
GP	05/27/12	250	5.31	6.87	8	124										
GP	06/11/12	50	9.39	7.07	18	280				79		22	0.6	266		768
GP	06/11/12	50	10.16	7.07	6	125				78		23	0.6	286		
GP	06/11/12	50	10.37	7.04	13	305				65		21	NA	298		
GP	06/11/12	50	10.59	6.93	28	257				69		17	0.3	128		
GP	06/11/12	50	10.73	6.84	15	293				63		21	0.9	388		
GP	06/11/12	100	6.97	6.87	15	306				105		56	0.2	244		
GP	06/11/12	100	7.28	6.71	16	272				127		47	NA	252		
GP	06/11/12	100	7.31	6.82	20	275				121		45	0.2	320		
GP	06/11/12	100	7.42	7.26	11	312				78		53	0.2	112		
GP	06/11/12	100	7.46	6.90	8	313				102		41	0.2	339		
GP	06/28/12	50	13.12	6.81	20	464				53		30	1.4	454		
GP	06/28/12	50	13.53	6.84	27	407				48		29	0.9	288		

GP	06/28/12	50	13.87	6.88	18	363				104		39	0.3	247		
GP	06/28/12	50	14.29		36	467				37		23	1.1	451		
GP	06/28/12	50	14.29	6.81	19	424				46		24	1.4	455		
GP	06/28/12	100	7.45	6.45	14	255				88		41	0.3	254		
GP	06/28/12	100	7.71	6.8	2	27				34		23	0.3	414		
GP	06/28/12	100	7.73	6.85	13	290				87		25	NA	161		
GP	06/28/12	100	7.74	6.87	20	318				110		44	0.4	287		
GP	06/28/12	100			23	286				48		33	0.3	214		
GP	07/03/12	50	15.86	6.87	24	441				30		19	1.6	432		
GP	07/03/12	50	16.63	6.60	26	432				36		21	NA	408		
GP	07/03/12	50	17.37	6.57	16	416				35		21	1.3	422		
GP	07/03/12	50	18.56	6.62	18	475				21		17	1.3	477		
GP	07/03/12	50	18.75	6.60	33	541				23		17	1.0	402		
GP	07/03/12	100	8.02	6.79	16	278				111		38	0.3	224		
GP	07/03/12	100	8.5	6.73	13	202				105		41	0.4	281		
GP	07/03/12	100	8.51	6.81	17	310				76		28	0.6	185		
GP	07/03/12	100	8.63	6.73	14	366				62		42	0.5	295		
GP	07/03/12	100			18	306				78		21	0.2	138		
GP	07/18/12	50	15.33	6.79	25	429				37		12	1.9	396		
GP	07/18/12	50	15.34	6.92	42	426				30		13	1.7	449		
GP	07/18/12	50	15.52	6.84	35	488										
GP	07/18/12	50	15.8	6.85	29	483				110		13	1.7	455		
GP	07/18/12	50	15.89	6.76	43	615				43		11	1.8	422		
GP	07/18/12	100	7.56	6.83	35	488										
GP	07/18/12	100	7.76	6.79	26	368				100		39	0.4	285		
GP	07/18/12	100	7.79	6.85	16	286				127		29	1.9	294		
GP	07/18/12	100	7.85	6.86	15	297				34		40	0.3	250		

GP	07/18/12	100	8.06	6.71	17	270				75		36	1.2	305		
CP	07/19/12	15	15.19	6.52	18	416	111									
CP	07/19/12	20	15.51	6.45	12	295	129									
CP	07/19/12	25	16.05	6.6	31	392	103			1.2		6			0.64	
SP	07/23/12	25	15.68	7.13	8	59										
SP	07/23/12	50	8.72	6.82	12	86	40									
SP	07/23/12	75	8.15	6.51	33	636										
SP	07/23/12	200	2.15	7.41	2	13										
IF	07/25/12	50	0.19	8.32	1	15	104									
IF	07/25/12	200	0.28	7.75	2	5										
IF	07/25/12	25*	5.68	7.7	10	56										
IF	07/25/12	25*	8.65	7.28	29	300										
IF	07/25/12	25*	14.97	7.3	37	605	399									
GP	07/30/12	50	14.17	6.8	11	344										
GP	07/30/12	100	7.5	6.77	23	287										
GP	07/30/12	150	7.9	6.78	8	401	138									
GP	07/30/12	200	5.23	6.88	4	92										
GP	07/30/12	250	5.97	6.83	2	51	60									
BB	08/01/12	50	12.67	4.41	95	1507										
BB	08/01/12	50	14.76	5.44	153	1599	94									
FL	08/09/12	25	3.35	6.94	11	138	39									
FL	08/09/12	50	9.61	6.91	45	551	138									
FL	08/09/12	100	5.47	6.92	25	289										
FL	08/09/12	150	7.87	6.9	51	900	416									
FL	08/09/12	200	10	6.92	58	1211										
GP	08/17/12	50	16.49	6.84	23	431	173	1167	102							
GP	08/17/12	100	7.67	6.92	11	278		975	259							

GP	08/17/12	150	7.11	6.76	11	261	128	893	211							
GP	08/17/12	200	5.84	6.75	6	122	90	723	349							
GP	09/05/12	25	11.01	6.71				2178	99							
GP	09/05/12	50	14.03	7.04				2773	185							
GP	09/05/12	50	9.08	6.77	20	419		1077	72							
GP	09/05/12	100	8.26	6.79	11	260		2060	208							
GP	09/05/12	140	7.46	6.92	18	268	104	686	134							
GP	09/05/12	190	5.84	6.75	4	112		635	282							
BB	09/12/12	10	13.72	6.93						202		31	1.9	198	2.25	2580
GP	09/12/12	50	8.42	7						92		23	0.7	197	1.69	233
CP	09/12/12	50	15.42	6.43						38		7	0.2	237	72.3	
IF	09/19/12	50	8.47	7.59						53		5	8.1	119	7.56	90
SP	09/19/12	50	15.46	6.57						12		7	1.8	168	4.92	ND
FL	09/19/12	50	16.08	6.79						27		3	3.8	279	18.88	11
WP	09/25/12	20	8.04	6.29	33	632	84									
WP	09/25/12	50	8	6.48	50	596										
GP	10/12/12	40	14.63	6.95	6	178	73	884	63			9	1.9	260	12.4	
GP	10/12/12	75	6.42	7.07	5	72		809	114	162	-48	35	0.9	141	3.92	
GP	10/12/12	140	7.11	6.81	9	193		835	280	135	145	42	0.2	154	4.98	
GP	10/12/12	200	5.77	6.83	7	223		556	382	144	238	33	0.2	70	0.23	
GP	11/22/12	25	17.93	6.44				899	85			4			4.52	
GP	11/22/12	50	16.9	6.73	22	413		671	117			13	3.1	346	20.8	
GP	11/22/12	90	12.4	7.02	17	373		915	166			30	0.5	324	1.1	
GP	11/22/12	130	7.5	6.81	14	277		825	238			45	0.2	267	0.75	
GP	11/22/12	200	5.6	6.86	1	50		556	373			32	0.1	63	0.42	
GP	12/08/12	25	17.06	6.33				690	30			2	3.8	150	2.3	
GP	12/08/12	50	15.68	6.84	24	457		538	67			12	1.3	368	12.5	

GP	12/08/12	70	9.24	7.07	17	248		939	146			27	0.5	193	1.19	
GP	12/08/12	130	8.17	6.81	11	195		808	223			40	0.2	246	0.45	
GP	12/08/12	200	5.63	6.89	3	89		518	380			32	0.1	68	0.26	
GP	01/29/13	30	15.89	7.03	28	304						3	7.5	198	0.51	
GP	01/29/13	50	7.17	7.34	13	175						9	2.1	92	8.3	
GP	01/29/13	80	6.76	7.21	7	116						15	0.7	93	2.1	
GP	01/29/13	110	7.98	7.01	9	258						27	0.2	91	0.25	
GP	01/29/13	150	5.25	6.8	4	67						26	0.1	44	0.23	
GP	01/29/13	190	4.88	6.78	5	102						32	0.1	92	0.52	
GP	02/25/13	50	6	7.14	8	133		884	63	33	30	9	1.9	94	13.3	
GP	02/25/13	75	6.1	6.77	9	123		923	106	66	41	13	0.8	95	2.86	
GP	02/25/13	110	6.6	6.98	18	269		735	217	145	71	26	0.3	112	3.52	
GP	02/25/13	155	5.2	6.78	5	119		540	244	123	121	26	0.1	55	0.47	
GP	02/25/13	200	4.8	6.79	8	141		429	301	134	167	22	0.1	76	0.08	
GP	02/25/13	310	2.8	7.44	2	51		259	165	104	61	16	0.3	11	0.86	
GP	03/27/13	50	6.51	7.28	10	162		813	59							
GP	03/27/13	75	6.86	7.22	8	136		819	102							
GP	03/27/13	110	6.55	7.07	18	245		728	206							
GP	03/27/13	155	5.35	6.93	4	114		519	248							
GP	03/27/13	200	4.98	6.95	4	127		452	290							
GP	03/27/13	310	2.96	7.51	2	47		298	170							

Table 2. PAH congeners in analysis method and if quantitatively detected in at least one sample.

Compound	Detected?
Naphthalene	yes
Benzo[b]thiophene	no
2-methyl napthalene	yes
1-methyl napthalene	yes
biphenyl	yes
2,6-dimethylnapthalene	yes
acenaphylene	yes
acenapthene	yes
dibenzofuran	no
2,3,5,-trimethylnapthalene	yes
fluorene	yes
dibenzothiophene	yes
phenanthrene	yes
anthracene	yes
carbazole	yes
1-methyl phenanthrene	yes
Flouranthene	yes
pyrene	yes
benz(a)anthracene	no
Chrysene	no
benzo(b)flouranthene	yes
benzo(k)flouranthene	yes
benzo(e)pyrene	yes
benzo(a)pyrene	yes
perylene	yes
indeno(1,2,3,cd)pyrene	yes
benzo(g,h,i)perylene	yes

Table 3. Chemical constituent concentrations in shallow pore water and surface water used to calculate SGD fluxes by season. Surface water sources in order: [a]Raymond and Bauer, 2001; [b]Reay, 2009; [c]Epstein and Zander, 1978; [d]Moore and Shaw, 2009; [e]Jian Shen, personal comm. * no error is included because concentration is a median value. Standard deviation is expected to be larger than the median value.

	Pore water Winter	**Pore water Summer**	**Surface Water**
DOC (uM)	1325±1080	750±120	350[a]
TDN (uM)	110±65	65±40	25[b]
TDP (uM)	33±6	13±8	0.9[b]
NH_4 (uM)	95±80	34±8	5[b]
Ba (nM)	230±130	430±140	200[c]
U (nM)	1.1±0.8	1.2±1.3	5.5[d]
ΣPAH_{30} (ng)	90*	90*	-
Salinity	13.87	17.44	15-19[e]

Table 4. Seasonal and annual constituent SGD fluxes in mmol/m^2/d other than as noted. *No statistical error was propagated for PAHs due to use of the median rather than mean; therefore error is expected to be larger than value shown for each. ^Error on seasonal averages is not propagated but is expected to be larger than values shown.

	^{224}Ra	^{223}Ra	^{226}Ra
	Summer		
DOC	39±19	34±16	2.4±1.2
TDN	3.8±4.5	3.3±3.9	0.2±0.3
TDP	1.2±0.8	0.9±0.7	0.07±0.05
NH_4	2.8±0.8	2.4±0.7	0.17±0.05
Ba	0.022±0.017	0.019±0.015	0.001±0.001
U	-0.0004±0.0001	-0.00036±0.00001	-0.00002±0.0004
ΣPAH_{30} (ng/m^2/d)	8.6*	7.6*	0.5*
	Winter		
DOC	120±140	10±15	19±22
TDN	10±10	9.3±11	1.7±1.3
TDP	3.9±2.1	3.4±3.2	0.6±0.1
NH_4	11±11	9.3±12	1.7±1.5
Ba	0.004±0.02	0.003±0.018	0.7±4
U	-0.0005±0.0004	-0.0005±0.0005	-0.00008±0.0007
ΣPAH_{30} (ng/m^2/d)	10.8*	9.5*	1.8*
	Annual^		
DOC	78	69	11
TDN	7.2	6.3	1
TDP	2.5	2.2	0.3
NH_4	6.7	5.9	1
Ba	0.013	12	0.001
U	0.0005	-0.0004	-0.0006
ΣPAH_{30} (ng/m^2/d)	9.7	8.6	1

Summary and Conclusions

Radium was enriched in pore water relative to surface waters and was used as a tracer of SGD in the YRE. Non-SGD sources and sinks of Ra were measured in the YRE and a significant imbalance was observed. SGD of Ra was determined the only way to satisfy this large mass imbalance. The Ra pore water end member was correlated with salinity, was seasonally variable, and was used to determine approximate annual SGD fluxes of 6-118L/m^2/d. Each Ra isotope provided a different SGD flux which together span more than order of magnitude. This study suggests that the calculated SGD fluxes vary according to the Ra isotope regeneration rate, which is a function of the Ra isotope half-life. These isotope-specific SGD fluxes therefore likely represent mixing occurring through different zones of the STE.

The behavior of dissolved DOC, TDN, NH_4, TDP, U, Ba, Fe, and PAHs in pore water was investigated and compared to the behavior Ra in the York River STE. Both TDN and NH_4 had either a deep groundwater source or were not removed, while DOC and TDP were added non-conservatively and U was removed non-conservatively within the subterranean estuary. PAHs and Fe had no distinct distribution with respect to salinity or Ra. Fe variability was likely related to the presence of Fe-oxides in the sediments while PAH variability was likely caused by near-shore land use. Only Ba was positively correlated with Ra (as well as salinity) in pore water, and a flux of 11-12 μmol/m^2/d was estimated. Because the behavior of each pore water constituent other than Ba was not correlated with Ra, Ra-derived SGD fluxes do not provide accurate flux estimates for these compounds. Therefore, this study provides only minimum and maximum estimates of these constituent fluxes through SGD using ^{226}Ra and ^{224}Ra, based on the assumption

that the regeneration rate of each constituent falls between the regeneration rate of these two isotopes in pore water. In order to accurately determine the flux of these compounds in SGD, a tracer with the same behavior must be used. This study suggests Ra-derived SGD fluxes are imprecise and should not be used to estimate nutrient or other pore water constituents unless the compound of interest has the same behavior in pore water as Ra.

Literature Cited

Addy, K., Gold, A., Nowicki, B., McKenna, J., Stolt, M., Groffman, P., 2005. Denitrification capacity in a subterranean estuary below a Rhode Island fringing salt marsh. Estuaries 28, 896-908.

Al-Masri, M.S., 2006. Spatial and monthly variations of radium isotopes in produced water during oil production. App. Rad. Iso. 64, 615-623.

Ballestero, T.P., Roseen, R.M., Bacca-Cortes, G.F., 2004. Land use influence on the characteristics of groundwater inputs to the Great Bay estuary, New Hampshire. CICEET Final report.

Barnes, C.E., Cochran, J.K., 1993. Uranium geochemistry in estuarine sediments: Controls on removal and release processes. Geochim. Cosmochim. Acta 57, 555-569.

Basu, A.R., Jacobsen, S.B., Poreda, R.J., Dowling, C.B., Aggarwal, P.K., 2001. Large groundwater strontium flux to the oceans from the Bengal basin and marine strontium isotope record. Science. 293, 1470-1473.

Beck, A.J., Rapaglia, J.P., Cochran, J.K., Bokuniewicz, H.J., 2007. Radium mass-balance in Jamaica Bay, NY: Evidence for a substantial flux of submarine groundwater. Mar. Chem. 106, 419-441.

Beck, A.J., Rapaglia, J.P., Cochran, J.K., Bokuniewicz, H.J., Yang, S. 2008. Submarine groundwater discharge to Great South Bay, NY, estimated using Ra isotopes. Mar. Chem. 109, 279-291.

Beck, A.J., Cochran, J.K., Sanudo-Wilhelmy, S.A., 2010. The distribution and speciation of dissolved trace metals in a shallow subterranean estuary. Mar. Chem. 121, 145-156.

Beck, A.J., Cochran, M.A., 2013. Controls on solid-solution partitioning of radium in saturated marine sands. Mar. Chem. http://dx.doi.org/10.1016/j.marchem.2013.01.008.

Bellucci, L.G., Frigani, M., Cochran, J.K., Albertazzi, S., Zaggia, L., Cecconi, G., Hopkins, H., 2007. ^{210}Pb and ^{137}Cs as chronometers for salt marsh accretion in the Venice Lagoon-links to flooding frequency and climate change. J. Env. Radio. 97, 85-102.

Bhat, S.G., Krishnaswamy, S., Lal, D. Rama, Moore, W.S., 1969. ^{234}Th/^{238}U ratios in the ocean. Earth Plan. Sci. Lett. 5, 483-491.

Bird, F.L., Ford, P.W., Hancock, G.J., 1999. Effect of burrowing macrobenthos on the flux of dissolved substances across the water-sediment interface. Mar. Freshwater Res. 50, 523-532.

Bollinger, M.S., Moore, W.S., 1984. Radium fluxes from a salt marsh. Nature 309, 444-446.

Bollinger, M.S., Moore, W.S., 1993. Evaluation of salt marsh hydrology using radium as a tracer. Geochim. Cosmochim. A. 57, 2203-2212.

Bone, S.E., Charette, M.A., Lamborg, C.H., Gonneea, M.E., 2007. Has submarine groundwater discharge been overlooked as a source of mercury to coastal waters? Environ. Sci. Technol. 41, 3090-3095.

Bromage, E.S.,Vadas, G.G., Harvey, E., Unger, M.A., Kaatari, S., 2007. Validation of an antibody-based biosensor for rapid quantification of 2,4,6-trinitrotoluene (TNT) contamination in ground water and river water. Environ. Sci. Technol. 41, 7067-7072.

Burnett, W.C., Taniguchi, M., Oberdorfer, J., 2001. Measurement and significance of the direct discharge of groundwater into the coastal zone. J. Sea Res. 46, 109-116.

Burnett, W.C., Bokuniewicz, H., Huettl, M., Moore, W.S., Taniguchi, M., 2003. Groundwater and pore water inputs to the coastal zone. Biogeochem. 66, 3-33.

Burnett, W.C., Aggarwal, P.K., Aureli, A., Bokuniewicz, H., Cable, J.E., Charette, M.A., Kontar, E., Krupa, S., Kulkarni, K.M., Loveless, A., Moore, W.S., Oberdorfer, J.A., Oliveira, J., Oyzurt, N., Povinec, P., Privitera, A.M.G., Rajar, R., Ramessur, R.T., Scholten, J., Stieglitz, T., Taniguchi, M., Turner, J.V., 2006. Quantifying submarine groundwater discharge in the coastal zone via multiple methods. Sci. Tot. Env. 367, 498-543.

Chabaux, F. Riotte, J., Dequincy, O., 2003. U-Th-Ra fractionation during weathering and river transport. Rev. Mineral. Geochem. 52, 533-576.

Charette, M.A., 2007. Hydrologic forcing of submarine groundwater discharge: Insight from a seasonal study of radium isotopes in a groundwater dominated salt marsh estuary. Limnol. Oceanog. 52, 230-239.

Charette, M.A., Allen, M.C., 2006. Precision ground water sampling in coastal aquifers using a direct-push, shielded-screen well-point system. Ground Water Monitoring and Remediation 26, 87-93.

Charette, M.A., Buesseler, K.O., Andrews, J.E., 2001. Utility of radium isotopes for evaluated the input of groundwater-derived nitrogen to a Cape Cod Estuary. Limnol. Oceanog., 46, 465-470.

Charette, M.A., Buesseler, K.O., 2004. Submarine groundwater discharge of nutrients and copper to an urban subestuary of Chesapeake Bay (Elizabeth River). Limnol. Oceanog. 49, 376-385.

Charette, M.A., Moore, W.S., Burnett, W.C., 2008. Uranium- and thorium- series nuclides as tracers of submarine groundwater discharge. Radio. Env. 13, 155-191.

Charette, M.A., Sholkovitz, E.R., 2002. Oxidative precipitation of groundwater-derived ferrous iron in the subterranean estuary of a coastal bay. Geophys. Res. Lett. 29,

Charette, M.A., Sholkovitz, E.R., 2006. Trace element cycling in a subterranean estuary: Part 2. Geochemistry of the pore water. Geochim. Cosmochim. Acta 70, 811-826.

Countway, R.E., Dickhut, R.M., Canuel, E.A., 2003. PAH distributions and associations with organic matter in surface waters of the York River, VA Estuary. Org. Geochem. 34, 209-224.

Conrad, C.F., Fugate, D., Daus, J., Chisolm-Brause, C.J., Kuehl, S.A., 2007. Assessment of the historical trace metal contamination of sediments in the Elizabeth River, Virginia. Mar. Poll. Bull. 54, 385-395.

Corbett, D.R., Cable, J.E., 2003. Seepage meters and advective transport in coastal environments: Comments on ''Seepage meters and Bernoulli's revenge'' by E. A. Shinn, C. D. Reich, and T. D. Hickey. 2002. Estuaries 25:126–132. Estuaries 26, 1383-1389.

Cornett, R.J., Risto, B.A., Lee, D.R., 1989. Measuring groundwater transport through lake sediments by advection and diffusion. Water Resources Res. 25, 1815-1823.

Crotwell, A.M., Moore, W.S., 2003. Nutrient and radium fluxes from submarine groundwater discharge to Port Royal Sound, SC. Aq. Geochem. 9, 191-208.

CWVa, 2005. Chesapeake Bay nutrient and sediment reduction tributary strategy for the York River and Lower York coastal basins. Commonwealth of Virginia, Richmond, 113pp.

Dale, A.W., Bertics, V.J., Treude, T., Sommer, S., Wallmann, K., 2013. Modeling benthic-pelagic nutrient exchange processes and porewater distributions in a seasonally hypoxic sediment: evidence for massive phosphate release by *Beggiatoa*? Biogeosci. 10, 629-651.

Dauer, D., Marshal, H., Donat, J., Lane, M., Morton, P., Doughten, S., Hoffman, F., 2005. Status and trends in water quality and living resources in the Virginia Chesapeake Bay: York River (1985-2004). Final Report. Virginia Department of Environmental Quality, Richmond, VA, 63p.

Diaz, R.J., 2001. Overview of hypoxia around the world. J. Environ. Equality 30, 275-281.

Doumlele, D.G., 1979. New Kent County tidal marsh inventory. Special report No. 208 in applied marine science and ocean engineering. Virginia Institute of Marine Science.

Dulaiova, H., Burnett, W.C., Wattayakorn, G., Sojisuporn, P., 2006. Are the groundwater inputs into river-dominated areas important? The Chao Phraya River-Gulf of Thailand. Limnol. Oceanog. 51, 2232-2247.

Duncan, T., Shaw, T.J., 2003. The mobility of rare earth elements and redox sensitive elements in the groundwater/seawater mixing zone of a shallow coastal aquifer. Aq. Geochem. 9, 233-255.

Epstein, M.S., Zander, A.T., 1979. Direct determination of barium in sea and estuarine water by graphite furnace atomic spectrometery. Anal. Chem. 51, 915-918.

Everett, L.G., Cullen, S.J., Rice, D.W., McNam., W.W.Jr., Dooher, B.P., Kavanaugh, M.C., Johnson, P.C., Kastenberg, W.E., Small, M.C., 1998. Risk-based assessment of appropriate fuel hydrocarbon cleanup strategies for the naval exchange gasoline station naval construction battalion center, Port Hueneme, CA. UCRL-AR-130891

Freeze RA, Cherry JA. Groundwater. Englewood Cliffs, NJ: Prentice- Hall Inc.; 1979. 604 pp.

French, P.W., Allen, J.R.L., Appleby, P.G., 1994. 210-Lead dating of modern period salt marsh deposit from the Severn estuary, and its implications. Mar. Geo. 118, 327-334.

Friedrichs, C.T., 2009. York River physical oceanography and sediment transport. J. Coast. Res. 57, 17-22.

Friedrichs, C.T., Wright, L.D., Hepworth, D.A., Kim, S.C., 2000. Bottom boundary layer processes associated with fine sediment accumulation in coastal seas and bays. Contin. Shelf Res. 20, 807-841.

Gallagher, D.L., Diettrich, A.M., Reay, W.G., Hayes, M.C., Simmons, G.M., 1996. Ground water discharge of agricultural pesticides and nutrients to estuarine surface water. GWMR, 118-129.

Gallardo, A.H., Marui, A., 2006. Submarine groundwater discharge: An outlook of recent advances and current knowledge. Geo-Mar. Lett. 26, 102-113.

Garcia-Orellana, J., Cochran, J.K., Bokuniewicz, H., Yang, S., Beck, A.J., 2010. Time-series sampling of ^{223}Ra and ^{224}Ra at the inlet to Great South Bay (New York): A strategy for characterizing the dominant terms in the Ra budget of the bay. J. Environ. Radio. 101, 582-588.

Garcia-Solsona, E., Garcia-Orellana, J., Masque, P., Dulaiova, H., 2008b. Uncertainties associated with ^{223}Ra and ^{224}Ra measurements in water via a Delayed Coincidence Counter (RaDeCC). Mar. Chem. 109, 198-219.

Garcia-Solsona, E., Masque, P., Garcia-Orellana, J., Rapaglia, J., Beck, A.J., Cochran, J.K., Bokuniewicz, H.J., Zaggia, L., Collavini, F., 2008a. Estimating submarine groundwater discharge around Isola La Cura, northern Venica Lagoon (Italy) by using the radium quartet. Mar. Chem. 109, 292-306.

Geibert, W., Rogers van der Loeff, M.M., Hanfland, C., Dauelsberg, H.-J., 2002. Actinium-227 as a deep-sea tracer: sources, distribution and applications. Earth Plan. Sci. Lett. 198, 147-165.

Gonneea, M., Mulligan, A.E., Charette, M.A., 2013. Climate-driven sea level anomalies modulate coastal groundwater dynamics and discharge. Geophys. Res. Lett. Accepted.

Harlow, G.E., Jr., Augenstein, T.W., Samsel, T.B., III, and Wilson, W.D., 1996, Geographic information system data base for the Elizabeth River watershed, Virginia [abs.], in Chesapeake Bay Symposium, Richmond, Va.: Virginia Journal of Science 46, 264.

Harsh, J.F., Laczniak, R.J., 1990. Conceptualization and analysis of ground-water flow system in the Coastal Plain of Virginia and adjacent parts of Maryland and North Carolina. USGS Professional Paper 1404-F.

Hayward, D., Welch, C.S., Haas, L.W., 1982. York River destratification: an estuary-subestuary interaction. Science 216, 1413-1414.

Helz, G.R., 1976. Trace element inventory of the northern Chesapeake Bay with emphasis on the influence of man. Geochim. Cosmochim. Acta 40, 573-580.

Heywood, C.E., Pope, J.P., 2009. Simulation of Groundwater Flow in the Coastal Plain Aquifer System of Virginia. USGS Scientific Investigations Report 2009-5093

Hu, C., Muller-Karger, F.E., Swarzenski, P.W., 2006. Hurricanes, submarine groundwater discharge, and Florida's red tides. Geophys. Res. Lett. 33, L11601, 1-5.

Hussain, N., Church, T.M., Kim, G. ^{222}Rn and ^{226}Ra to trace groundwater discharge into the Chesapeake Bay. Mar. Chem. 65, 127-134.

Huzzey, L.M., Brubaker, J.M., 1988. The formation of longitudinal fronts in a coastal plains estuary. J. Geophys. Res. 93, 1329-1334.

Jahnke, R., Richards M., Nelson J., Robertson C., Rao A., Jahnke, D., 2005. Organic matter remineralization and porewater exchange rates in permeable South Atlantic Bight continental shelf sediments. Cont. Shelf Res. 25, 1433–1452.

Kellum, A., Beck, A.J., Luek, J.L., Cochran, M.A. Controls on submarine groundwater discharge in the York River estuary. *In progress*.

Kelly, R.P., Moran, S.B., 2002. Seasonal changes in groundwater input to a well-mixed estuary estimated using radium isotopes and implications for coastal nutrient budgets. Limnol. Oceanogr. 47, 1796-1807.

Kim, G., Burnett, W.C., Dulaiova, H., Swarzenski, P.W., Moore, W.S., 2001. Measurement of ^{224}Ra and ^{226}Ra activities in natural waters using a radon-in-air monitor. Environ. Sci. Technol. 35, 4680-4683.

King, J.N., Mehta, A.J., Dean, R.G., 2009. Generalized analytical model for benthic water flux forced by surface gravity waves. J. Geophys. Res. 114, C04004, doi:10.1029/2008JC005116

King, J.N., 2012. Synthesis of benthic flux components in the Patos Lagoon coastal zone, Rio Grande do Sul, Brazil. Water Resour. Res. 48, W12530, doi:10.1029/2011WR011477

Koroleff F. Determination of nutrients. In: Grasshoff K., Ehrhardt M., Kremling K., editors. Methods in Seawater Analysis. New York: Verlag Chemie; 1983. p. 125-187

Kroeger, K.D., Swarzensi, P.W., Greenwood, W.J., Reich, C., 2007. Submarine groundwater discharge to the Tampa Bay: Nutrient fluxes and biogeochemistry of the coastal aquifer. Mar. Chem. 104, 85-97.

Langland, M., Moyer, D., Blomquist, J., 2007. Changes in streamflow concentration in selected nontidal basins in the Chesapeake Bay watershed, 1985-2006. USGS Open File Report 2007-1372, 58p. plus appendices.

Lapointe, B.E., O'Connell, J.D., Garrett, G.S., 1990. Nutrient couplings between on-site sewage disposal systems, groundwaters, and nearshore surface waters of the Florida Keys. Biogeochem.10, 289-307.

Lee, D.R., 1977. A device for measuring seepage flux in lakes and estuaries. Limnol. Oceanogr. 22, 140-147.

Lee, Y.-W., Kim, G., 2007. Linking groundwater-borne nutrients and dinoflagellates red-tide outbreaks in the southern sea of Korea using a Ra tracer. Est. Coast. Shelf. Sci. 71, 309-317.

Leister, D.L., Baker, J.E., 1994. Atmospheric deposition of organic contaminants to the Chesapeake Bay. Atmos. Environ. 28, 1499-1520.

Li, L., Barry, A., Stagnitti, F., Parlange, J.-Y., 1999. Submarine groundwater discharge and associated chemical input to a coastal sea. Water Resources Res. 35, 3253-3259.

Li, Y.-H., Mathieu, G., Biscaye, P., Simpson, H.J., 1977. The flux of 226Ra from estuarine and continental shelf sediments. Earth Plan. Sci. Lett. 37, 237-241

Li, Y.-H., Chan, L.-H., 1979. Desorption of Ba and ^{226}Ra from river-borne sediments in the Hudson estuary. Earth Plan. Sci. Lett. 43, 343-350.

Lin, J., and Kuo, A.Y., 2001. Secondary turbidity maximum in a partially mixed microtidal estuary. Estuaries 24, 707-720.

Loveless, A.M., Oldham, C.E., Hancock, G.J., 2008. Radium isotopes reveal seasonal groundwater inputs to Cockburn Sound, a marine embayment in Western Australia. J. Hydrol. 351, 203-217.

Lovley, D.R., Phillips, E.J., Gorby, Y.A., Landa, E.R., 1990. Microbial reduction of uranium. Nature 350, 413-416.

Metcalfe, C.D., Beddows, P.A., Bouchot, G.G., Metcalfe, T.L., Li, H., Van Lavieren, H., 2011. Contaminants in the coastal karst aquifer system along the Caribbean coast of the Yucatan Peninsula, Mexico. Environ. Poll., 159, 991-997.

McKee, B.A., 2008. U- and Th-series nuclides in estuarine environments. Radio. Env. 13, 193-225.

Michael, H.A., Charette, M.A., Harvey, C.F., 2011. Patterns and variability of groundwater flow and radium activity at the coast: A case study from Waquoit Bay, Massachussetts. Mar. Chem. 127, 100-114.

Milliman, J.D., 1993. Production and accumulation of calcium carbonate in the ocean: Budget of a nonsteady state. Global Biogeochem. Cycles 7, 927–57.

Milliman, J.D., Syvitski, J.P.M., 1992. Geomorphic/tectonic control of sediment discharge to the ocean: The importance of small mountainous rivers. J. Geol. 100, 525–544.

Mitchell, M.M., M.R. Berman, J., H. Berquist, Bradshaw, K. Duhring, S. Killeen and C.H. Hershner, 2011. Strengthening Virginia's Wetlands Management Programs, final report to US EPA.

Mitra, S., Dickhut, R.M., Kuehl, S.A., Kimbrough, K.L., 1999. Polycyclic aromatic hydrocarbon (PAH) source, sediment deposition patterns, and particle geochemistry as factors influencing PAH distribution coefficients in sediments of the Elizabeth River, VA, USA. Mar. Chem. 66, 113-127.

Monson, N.E., Cloern, J.E., Lucas, L.V., Monismith, S.G., 2002. A comment on the use of flushing time, residence time, and age as transport time scales. Limnol. Oceanog. 47, 1545-1553.

Moore, K.A., 1976. Gloucester County tidal marsh inventory. Special report No. 64 in applied marine science and ocean engineering. Virginia Institute of Marine Science.

Moore, K.A., 1980. James City County tidal marsh inventory. Special report No. 188 in applied marine science and ocean engineering. Virginia Institute of Marine Science.

Moore, K.A., Reay, W.G., 2009. CBNERRVA Research and monitoring program. J. Coast. Res. 10057, 118-125.

Moore, W.S., 1981. Radium isotopes in the Chesapeake Bay. Estuarine, Coastal and Shelf Sci. 12, 713-723.

Moore, W.S., 1999. The subterranean estuary: A reaction zone of ground water and sea water. Mar. Chem. 65, 111-125.

Moore, W.S., 2000. Ages of continental shelf waters determined from ^{223}Ra and ^{224}Ra. J. Geophys. Res. 105, 22117-22122.

Moore, W.S., 2003. Sources and fluxes of submarine groundwater discharge delineated by radium isotopes. Biogeochem. 66, 75-93.

Moore, W.S., 2008. Fifteen years experience in measuring ^{224}Ra and ^{223}Ra by delayed-coincidence counting. Mar. Chem. 109, 188-197.

Moore, W.S., 2010. The effect of submarine groundwater discharge on the ocean. Annu. Rev. Marine. Sci. 2, 59-88.

Moore, W.S., Arnold, R., 1996. Measurement of ^{223}Ra and ^{224}Ra in coastal waters using a delayed coincidence counter. J. Geophys. Res. 101, 1321-1329.

Moore, W.S., Blanton, J.O., Joye, S.B., 2006. Estimates of flushing times, submarine groundwater discharge, and nutrient fluxes to Okatee Estuary, South Carolina. J. Geophys. Res. 111, doi:10.1029/2007jc004199

Moore, W.S., Kjerfve, B., Todd, J.F. 1998. Identification of rain-freshened plumes in the coastal ocean using Ra isotopes and Si. J. Geophys. Res. 103, 7709-7717.

Moore, W.S., Krest, J., 2004. Distribution of ^{223}Ra and ^{224}Ra in the plumes of the Mississippi and Atchafalaya Rivers and the Gulf of Mexico. Mar. Chem. 86, 105-119.

Moore, W.S., Reid, D.F., 1973. Extraction of radium from natural waters using manganese-impregnated acrylic fibers. J. Geophys. Res. 78, 8880-8886.

Moore, D.G., Scott, M.R., 1986. Behavior of ^{226}Ra in the Mississippi River mixing zone. J. Geophys. Res. 91, 14317-14329.

Moore, W.S., Shaw, T.J., 2008. Fluxes and behavior of radium isotopes, barium, and uranium in seven Southeastern US rivers and estuaries. Mar. Chem. 108, 236-254.

Nichols, M.M., S.C. Kim, and C.M. Brouwer, 1991. Sediment characterization of the Chesapeake Bay and its tributaries, Virginian Province. National estuarine inventory: supplement. NOAA Strategic Assessment Branch. 88p.

Nittrouer, C.A., Sternberg, R., Carpenter, R., Bennett, J.T., 1979. The use of Pb-210 geochronology as a sedimentological tool: application to the Washington continental shelf. Mar. Geo. 31, 297-316.

NOAA. Tides and Currents. Yorktown USCG Training Center, VA: 8637689, 2013. National Oceanic and Atmospheric Administration. <tidesandcurrents.noaa.gov>.

Nozaki, Y., Yamamoto, Y., Manaka,T., Amakawa, H., Snidvongs, A., 2001. Dissolved barium and radium isotopes in the Chao Phraya River estuarine mixing zone in Thailand. Cont. Shelf Res. 21, 1435-1448.

Peeler, K.A., Opsahl, S.P., Chanton, J.P., 2006. Tracking anthropogenic inputs using caffeine, indicator bacteria, and nutrients in rural freshwater and urban marine systems. Environ. Sci. Technol. 40, 7616-7622.

Peterson, P.N., Burnett, W.C., Taniguchi, M., Chen, J., Santos, I.R., Ishitobi, T., 2009. Radon and radium isotope assessment of submarine groundwater discharge in the Yellow River delta, China. J. Geophys. Res., 113, 1-14.

Petrackis, N., Berman, M.R., Hershner, C., 1995. Current and Projected Land Use in The York River Basin, Gloucester Point: Virginia Institute of Marine Science, CMAP.

Porcelli, D., 2008. Investigating groundwater processes using U- and Th-series nuclides. Radioa. Env. 13, 105-147.

Porcelli, D., Swarzenski, P.W., 2003. The behavior of U- and Th-series nuclides in groundwater. Rev. Mineral. Geochem. 52, 317-361.

Priest, W.I., Silberhorn, G.M., Zacherle, A.W., 1987. King and Queen County tidal marsh inventory. Special report No. 208 in applied marine science and ocean engineering. Virginia Institute of Marine Science.

Rama and Moore, W.S., 1996. Using the radium quartet for evaluating groundwater input and water exchange in salt marshes. Geochim. Cosmochim. Acta 60, 4645-4652.

Raymond, P.A., Bauer, J.E., 2001. DOC cycling in a temperate estuary: A mass balance approach using natural ^{14}C and ^{13}C isotopes. Limnol. Oceanog. 46, 655-667.

Reay, W.G. Gallagher, D.L., Simmons, G.M. Jr., 1992. Groundwater discharge and its

impact on surface water quality in a Chesapeake Bay inlet. Water Res. Bull. 28, 1121-1134.

Reay, W.G., 2004. Septic tank impacts on ground water quality and nearshore sediment nutrient flux. Groundwater 42, 1079-1089.

Reay, W.G., 2009. Water quality within the York River estuary. J. Coast. Res. Special Issue 57. 23-39.

Redfield A.C., 1934. On the proportions of organic derivations in sea water and their relation to the composition of plankton. In *James Johnstone Memorial Volume*. (ed. R.J. Daniel). University Press of Liverpool 177–192.

Robinson, C., Brovelli, A., Barry, D.A., Li, L., 2009. Tidal influence on BTEX biodegradation in sandy coastal aquifers. Adv. Water Res. 32, 16-28.

Rutkowski, C.M., Burnett, W.C., Iverson, R.L., Chanton, J.P., 1999. The effect of groundwater seepage on nutrient delivery and seagrass distribution in the Northeastern Gulf of Mexico. Estuaries 22, 1033-1040.

Salisbury, S.K., 2011. Dynamics and composition of the extracellular polymeric substances produced by benthic macroalgae: An in situ ^{13}C and ^{15}N approach. Virginia Institute of Marine Science, *Master's Thesis*.

Santos, I.R., Burnett, W.C., Chanton, J., Mwashote, B., Suryaputra, I G.N.A., Dittman, T., 2008. Nutrient biogeochemistry in a Gulf of Mexico subterranean estuary and groundwater-derived fluxes to the coastal ocean. Limnol. Oceanogr. 53, 705-718.

Santos, I.R., Burnett, W.C., Dittmar, T., Suryaputra, I G.N.A., Chanton, J., 2009. Tidal pumping drives nutrient and dissolved organic matter dynamics in a Gulf of Mexico subterranean estuary. Geochim. Cosmochim. Acta. 73, 1325-1339.

Santos, I.R, Burneet, W.C., Misra, S., Suryapytra, I.G.N.A., Chanton, J., Dittmar, T., Peterson, R.N., Swarzenski, P.W., 2011. Uranium and barium cycling in a salt wedge subterranean estuary: The influence of tidal pumping. Chem. Geo. 287, 114-123.

Santos, I.R., Eyre, B.D., Huettel, M., 2012. Driving forces of porewater and groundwater flow in permeable coastal sediments: A review. Estuar. Coast. Shelf Sci. 98, 1-15.

Scholten, J.C., Pham, M.K., Blinova, O., Charette, M.A., Dulaiova, H., Eriksson, M., 2010. Preparation of Mn-fiber standards for the efficiency calibration of the delayed coincidence counting system (RaDeCC). Mar. Chem. 121, 206-214.

Schwarzenbach, R.P., Gschwend, P.M., Imboden, D.M., 2003. Environmental Organic Chemistry. Wiley, New York, ed. 2.

Seitz, R.C., 1971. Drainage area statistics for the Chesapeake Bay freshwater drainage basin. Chesapeake Bay Institute, Special Report No. 119. The Johns Hopkins University, Baltimore, MD.

Sharp J. H. Analytical methods for total DOM pools. In: Hansell D. A., Carlson C. A., editors. Biogeochemistry of Marine Dissolved Organic Matter. San Diego, USA: Academic Press; 2002. p. 35-58

Shaw, T.J., Sholkovitz, E.R., Klinkhammer, G., 1994. Redox dynamics in the Chesapeake Bay: The effect of sediment/water uranium exchange. Geochim. Cosmochim. Acta 58, 2985-2995.

Shaw, T.J., Moore, W.S., Kloepfer, J., Sochaski, M.A., 1998. The flux of barium to the coastal waters of the south eastern USA: the importance of submarine groundwater discharge. Geochim. Cosmochim. Acta 62, 3047-3054.

Shen, J., Haas, L., 2004. Calculating age and residence time in the tidal York River using a three-dimensional model experiments. Estuar. Coast. Shelf Sci., 61, 449-461.

Shinn, E.A., Reich, C.D., Hickey, T.D., 2002. Seepage meters and Bernoulli's revenge. Estuaries, 25, 126–132.

Simmons, G.M. Jr., 1988. The importance of submarine ground- water discharge to nutrient flux in coastal marine environ- ments. In *Proceedings of Understanding the Estuary: Advances in Chesapeake Bay Research*, March 29-31, Baltimore, MD, ed. M.P. Lynch and E.C. Krome, 255–269. Baltimore, Maryland: Chesapeake Research Consortium.

Simmons, G.M. Jr., 1992. Importance of submarine ground water discharge and seawater cycling to material flux across sediment/water interfaces in marine environments. Mar. Ecol. Prog. Ser. 84, 173–184

Sisson, G.M., Shen, J., Kim, S.C., Kuo, A.Y., Boon, J.D., 1997. VIMS three-dimensional hydrodynamic-eutrophication model (HEM- 3D): application of the hydrodynamic model to the York River system. Special Report in Applied Marine Science and Ocean Engineering, No. 341. Virginia Institute of Marine Science, Gloucester Point, VA 23062.

Slomp, C.P., Van Cappellen, P., 2004. Nutrient inputs to the coastal ocean through submarine groundwater discharge: controls and potential impact. J. Hydrol. 295, 64-86.

Spier, C.R., Vadas, G.G., Kaatari, S.L., Unger, M.A., 2011. Near real-time, on-site, quantitative analysis of PAHs in the aqueous environment using antibody-based biosensor. Environ. Tox. Chem. 30, 1557-1563.

Spiteri, C., Regnier, P., Slomp, C.P., Charette, M.A., 2006. pH-Dependent iron oxide precipitation in a subterranean estuary. J. Geochem. Explor. 88, 399-403.

Sprague, L.M, Langland, M., Yochum, S., Edwards, R., Blomquist, J., Phillips., S., Shenk, G., Preston, S., 2000. Factors affecting nutrient trends in major rivers of the Chesapeake Bay watershed. USGS Water Resources Investigations Report 00-4218, 109p.

Sun, Y., Torgersen, T., 1998. The effects of water content and Mn-fiber surface conditions on ^{224}Ra measurement by ^{220}Rn emanation. Mar. Chem. 62, 299-306.

Swarzenski, P.W., Baskaran, M., 2007. Uranium distribution in coastal waters and pore waters of Tampa Bay, Florida. Mar. Chem. 104, 43-57.

Swarzenski, P.W., Porcelli, D., Andersson, P.S., Smoak, J.M., 2003. The behavior of U- and Th-series nuclides in the estuarine environment. Rev. Mineral. Geochem. 52, 577-606.

Swarzenski, P.W., Reich, C.D., Spechler, R.M., Kindinger, J.L., Moore, W.S., 2001. Using multiple geochemical tracers to characterize the hydrogeology of the submarine spring off Crescent Beach, Florida. Chem. Geo. 179, 187-202.

Szabo, Z., DePaul, V.T., Fischer, J.M., Kraemer, T.F., Jacobsen, E., 2012. Occurrence and geochemistry of radium in water from principal drinking-water aquifer systems of the United States. App. Geochem. 27, 729-752.

Taniguchi, M., Burnett, W.C., Cable, J.E., Turner, J.V., 2002. Investigation of submarine groundwater discharge. Hydrol. Process. 16, 2115-2129.

Uchiyama, Y., Nadaoka, K., Rolke, P., Adachi, K., Yagi, H., 2000. Submarine groundwater discharge into the sea and associated nutrient transport in a sandy beach. Water Resour. Res. 36, 1467-1479.

Ullman W.J., Chang B., Miller D.C., Madsen J.A., 2003. Groundwater mixing, nutrient diagenesis, and discharges across a sandy beachface, Cape Henlopen, Delaware (USA). Estua- rine, Coast. Shelf Sci, 57, 539–552.

U.S. Geological Survey, 2013, National Water Information System data available on the World Wide Web (USGS Water Data for the Nation), accessed [June 9, 2013], at [http://waterdata.usgs.gov/nwis/].

USGAO, 2005. Groundwater Contamination: DOD uses and develops a range of remediation technologies to clean up military sites. GAO-05-666, 46p.

VaDEQ, 2005. PCB strategy for the Commonwealth of Virginia. Virginia Department of Environmental Quality. Richmond, VA, 32 p. plus appendices.

VaDEQ, 2010. TMDL Report for Chesapeake Bay Shellfish Waters: in Ware Creek, Taskinas Creek, and Skimino Creek Bacterial Impairment. Virginia Department of Environmental Quality.

VaDEQ, 2012. Status of Virginia's Water Resources: A report on Virginia's Water Resources
Management Activities. Virginia Department of Environmental Quality.

Valeila, I., Foreman, K., LaMontagne, M., Hersh, D., Costa, J., D'Avanzo, C., Babione, M., Peckol, P., DeMeo-Anderson, B., Sham, C.-H., Brawley, J. Lajtha, K., 1992. Coupling of watersheds and coastal waters: Sources and consequences of nutrient enrichment in Waquoit Bay, MA. Estuaries 15, 443-457.

van Beek, P., Bourquin, M., Reyss, J.-L., Souhaut, M., Charette, M.A., Jeandel, C., 2008. Radium isotopes to investigate the water mass pathways of Kerguelen Plateau (Southern Ocean). Deep-Sea Res. II. 55, 622-637.

Virginia Estuarine and Coastal Observing System (VECOS), 2013. Virginia Institute of Marine Science, Gloucester Pt., VA. <www.vims.edu/vecos>.

Waska, H., Kim, S., Kim, G., Peterson, R.N., Burnett, W.C., 2008. An efficient and simple method for measuring 226Ra using the scintillation cell in a delayed coincidence counting system (RaDeCC). J. Environ. Radio. 99, 1859-1862.

Webster, I.T., Hancock, G.J., Murray, A.S., 1995. Modeling the effect of salinity on radium desorption from sediments. Geochim. Cosmochim. Acta 59, 2469-2476.

Wendt, P.H., Van Dolah, R.F., Bobo, M.Y., Mathews, T.D., Levisen, M.V., 1996. Wood preservative leachates from docks in an estuarine environment. Envrion. Contamin. Toxicol. 31, 24-37.

Westbrook, S.J., Rayner, J.L., Davis, G.B., Clement, T.P., Bjerg, P.L., Fisher, S.J., 2005. Interaction between shallow groundwater, saline surface water and contaminant discharge at a seasonally and tidally forced estuarine boundary. J. Hydrol. 302, 255-269.

Windom, H., and Niechenski, F., 2003. Biogeochemical processes in a freshwater-seawater mixing zone in permeable sediments along the coast of Southern Brazil. Mar. Chem. 83, 121-130.

Yehdegho, B., Rozanski, K., Zojer, H., Stichler, W., 1997. Interaction of dredging lakes with the adjacent groundwater field: An isotope study. J. Hydrol. 192, 247-270.

Zhao, S., Zhang, P., Crusius, J., Kroeger, K.D., Bratton, J.F., 2011. Use of pharmaceuticals and pesticides to constrain nutrient sources in coastal groundwater of northwestern Long Island, New York, USA. J. Environ. Monit. 13, 1337-1343.

Vita

Jenna Lynn Luek

Jenna was born in Elwood City, Pennsylvania on May 12, 1988. She attended Seneca Valley High School in Harmony, PA and graduate with high honors in 2006. She went on to earn a B.S. in Chemistry with a minor in Environmental Studies from Chatham University in Pittsburgh Pennsylvania. In 2010, she defended a senior tutorial on persistent organic pollutants in the Atlantic and Southern Oceans and graduated summa cum laude. She entered the Masters program at the Virginia Institute of Marine Science, College of William and Mary, under graduate advisor Dr. Rebecca Dickhut in 2010. Following the death of Dr. Dickhut in 2011, Jenna became the student of Dr. Aaron Beck, under whom she pursued the research presented here.